Local mass transport rates and local activity of heterogeneous biofilms
by Kjetil Rasmussen

A thesis submitted in partial fulfillment of the requirements for the degree of Master of Science in Environmental Engineering
Montana State University

Abstract:
Biofilms have been modeled as homogeneous layers of cells and extracellular polymers covered by a uniform liquid layer. Modelers have assumed that water within and in close vicinity to the biofilm is stagnant. However, scanning confocal laser microscopy has shown that biofilms are highly heterogeneous, and consist of cell clusters separated by voids and channels. The heterogeneous structure makes the mass transport near and within biofilms very complicated. To be able to describe mass transport in biofilms mathematically some simplifying assumptions based on experimental data are needed.

Microelectrodes have been used here to measure oxygen profiles and local mass transfer coefficient profiles in biofilm clusters and interstitial voids. Both dissolved oxygen- and local mass transfer coefficient profiles were measured at the same locations to make it possible to superimpose the two profiles. From the oxygen profiles the effective diffusive boundary layer thickness was determined. The local mass transfer coefficient profiles provided information about the nature of mass transport near and within the biofilm. All profiles were measured at three different flow velocities to determine the influence of fluid flow on mass transport.

Convective mass transport was found to be active within the mass boundary layer and in the upper region of the biofilm, independent of biofilm's thickness and flow velocity. The effective diffusive boundary layer thickness, however, varied strongly at different locations when the same flow velocities were applied. Oxygen-and local mass transfer coefficient profiles collected through a 70 μm thick cluster revealed that the thin cluster did not cause any significant changes in local mass transfer resistance. The same conclusion was drawn from profiles measured through a void filled with a 200 μm thick extracellular polymer layer when the flow velocity was higher than 1.53 cm sec^-1. In a 350 μm thick biofilm cluster the local mass transfer coefficient decreased gradually and approached zero near the substratum.

LOCAL MASS TRANSPORT RATES AND LOCAL ACTIVITY OF HETEROGENEOUS BIOFILMS

by

Kjetil Rasmussen

A thesis submitted in partial fulfillment
of the requirements for the degree

of

Master of Science

in

Environmental Engineering

MONTANA STATE UNIVERSITY-BOZEMAN
Bozeman, Montana

September, 1996

APPROVAL

of a thesis submitted by

Kjetil Rasmussen

This thesis has been read by each member of the thesis committee and has been found to be satisfactory regarding content, English usage, format, citations, bibliographic style, and consistency, and is ready for submission to the College of Graduate Studies.

Zbigniew Lewandowski (chair) _____ (Signature) Sep. 17, 1996 (Date)

Approved for the Department of Civil Engineering

Bob Oakberg (Dept. Head) Robert G. Oakberg (Signature) 9/17/96 (Date)

Approved for the College of Graduate Studies

Robert Brown (Graduate Dean) _____ (Signature) 9/18/96 (Date)

STATEMENT OF PERMISSION TO USE

In presenting this thesis in partial fulfillment of the requirements for a master's degree at Montana State University-Bozeman, I agree that the Library shall make it available to borrowers under rules of the Library.

If I have indicated my intention to copyright this thesis by including a copyright notice page, copying is allowable only for scholarly purposes, consistent with "fair use" as prescribed in the U.S. Copyright Law. Requests for permission for extended quotation from or reproduction of this thesis in whole or in parts may be granted only by the copyright holder.

Signature 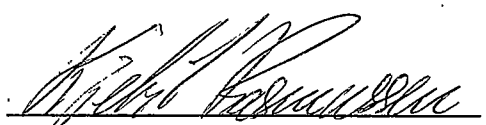

Date Sep. 17 1996

TABLE OF CONTENTS

Page

INTRODUCTION 1

MATERIALS AND METHODS 16

Construction of dissolved oxygen microelectrode 16
Calibration of dissolved oxygen microelectrode 19
Construction of local mass transfer coefficient microelectrode 20
Testing the local mass transfer coefficient microelectrode 23
Effect of changing position of the reactive surface relative to flow direction 23
Respiratory activity in a biofilm submerged by electrolyte solution 26
Influence of oxygen on local mass transfer coefficient measurements 28
Dissolved oxygen and local mass transfer coefficient profiles at the same locations of a biofilm 32
Experimental setup 32
Biofilm growth 34
Data acquisition system 35
Measurement of local mass transfer coefficient profiles in sterile reactor 35
Local mass transfer coefficient- and oxygen profiles at the same locations 36
Theoretical calculations 36
Calculation of the local mass transfer coefficient 36
Calculation of effective diffusive boundary layer thickness 37

RESULTS 39

Local mass transfer coefficient profiles in a sterile reactor 39
Dissolved oxygen- and local mass transfer coefficient profiles collected at the same locations 39
Thin cluster 39
Void filled with polymers 43
Thick cluster 47

DISCUSSION 52

Local mass transfer coefficient profiles in a sterile reactor 52
Dissolved oxygen- and local mass transfer coefficient profiles collected at the same locations 53
Thin cluster 53
Void filled with polymers 53
Thick cluster 55

CONCLUSIONS 63

LITERATURE CITED 65

NOMENCLATURE 70

APPENDIX - Experimental raw data 73

LIST OF TABLES

Table Page

1. Effective diffusive boundary layer thicknesses at different locations and flow velocities 55

LIST OF FIGURES

Figure		Page
1.	Biofilm structure.	2
2.	Concept of mass transport in homogeneous biofilms	5
3.	Construction of a dissolved oxygen microelectrode	17
4.	Calibration curve for a dissolved oxygen microelectrode	21
5.	Construction of a local mass transfer coefficient microelectrode	22
6.	Effect of changing position of electrode tip relative to flow direction	25
7.	Calibration of oxygen electrode in water and electrolyte	27
8.	Oxygen profile through biofilm submerged by electrolyte	29
9.	Oxygen influence on limiting current	31
10.	Experimental setup	33
11.	Local mass transfer coefficient profiles in sterile reactor	40
12.	Oxygen- and local mass transfer coefficient profiles in thin cluster, $v = 0.62$ cm sec^{-1}	41
13.	Oxygen- and local mass transfer coefficient profiles in thin cluster, $v = 1.53$ cm sec^{-1}	42
14.	Oxygen- and local mass transfer coefficient profiles in void, $v = 0.62$ cm sec^{-1}	44
15.	Oxygen- and local mass transfer coefficient profiles in void, $v = 1.53$ cm sec^{-1}	45

16. Oxygen- and local mass transfer coefficient profiles in void, $v = 2.60$ cm sec^{-1} 46

17. Oxygen- and local mass transfer coefficient profiles in thick cluster, $v = 0.62$ cm sec^{-1} 48

18. Oxygen- and local mass transfer coefficient profiles in thick cluster, $v = 1.53$ cm sec^{-1} 49

19. Oxygen- and local mass transfer coefficient profiles in thick cluster, $v = 2.60$ cm sec^{-1} 50

ABSTRACT

Biofilms have been modeled as homogeneous layers of cells and extracellular polymers covered by a uniform liquid layer. Modelers have assumed that water within and in close vicinity to the biofilm is stagnant. However, scanning confocal laser microscopy has shown that biofilms are highly heterogeneous, and consist of cell clusters separated by voids and channels. The heterogeneous structure makes the mass transport near and within biofilms very complicated. To be able to describe mass transport in biofilms mathematically some simplifying assumptions based on experimental data are needed.

Microelectrodes have been used here to measure oxygen profiles and local mass transfer coefficient profiles in biofilm clusters and interstitial voids. Both dissolved oxygen- and local mass transfer coefficient profiles were measured at the same locations to make it possible to superimpose the two profiles. From the oxygen profiles the effective diffusive boundary layer thickness was determined. The local mass transfer coefficient profiles provided information about the nature of mass transport near and within the biofilm. All profiles were measured at three different flow velocities to determine the influence of fluid flow on mass transport.

Convective mass transport was found to be active within the mass boundary layer and in the upper region of the biofilm, independent of biofilm's thickness and flow velocity. The effective diffusive boundary layer thickness, however, varied strongly at different locations when the same flow velocities were applied. Oxygen- and local mass transfer coefficient profiles collected through a 70 μm thick cluster revealed that the thin cluster did not cause any significant changes in local mass transfer resistance. The same conclusion was drawn from profiles measured through a void filled with a 200 μm thick extracellular polymer layer when the flow velocity was higher than 1.53 cm sec^{-1}. In a 350 μm thick biofilm cluster the local mass transfer coefficient decreased gradually and approached zero near the substratum.

INTRODUCTION

Recent studies of biofilm architecture strongly influence our concepts of mass transport mechanism in biofilms. Images of living biofilms using confocal laser microscopy show that biofilms form cellular aggregates (microcolonies) separated by interstitial void spaces filled either with water or low density biopolymers as shown in figure 1 (Lawrence et al., 1991, Korber et al., 1994, Wolfaardt et al., 1994, Keevil and Walker, 1992). Structural heterogeneity of biofilms was demonstrated using scanning electron microscopy (Stewart et al., 1995), scanning confocal laser microscopy (SCLM) (Lawrence et al., 1991), and cryoembedding (Murga et al., 1994). It is well known that the nonuniform distribution of biomass in biofilms may influence the mass transport mechanism. The study of the nature of oxygen distribution within structurally heterogeneous biofilms clearly demonstrated the importance of biofilm architecture to oxygen transport (De Beer et al, 1994 a). Reports of such influence were published even before the importance of biofilm's architecture was fully realized. Siegrist and Gujer (1985) observed an increased average diffusion coefficient with increased biofilm thickness and hypothetically explained this as a result of irregularities of thick biofilms penetrating the boundary layer causing eddy diffusion. Similar explanation may be employed to the observations of Larsen and Harremoës (1994) and Horn and Hempel (1995) who

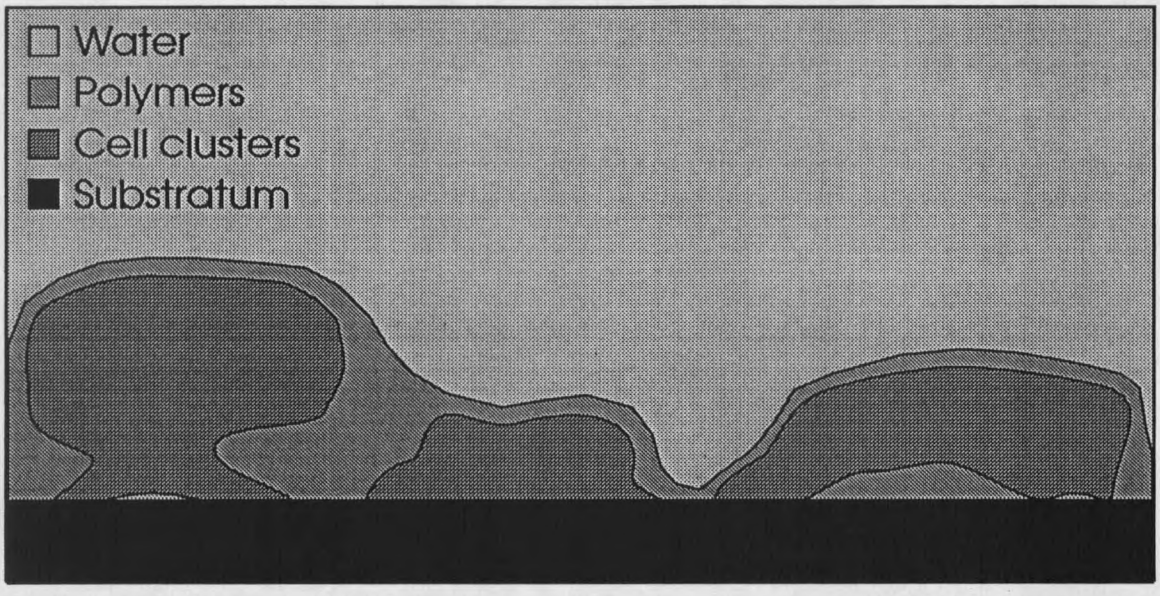

Figure 1. Biofilm structure; cell clusters separated by void spaces filled with extracellular polymers.

report that the oxygen diffusion coefficient in a biofilm is higher than in pure water. The concept of structurally heterogeneous biofilms constitutes an intellectual platform to accommodate those, otherwise difficult to interpret, observations. At the recent meeting of the International Association on Water Quality (IAWQ) Specialist Group on Biofilm Systems in Leeuwenhorst, the Netherlands, biofilm's heterogeneity was defined as "spatial differences in any parameter we think is important" (Bishop and Rittmann, 1995). Despite the awareness of biofilm heterogeneity there is no clear notion on what causes it and how the heterogeneity influences biofilm processes. Van Loosdrecht et al. (1995) discussed the influence of substrate loading rate, shear, and growth rate on the biofilm structure. Some qualitative opinions of how the process parameters influence biofilm structure have been established among biofilm researchers. A high shear rate tends to increase the biofilm's density and mechanical stability. Higher substrate loadings as well as presence of fast growing microorganisms result in thicker and less smooth biofilms. Some researchers initiated the quantification of parameters influencing structural heterogeneity. Zhang and Bishop (1994 a,b) determined the densities, porosities, specific surface area, and mean pore radius of biofilms. They determined the distribution of the tortuosity factor and the ratio of the effective diffusivity to the diffusivity in bulk solution of a biofilm. Fu et al. (1994) estimated the effective diffusivity in different layers of a biofilm using a dissolved oxygen microelectrode. Hermanowicz et al. (1995) used SCLM images to estimate the fractal dimension and biofilm morphology.

Biofilm reactivity is controlled by the rate of substrate consumption and by the rate of mass transport. Bird et al. (1960) describe two models for mass transfer; (1) the film theory; and (2) the boundary-layer theory. The film theory is a unnidirectional transport model, whereas the boundary-layer theory considers two-dimensional velocity profiles. The film theory says that a stagnant or laminar, fictitious film of fluid is present next to the boundary in which all resistance to transfer exists (Welty et al., 1976). Transport in this layer is only due to molecular diffusion. The mass transfer coefficient, k, is defined as the molecular diffusivity, D, divided by the film thickness, L_D:

$$k = D/L_D \qquad (1)$$

Although the disadvantages of the film model are well known, its conceptual simplicity and computational convenience are so appealing that it is frequently intermixed with the boundary layer concept. From its beginning biofilm modeling relied on the assumption that water near the biofilm, and within the biofilm, is stagnant (Atkinson and Davies, 1974, Rittmann and McCarty, 1978, Wanner and Gujer, 1984). It is a common practice to substitute the film thickness in the film model with the thickness of the mass boundary layer (MBL) determined with microelectrodes (Zhang and Bishop, 1994 c). This approach implicitly assumes that the mass transport in the mass boundary layer is due to molecular diffusion only. Figure 2 shows how a concentration profile through the bulk liquid, MBL, and biofilm should appear based on this concept. The assumptions that molecular diffusivity is the major factor influencing the mass transport rate inside the MBL and

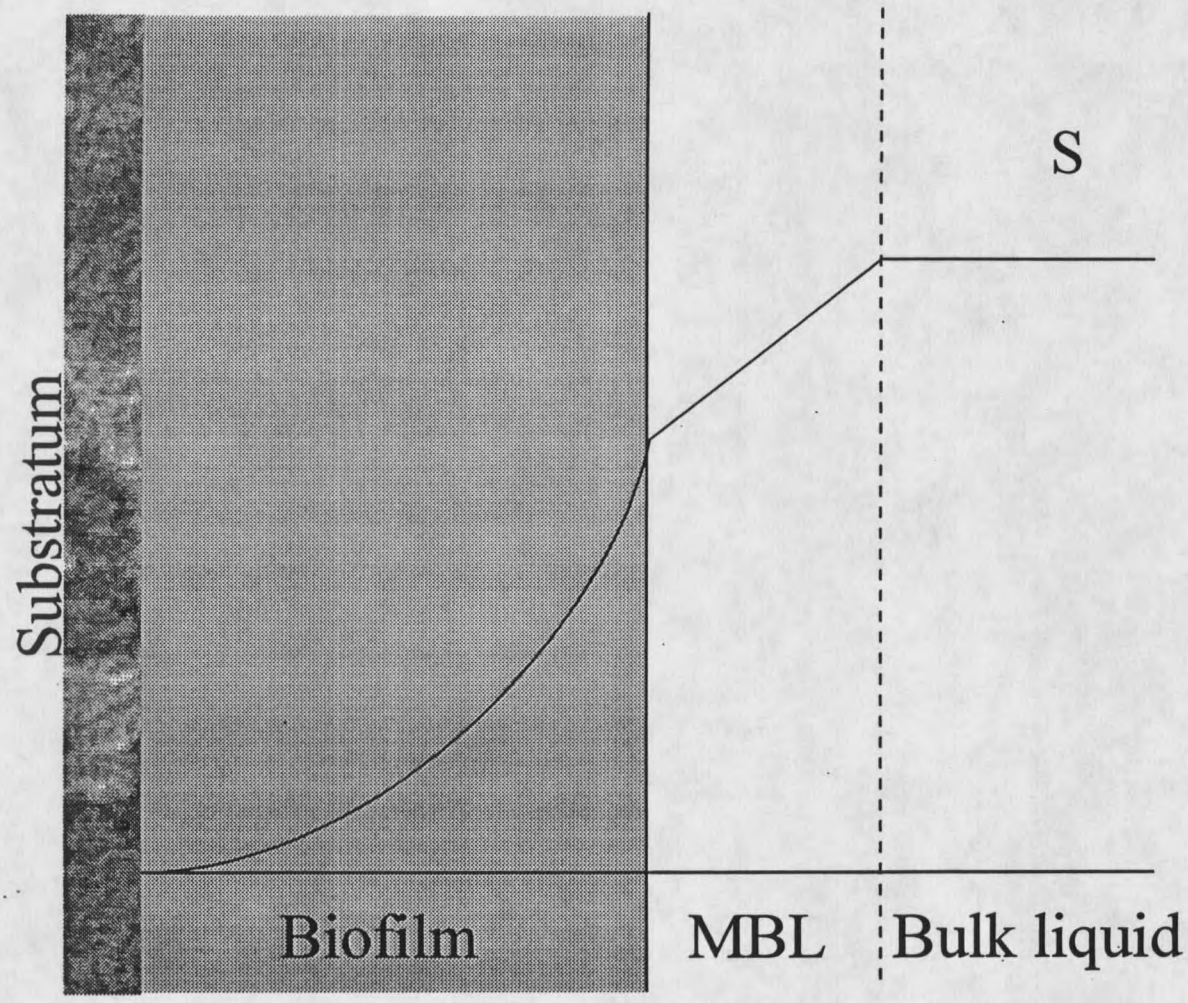

Figure 2. Substrate concentration profile, S, through bulk liquid, mass boundary layer, and biofilm based on concept of homogeneous biofilms. The substrate concentration is constant in the bulk solution. In the MBL the gradient is linear because transport is only due to molecular diffusion. The profile is curved in the biofilm due to substrate consumption.

biofilm influences the ways the kinetic data are extracted from substrate concentration profiles. Revsbech (1989 a) evaluated the kinetics of oxygen transport from the oxygen concentration profiles. Lewandowski (1994) used an oxygen profile to determine the diffusivity, maximum reaction rate, half-saturation coefficient, and oxygen flux. Kühl and Jørgensen (1992) calculated the rates of oxygen consumption, sulfide oxidation, and sulfite reduction from oxygen-, sulfide-, and pH profiles through a trickling filter biofilm. Denitrification rates were determined from nitrous oxide concentration profiles by Dalsgaard et al. (1995).

When transport is governed by molecular diffusion, the mass transfer coefficient, introduced in equation 1, is used to determine the flux, J, of a species caused by a concentration gradient:

$$J = k\Delta C \qquad (2)$$

Models using the film theory implicitly assume that the boundary layer is uniform and the overall mass transfer coefficient is constant. Thus, the mass transfer coefficient is just the ratio of the diffusion coefficient of the substrate in stagnant water to the thickness of the effective diffusive boundary layer.

The mass transfer coefficient is an important parameter for biofilm modeling. Following are some examples how the mass transfer coefficient has been applied in biofilm research. Logan and Dettmer (1989) examined the effect of fluid flow on leucine uptake by cells attached to a surface. Based on the leucine uptake rate, Q, cell radius, α, and the assumption that the leucine concentration at the cell surface was

negligible, they calculated the mass transfer coefficient for different flow velocities according to:

$$k = Q[4\pi\alpha^2(C_\infty - C_s)]^{-1} \quad (3)$$

The mass transfer coefficient was converted to a dimensionless parameter called the Sherwood number, Sh:

$$Sh = kL/D \quad (4)$$

The Sherwood number, Sh, also referred to as the mass transfer Nusselt number, Nu can be considered as the ratio of the molecular mass transport resistance to the convective mass transport resistance of the fluid. Based on the flow velocity, cell radius, kinematic viscosity, and the diffusivity of leucine Logan and Dettmer calculated the Reynolds number and the Peclet number for the velocities used in the experiment. By definition the Reynolds number is the ratio of the inertia force to the viscous force:

$$Re = Lvv^{-1} \quad (5)$$

The Peclet number relates the effectiveness of mass transport by advection to the effectiveness of mass transport by diffusion (Fetter, 1993):

$$Pe = vL/D \quad (6)$$

Knowing Re and Pe, Logan and Dettmer calculated the Sherwood number according to three different models:

1. Sherwood number for a sphere fixed in a flow stream;

$$Sh = (1 + 0.48Pe^{2/3})^{1/2} \quad (7)$$

2. Effect of sinking velocity on mass transport to phytoplankton;

$$Sh = 1 + 0.5Pe + 0.6Pe^2 \quad (8)$$

3. Effect of fluid velocity on phosphorous uptake by a diatom;

$$Sh = 1.45Re^{0.57} \quad (9)$$

The Sherwood numbers calculated using the models and the mass transfer coefficient were plotted versus flow velocity in the same diagram. For the experimental results in this study the model of the effect of fluid velocity on phosphorous uptake by a diatom appeared to give the best fit.

Gantzer et al. (1988 b) examined the sensitivity of substrate flux into streambed biofilms to short-term changes in flow velocity. They developed an equation describing mass transfer of substrate into biofilms growing in gravel and cobble streambeds:

$$k = [n_1 + n_3 Re^m Sc^{1/3} d^{-1}] D d_p^{-1} \quad (10)$$

In this equation the Schmidt number, Sc, occurs. This is the ratio of the molecular diffusivity of momentum to the molecular diffusivity of mass (Welty et al., 1976):

$$Sc = \nu D^{-1} \quad (12)$$

Biofilms were grown at an acclimation flow velocity until it reached steady state. Batch tests for COD removal were performed at flow velocities above and below the acclimation velocity. Gantzer et al. (1988 b) found that substrate flux into the cobble-streambed was more sensitive to short-term changes in water velocity than flux into gravel-streambed biofilms. The substrate removal rates of both biofilms were more sensitive to changes in flow velocity than predicted by previous models.

Gantzer et al. (1988 a) demonstrated that a mechanistic biofilm model was suited for predicting the removal rate of trace organics by natural biofilms. Biofilms were grown in pond and river water on Teflon strips. These were attached to the inner walls of a beaker stirred by paddles. The equation used to calculate the mass transfer coefficient was originally designed to determine the heat transfer coefficients for walls of a jacket lined reactor stirred by an anchor agitator:

$$k = 0.38Re^{2/3}Sc^{1/3}Dd^{-1} \quad (11)$$

Chang and Rittmann (1987 a&b) used column reactors filled with spherical activated carbon to verify a model of biofilm on activated carbon. The model incorporated film transfer, biodegradation, adsorption of substrate, and biofilm growth. The overall mass transfer coefficient was estimated by:

$$k = 2.40v_s(Re\epsilon^{-1})^{-0.66}(Sc)^{-0.58} \quad (13)$$

Christiansen et al. (1995) investigated the influence of liquid film diffusion on reaction rate in a submerged biofilter with denitrification and to compare with a theoretical study of the mass transfer coefficient. They used an equation for mass transfer in fixed beds:

$$k = DD_p^{-1}\{2+0.51[\xi(D_pU_0(e\nu)^{-1})^{\delta}]^{0.6}\}(\nu D^{-1})^{1/3} \quad (14)$$

The mass transfer coefficient was found for different flow velocities. They plotted the rate of nitrate removal versus nitrate concentration for the experimental data and from theoretical calculations applying the determined mass transfer coefficients and a mass transfer coefficient several orders of magnitude higher. The magnitude of k had no influence on the graphs, and it was concluded that the influence of liquid film

diffusion on reaction rate can be ignored for velocities in the range, $1.3 < v < 10.9$ m/h.

The major factor influencing the intensity of local mass transport and the shape of substrate concentration profiles in biofilms is hydrodynamics. Experiments demonstrated the true nature of hydrodynamics near biofilms. Lewandowski et al. (1993) showed, using Nuclear Magnetic Resonance Imaging (NMRI), that water was moving in the space occupied by the biofilm. This study was followed by quantification of the intrabiofilm flow using a combination of particle tracking and SCLM. De Beer et al. (1994 b) and Stoodley et al. (1994) determined the flow velocity profiles in voids and channels. The water flow in biofilms occurs in two flow fields, one inside the biofilm and one outside. The external and internal flow fields influence each other in a complex way (Lewandowski et al., 1995). Consequently, recent experiments suggest the possibility that in the biofilms neither the film nor the boundary layer theory are directly applicable. Also these results indicate that the mass transport in biofilms is affected by convection to a much larger extent than previously suspected.

Mass transfer by convection involves the transport of material between a boundary surface and a moving fluid (Welty et al., 1976). Similar to the mass transfer coefficient for diffusive mass transport (equation 2), the convective mass transfer coefficient, k_c, is defined by:

$$J = k_c \Delta C \qquad (15)$$

When determining k_c, one have to consider the properties of the fluid, the dynamic characteristics of the flowing fluid and the geometry of the system. Use of dimensionless parameters makes it easier to determine the mass transfer coefficient. Welty et al. (1976) discussed four methods of evaluating the convective mass transfer coefficient. These are; (1) dimensional analysis; (2) exact boundary-layer analysis; (3) approximate boundary-layer analysis; and (4) analogy between momentum, energy, and mass transfer.

Dimensional analysis can be used to predict which dimensionless parameters are helpful in correlating experimental data. Welty et al. (1976) used the Buckingham method. All significant variables and their dimensions for the system are listed. The variables and dimensions are then tabulated in a matrix where the numbers represent the exponent of the corresponding dimension and variable. The number obtained by subtracting the number of rows, in the largest nonzero determinant which can be formed from the matrix, from the number of variables involved, indicates how many independent dimensionless groups can be formed. A core group of variables, which will appear in each dimensionless group and contain all of the fundamental dimensions, is then selected. Each of the remaining variables are combined with the core group. These groups are made dimensionless by changing the exponents of the variables in the core group. By using this method Welty et al. (1976) showed that Nu for transfer into a stream flowing under forced convection is a function of Re and Sc.

For laminar flow parallel to a flat surface, Blasius (1908) developed an exact solution for the hydrodynamic boundary layer. Welty et al. (1976) extended this

solution to include convective mass transfer. They assumed low mass transfer rates between the flat plate and the boundary layer, and a Schmidt number of one. The following expression for the mass transfer Nusselt number was found:

$$Nu = 0.332Re^{1/2} \tag{16}$$

To make the equation applicable for situations where the Schmidt number is not equal to unity, the relation between the concentration boundary layer thickness, δ_c, and the hydrodynamic boundary layer thickness, δ, was used:

$$\delta/\delta_c = Sc^{1/3} \tag{17}$$

As predicted by the dimensional analysis the mass transfer Nusselt number was determined as a function of Re and Sc:

$$Nu = 0.332Re^{1/2}Sc^{1/3} \tag{18}$$

Few exact solutions exist for transport in the boundary layer when the flow is not laminar, and the configuration is other than a flat plate. If no exact solution exists one has to assume the concentration and velocity profiles. To obtain an approximate solution the von Kármán integral equation can be used:

$$d/dx\int(C - C_\infty)v_x dy = k_c(C_s - C_\infty) \tag{19}$$

In this thesis it has been described how microelectrodes can be used to measure concentration profiles, and study the nature of mass transfer near and within biofilms.

The equations for momentum, energy, and mass transfer are similar. Several analogies among transfer phenomena have been proposed because of the similarity in their mechanisms. These analogies are useful in predicting behavior of systems for which limiting quantitative data are available. Reynolds (1874) postulated that the

mechanisms for transfer of momentum and energy were identical. This has been found to be true when the Prandtl number, Pr, is unity (Welty et al., 1976). The Prandtl number is the ratio of the molecular diffusivity of momentum to the molecular diffusivity of heat:

$$Pr = \mu c_p/k \tag{20}$$

Chilton and Colburn (1934) found an analogy beween convective heat and mass transfer. They found that the dimensionless j factor for mass transfer, j_D, is equal to the j factor for heat transfer, j_H:

$$j_D = k_c/v_\infty(Sc)^{2/3} = j_H = StPr^{2/3} \tag{21}$$

where St is the Stanton number which is the Nusselt number divided by the product of the Reynolds number and the Prandtl number. Equation 21 is valid for gases and liquids within the ranges, $0.6 < Sc < 2500$ and $0.6 < Pr < 100$.

Convective mass transport in biofilm systems is difficult to quantify. Addressing this problem, Yang and Lewandowski (1995) developed a microtechnique to evaluate the local mass transport coefficient in biofilms by measuring the limiting current drawn from a mobile microelectrode. The limiting current technique is often used to determine mass transfer rates to surfaces (Hanratty, 1991, Juhasz and Deen, 1993, Dawson and Trass, 1972). Electroactive species are consumed at the polarized electrode surface. In the experiment of Yang and Lewandowski a ferricyanide solution was used as electrolyte. Ferricyanide was not consumed by the biofilm, and the only sink for those species was the tip of the microelectrode. All physical elements of the system, like the reactor's walls and the biofilm, obstruct mass

transport to the tip of the electrode. The extent of this obstruction is measured on a relative scale. The potential applied to the microelectrode is high enough to assure that the concentration of electroactive species at the electrode surface is zero. Under such conditions the rate of consumption of the electroactive species at the electrode surface is limited only by mass transport, and the measured limiting current is directly proportional to the mass transfer rate. By positioning the tip of the electrode at different locations in biofilms, the local mass transport coefficient to the electrode can be determined. The concept of the local mass transport coefficient is similar to the concept of the overall mass transfer coefficient. Local mass transfer coefficient describes the ratio of the flux of electroactive species to the tip of the microelectrode to the concentration difference at a specific location. It should not be, however, identified with the overall mass transport coefficient. The local mass transport coefficient describes only the mass transfer resistance in the immediate vicinity of the electrode tip, and thus reflects the relationship between local hydrodynamics, local effective diffusivity, and local biofilm structure. Conversely, the overall mass transport coefficient reflects mass transport rate to the biofilm surface through the entire mass boundary layer. Yang and Lewandowski (1995) report that the local mass transfer coefficient varied both horizontally and vertically in biofilms.

It is clear that the mass transport dynamics in biofilms is much more complex than previously assumed; 1) the biofilms are heterogenous and consist of discrete cell clusters separated by interstitial voids, 2) the hydrodynamics in biofilms is controlled by two flow fields, and 3) the mass transfer coefficient in biofilms behaves

unexpectedly. Although the newly proposed concept of biofilm structure helps to interpret the experimental observations, the new experiments reveal further dimensions of complexity. Researchers are becoming progressively aware that it may not be possible to completely describe mass transport in biofilms mathematically. Some simplifying assumptions are, therefore, urgently needed to establish empirical equations serving purely practical purposes. It is important that these assumptions are established as a result of experimentation rather than computational convenience.

To study the nature of mass transport near and within biofilms the measurements of the local mass transfer coefficients were combined with the measurement of local dissolved oxygen concentrations. A bacterial biofilm composed of aerobic microorganisms was grown in an open channel flow reactor. Profiles of dissolved oxygen and local mass transfer coefficient were measured through the cell clusters and through the interstitial voids for different flow velocities. Superimposing those two profiles permits evaluating the effect of biofilm architecture on the rate of transport related to hydrodynamics. The goal of this work was to get a better understanding of mass transport in biofilms, and thereby be able to make some simplifying assumptions about this process.

MATERIALS AND METHODS

Construction of dissolved oxygen microelectrode

The dissolved oxygen microelectrode was constructed as described by Revsbech (1989 b). As shown in figure 3 the electrode had five components: (1) a platinum cathode; (2) a silver/silver chloride reference electrode; (3) a silver guard cathode; (4) an outer casing; and (5) a potassium chloride electrolyte solution.

The platinum cathode was made from a 0.004 inch (pure TC grade) platinum wire (California Wire Company, Grover Beach, CA). One end was electrochemically etched (7 volts AC) in a saturated KCN solution to a diameter of 5-10 μm, and then rinsed in distilled water. The wire was inserted into a glass capillary of Schott 8533 glass (Schott Glaswerke, F.R.G.). The capillary was obtained by heating a glass tube over a propane torch and pulling on the ends by hand. Heat was then applied where the glass tube started to taper, and a second pull was performed. This resulted in a glass bulb with two capillaries on opposite ends. The capillaries were separated using a file. Soda-lime glass was used as shaft. A glass tube (15 cm in length) was pulled once over a propane torch, and the capillary was broken off. The tapered end of the shaft was then inserted into the 8533 capillary containing the platinum wire, and the two were fused in a flame. The glass capillary was positioned in a Micro Electrode Puller (Stoelting Co., Wooddale, IL) with the etched tip of the platinum wire 1.5-2.0

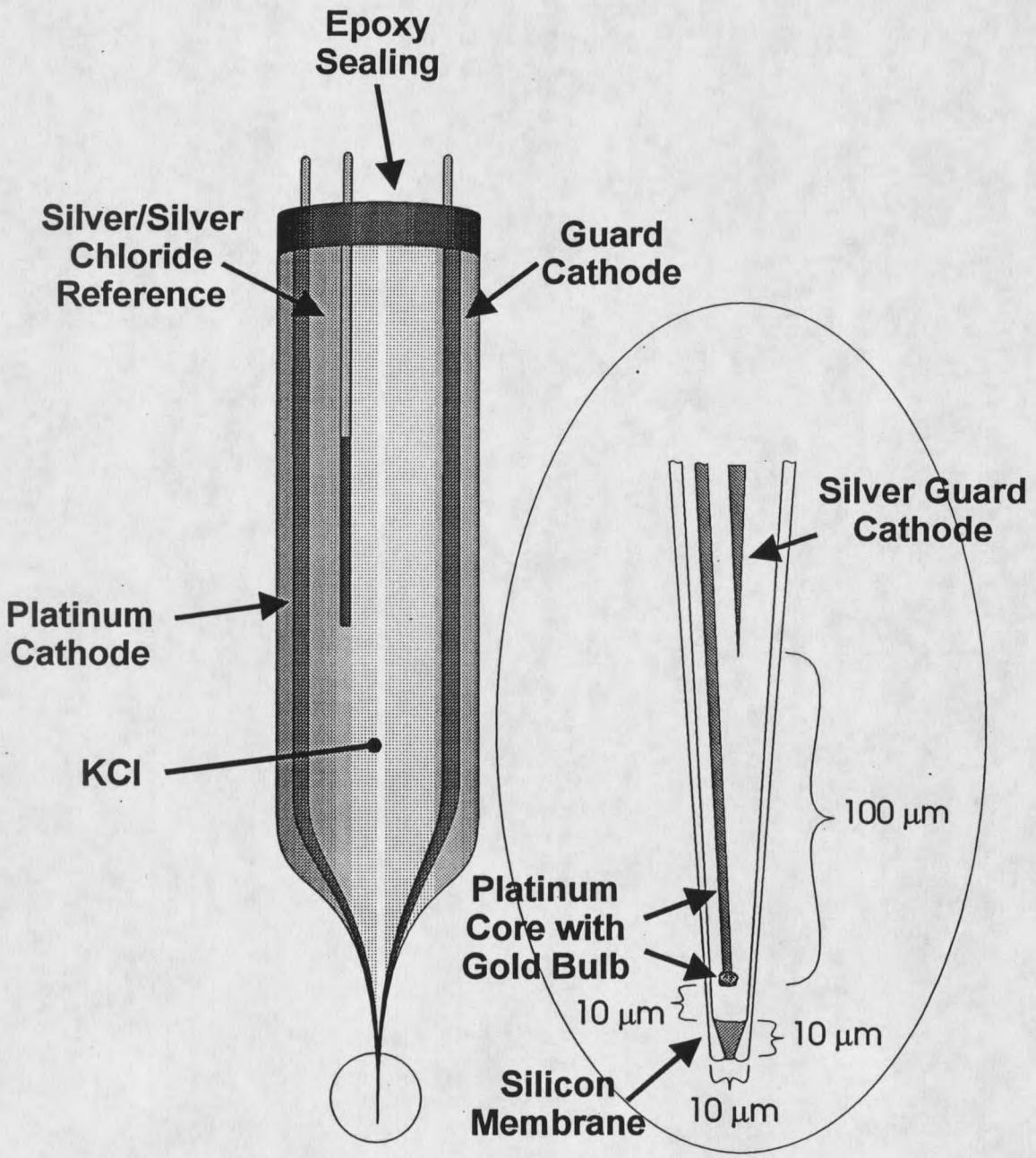

Figure 3. Construction of a dissolved oxygen microelectrode.

cm higher than the Ni-Cr heating coil. Heat was gradually increased until the glass collapsed around the wire and the electrode dropped down. Under a microscope the glass was recessed 5-10 μm by moving a platinum heating loop close to the electrode tip. The exposed platinum was then electroplated with gold by inserting the tip into a $HAuCl_4$ solution and applying a potential of 2.0 volts for 2-3 seconds.

A 0.5 mm diameter, 99.99% pure silver wire was used for the silver/silver chloride reference electrode. The tip of a 3 cm long wire was polished with fine grained sandpaper followed by cleaning in nitric acid and rinsing in distilled water. One centimeter of the wire was then submerged in a 0.1M HCl solution, and a current density of 0.4 mA/cm^2 was applied for 1-2 hours until the wire was uniformly covered with AgCl. It was then rinsed with distilled water.

A 0.004 inch diameter, 99.99% pure silver wire (California Fine Wire Company, Grover Beach, CA) was used for the guard cathode. A 10 cm long wire was inserted into a thin glass capillary obtained by pulling a soda-lime glass tube over a propane torch. Approximately 1.5 cm of the wire was sticking out of the capillary in both ends. The wire was fixed to the glass by dipping one end of the capillary in epoxy. One end was then electrochemically etched (3.5 volts AC) in a saturated KCN solution followed by rinsing with distilled water.

The outer casing was made from $5^3/_4$ inch Pasteur Pipets (Fisher Scientific, Pittsburgh, PA). Heat was applied to the narrow end by a propane torch, and the glass was pulled by hand. The second pull was done by gravity, and a thin capillary was obtained by slowly moving a platinum heating loop towards the glass. The

desired tip diameter was obtained by pushing the tip against a solid glass rod under a microscope. The tip opening was then shrunk to 2-3 μm by moving a platinum heating loop close to the tip. It was then filled with uncured silicone, by capillary suction, to a depth of 10-15 μm.

The platinum cathode was fixed to the outer casing with epoxy, and the distance between the gold tip and the silicon membrane was 10 μm. When the epoxy was dry, the reference- and the guard cathode were fixed to the outer casing with epoxy. The distance between the tip of the platinum cathode and the tip of the guard cathode was 100 μm. The outer casing was filled with electrolyte containing K_2CO_3 (0.3 M), $KHCO_3$ (0.2 M), and KCl (1.0 M). Epoxy was then used to seal the top.

Calibration of dissolved oxygen microelectrode

When a potential of -0.8 volts is applied between the platinum cathode and the silver/silver chloride reference electrode, oxygen is reduced on the gold-tip of the cathode. This creates a current which is proportional to the oxygen concentration in the solution surrounding the tip of the probe. Since the calibration curve is linear, only two points are required; the currents associated with zero and saturated oxygen concentration. A picoammeter / DC voltage source (Hewlet Packard 4140B) was used to apply a potential of -0.8 volts between the platinum cathode and the Ag/AgCl reference electrode, and between the guard cathode and the reference. Some of the nutrient solution used in the experiments was transferred to a 300 ml beaker. The tip of the microelectrode was then submerged in the solution. Air from a compressed air

tank was supplied to obtain a saturated oxygen concentration. When the current stabilized, the current reading was associated with the saturated oxygen concentration. Next, nitrogen gas was supplied to the solution to remove all the dissolved oxygen. When the current stabilized, the current reading was associated with the zero oxygen concentration. An example of a calibration curve is shown in figure 4.

Construction of local mass transfer coefficient microelectrode

The microelectrode used for local mass transfer coefficient measurements was constructed according to Yang and Lewandowski (1995). Figure 5 shows the construction of the electrode. It was made from a 0.004 inch (pure TC grade) platinum wire (California Wire Company, Grover Beach, CA). One end was electrochemically etched (7 volts AC) in a saturated KCN solution to a diameter of 5-10 μm, and then rinsed in distilled water. The wire was inserted into a glass capillary of Schott 8533 glass (Schott Glaswerke, F.R.G.). The capillary was obtained by heating a glass tube over a propane torch and pulling on the ends by hand. Heat was then applied where the glass tube started to taper, and a second pull was performed. This resulted in a glass bulb with two capillaries on opposite ends. The capillaries were separated using a file. Soda-lime glass was used for shaft. A glass tube (15 cm in length) was pulled once over a propane torch, and the capillary was broken off. The tapered end of the shaft was then inserted into the 8533 capillary containing the platinum wire, and the two were fused in a flame. The glass capillary was positioned

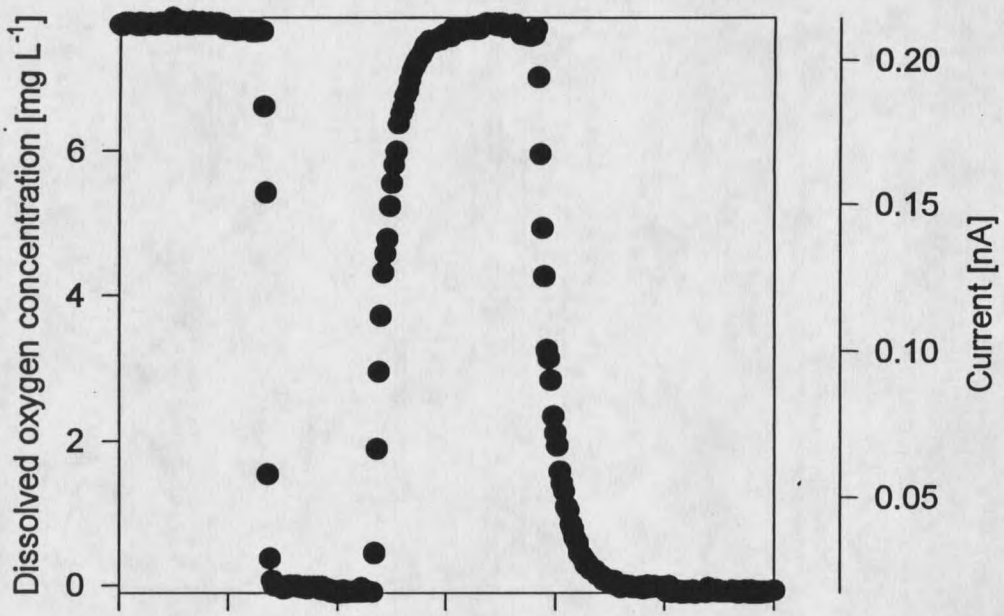

Figure 4. Calibration curve for a dissolved oxygen microelectrode. The secondary Y-axis indicates the current associated with the oxygen concentration on the primary Y-axis.

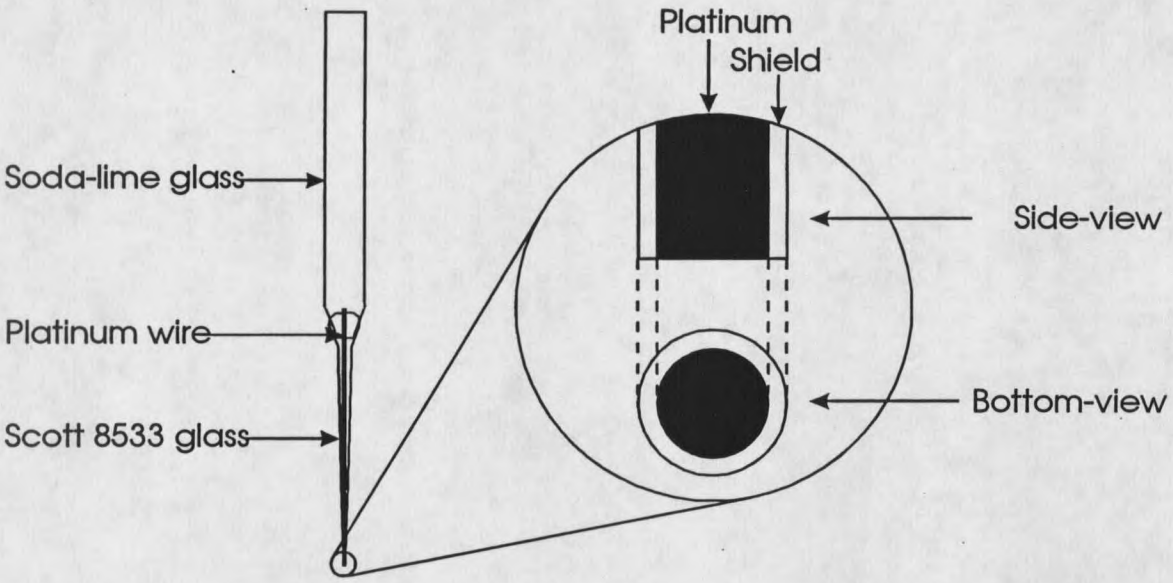

Figure 5. Construction of a local mass transfer coefficient microelectrode.

in a Micro Electrode Puller (Stoelting Co., Wooddale, IL) with the tip of the wire 1.5-2.0 cm higher than the Ni-Cr heating coil. Heat was gradually increased until the glass collapsed around the wire and the electrode dropped down. The tip of the wire was then exposed by grinding on a rotating grinding wheel (Model EG-4, Narishige Co., Tokyo, Japan), followed by cleaning in a sonication bath with deionized water and then acetone. To calculate the surface area, the tip radius was measured microscopically. Each electrode was tested in the electrolyte solution before it was used. The electrolyte solution consisted of 25 mM $K_3Fe(CN)_6$ and 0.5 M KCl as supporting electrolyte. To test the electrode the potential between the microelectrode and the reference was scanned from 0 to -1.2 volts. From the voltammogram the potential range in which the limiting current occurred was determined. A range between -0.6 and -0.9 volts was accepted.

Testing the local mass transfer coefficient microelectrode

Effect of changing the position of reactive surface relative to flow direction

The local mass transfer coefficient is influenced by the local hydrodynamics around the tip of the microelectrode. From equation 1 it is clear that by changing the boundary layer thickness the local mass transfer coefficient will change if the diffusivity is constant. When the tip of the microelectrode faces towards the flow, the boundary layer will be compressed compared to thickness when the tip is positioned perpendicular to the flow. Likewise, the boundary layer thickness will increase by

moving the electrode from the vertical position to one where the tip faces away from the flow. The effect of changing the position of the electrode tip, relative to the flow direction, on the local mass transfer coefficient measurements was tested. Ferricyanide electrolyte solution was added to a 1 L beaker. The solution was stirred by a magnet stirrer at a constant rotational speed throughout the experiment. A standard calomel electrode (Model 13-620-51, Fisher Scientific, Pittsburgh, PA) was positioned in the center of the beaker to minimize any influence of the electrode on the hydrodynamics. The local mass transfer coefficient microelectrode was polarized at -0.8 volts against the reference electrode by a Picoammeter / DC Voltage Source (Hewlett Packard 4140B). A data acquisition system (Model CIO-DAS08PGL, Computer Boards, Inc., Mansfield, MA) collected the current signal. The microelectrode tip was positioned in three different ways; (1) facing away from the flow; (2) facing the bottom of the beaker; and (3) facing towards the flow. Results are shown in figure 6. From this figure it can be found that the local mass transfer coefficient decreased by 30% when the electrode was moved from the vertical position to one where the tip faced away from the flow. When the tip faced towards the flow, the local mass transfer coefficient was 30% higher than when the electrode was in the vertical position. These measurements were measured at the same location of the beaker which means that the diffusivity was constant. Moreover, the only parameter that changed the local mass transfer coefficient was the boundary layer thickness. This experiment shows the importance of being consistent with the positioning of the electrode tip relative to the flow direction.

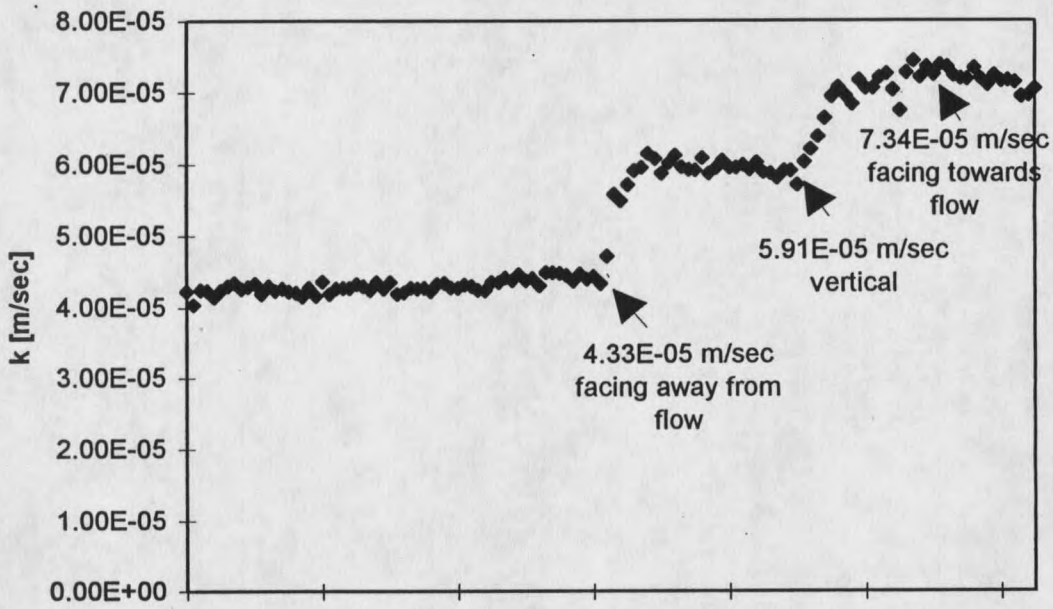

Figure 6. Effect of changing the position of the local mass transfer coefficient microelectrode tip relative to the flow direction.

Respiratory activity in a biofilm submerged by electrolyte solution

Yang and Lewandowski (1995) report that the number of viable cells remained relatively constant the first four hours after the biofilm was exposed to the electrolyte solution. This does not mean that the bacteria respired under these conditions. The high potassium chloride concentration (0.5 M) is very likely to injure the cells. When these viable cells are transferred to a rich medium, normal cell activity can resume. To examine if respiration occurred when the biofilm was submerged in the electrolyte solution, oxygen profiles were measured through it. Before this experiment was performed the dissolved oxygen microelectrode was calibrated in both water and the electrolyte solution. This was done to see if ferricyanide or potassium chloride influenced the oxygen measurement. The calibration procedure is described under Calibration of dissolved oxygen microelectrode. Figure 7 shows the calibration curves for oxygen in water and the ferricyanide electrolyte solution. The calibrations were done separately, but the curves are in the same figure for comparison. Both curves start out with a saturated oxygen concentration between 7.5 and 8.0 mg L^{-1}. At the point where the curves suddenly drop, nitrogen gas was added to remove the dissolved oxygen from the solutions. Both curves reached the same level when oxygen was depleted. The sudden increase in the oxygen concentrations indicates that compressed air was added to the solutions. Both curves reached the same level for oxygen saturation as before nitrogen gas was added. When nitrogen gas was supplied again, the slope of the calibration curve for oxygen in water decreased. This happened

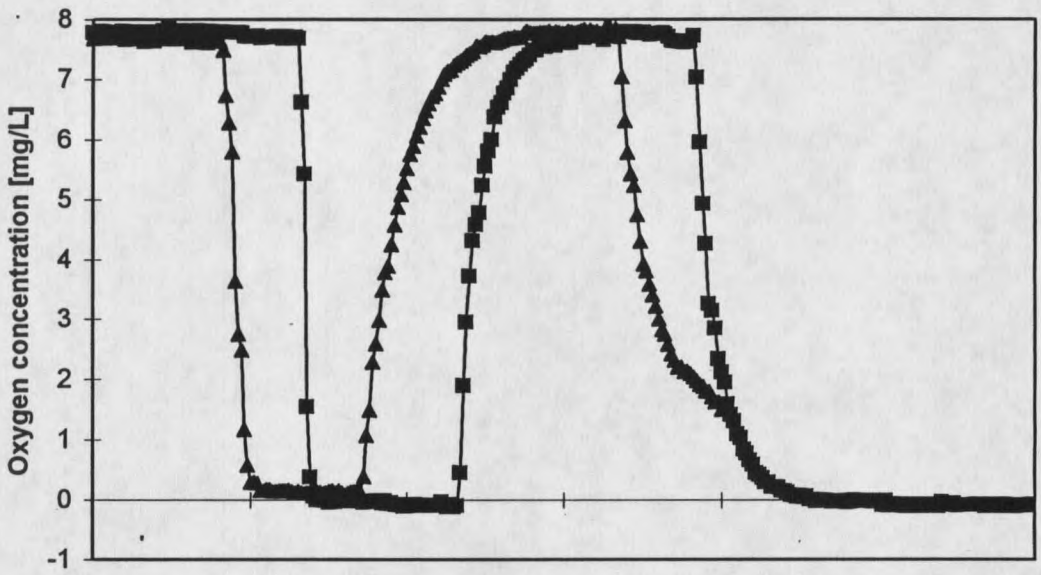

Figure 7. Calibration of the dissolved oxygen microelectrode in water (▲) and ferricyanide electrolyte solution (■).

simply because the supply of nitrogen was terminated right before the end of the calibration. These calibration curves show that the signal for zero and saturated oxygen concentration were the same in water and electrolyte. Hence, ferricyanide and potassium chloride did not affect the oxygen measurement by the electrode. Figure 8 shows an oxygen profile through a biofilm five hours after the electrolyte solution was added. The biofilm thickness was approximately 200 μm, and the oxygen concentration was close to 4 mg L^{-1} throughout the biofilm. The curve is nearly horizontal inside the biofilm indicating no oxygen flux. This means that oxygen was not consumed within the biofilm.

Influence of oxygen on local mass transfer coefficient measurements

Local mass transfer coefficient microelectrodes were only used if the limiting current occurred at a potential in the range -0.6 - -0.9 volts against a standard calomel electrode. During the experiments the electrode was polarized at -0.8 volts against a standard calomel electrode. The limiting current of oxygen occurs at a potential of -0.8 volts against a silver/silver chloride reference electrode. The standard calomel electrode and the silver/silver chloride reference electrode have similar reduction potentials; 0.241 and 0.222, respectively (Lide, 1994), which means that the potentials at the tip of the local mass transfer microelectrode and the oxygen sensor are similar. Moreover, oxygen may be reduced by the local mass transfer coefficient electrode. However, the concentration of ferricyanide (25 mM) in the electrolyte

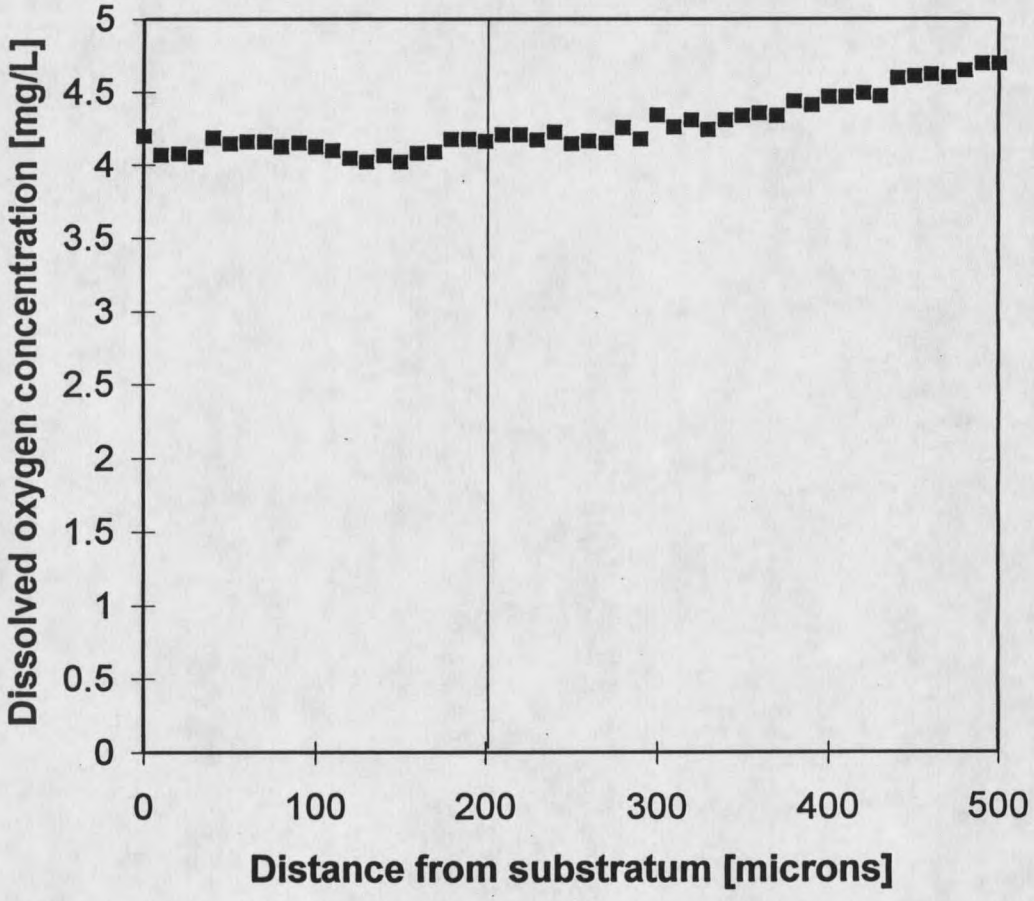

Figure 8. Dissolved oxygen measured through a biofilm submerged by ferricyanide electrolyte solution. The solid line parallel to the Y-axis indicates the biofilm thickness.

solution was approximately a hundred times higher than the saturated oxygen concentration in water (0.25 mM). Consequently, the influence of oxygen should be negligible. To confirm this hypothesis the influence of oxygen present in the electrolyte solution was examined. The tip of the local mass transfer coefficient microelectrode was submerged in electrolyte contained in a beaker. It was polarized at -0.8 volts against a standard calomel electrode (Model 13-620-51, Fisher Scientific, Pittsburgh, PA) by a picoammeter / DC voltage source (Hewlet Packard 4140B). The current was recorded by a data acquisition system (Model CIO-DAS08PGL, Computer Boards, Inc., Mansfield, MA). When the current reading had stabilized the solution was aerated for one minute with compressed air through a diffuser. The current stabilized again, and the oxygen was removed by adding nitrogen gas to the solution. Figure 9 shows the result from this test. Addition of air caused a sudden increase in the limiting current from 4.0E-8 A to 8.9E-8 A. Following termination of the air supply, the current stabilized at its original level. When nitrogen gas was added to remove the dissolved oxygen, the limiting current increased to 7.4E-8 A. After the gas flow was terminated, the current stabilized around 4.0E-8 A. From these results it can be concluded that the limiting current is the same in the presence and absence of oxygen.

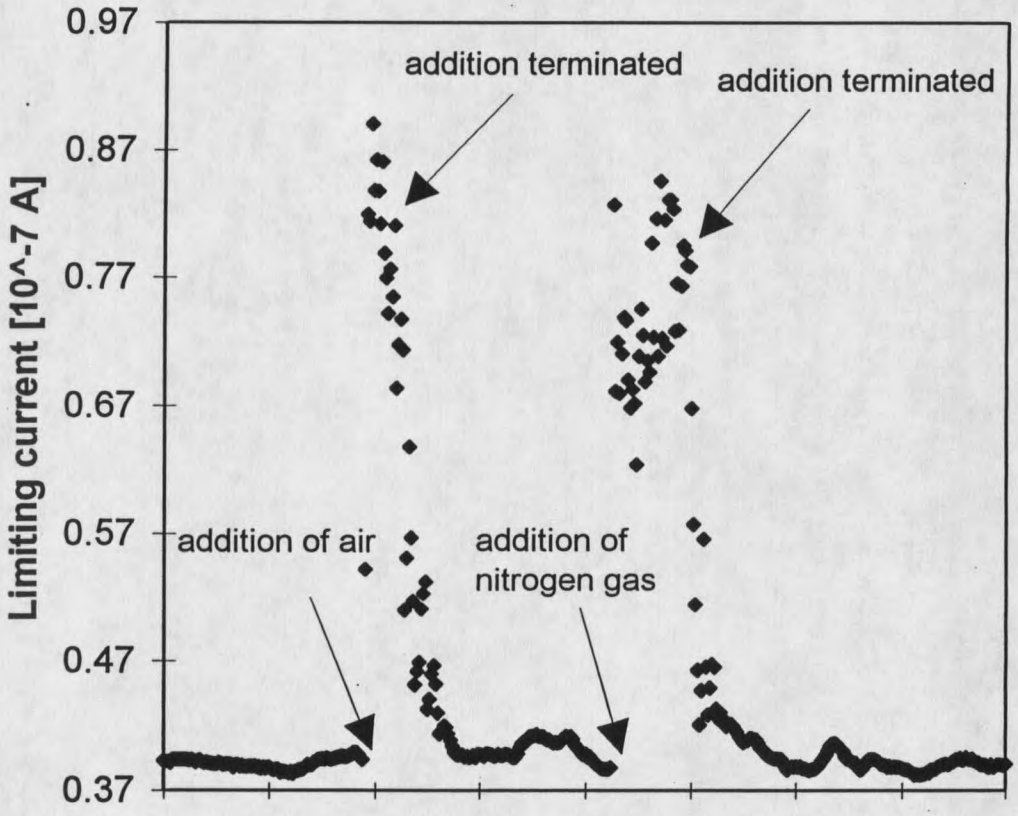

Figure 9. Influence of dissolved oxygen on the local mass transfer coefficient measurements.

Dissolved oxygen and local mass transfer coefficient profiles at the same locations of a biofilm

Experimental setup

The experimental setup is shown in figure 10. The biofilm was grown in an open channel reactor 40 mm wide and 500 mm long, made of polycarbonate. Measurements were conducted at flow velocities of 0.62, 1.53, and 2.60 cm sec^{-1}, corresponding to Reynolds numbers of 100, 300, and 600, respectively. A micromanipulator (Model M3301L, World Precision Instruments, New Haven, CT) was used to move the microelectrodes. It was equipped with a stepper motor (Model 18503, Oriel, Stratford, CT) and manipulated by a computer controller (Model 20010, Oriel, Stratford, CT). The electrodes were moved from the bulk down through the biofilm with 10 μm increments. A Picoammeter / DC voltage source (Hewlet Packard 4140B) was used to polarize the electrodes. The measured signal was directed to a computer containing a data acquisition system (Model CIO-DAS08PGL, Computer Boards, Inc., Mansfield, MA). Dissolved oxygen profiles were measured first. After the measurement the nutrient solution was replaced by the solution of electroactive species. Local mass transfer coefficient profiles were then collected in the same locations as the prior dissolved oxygen profiles. The reactor was fixed to an X-Y micropositioner stage (Model CTC-462-2S, MicroKinetics, Laguna Hills, CA). The stage was computer controlled through a controller (Model CTC-283-3, MicroKinetics, Laguna Hills, CA) with a positioning precision of 0.1 μm. A

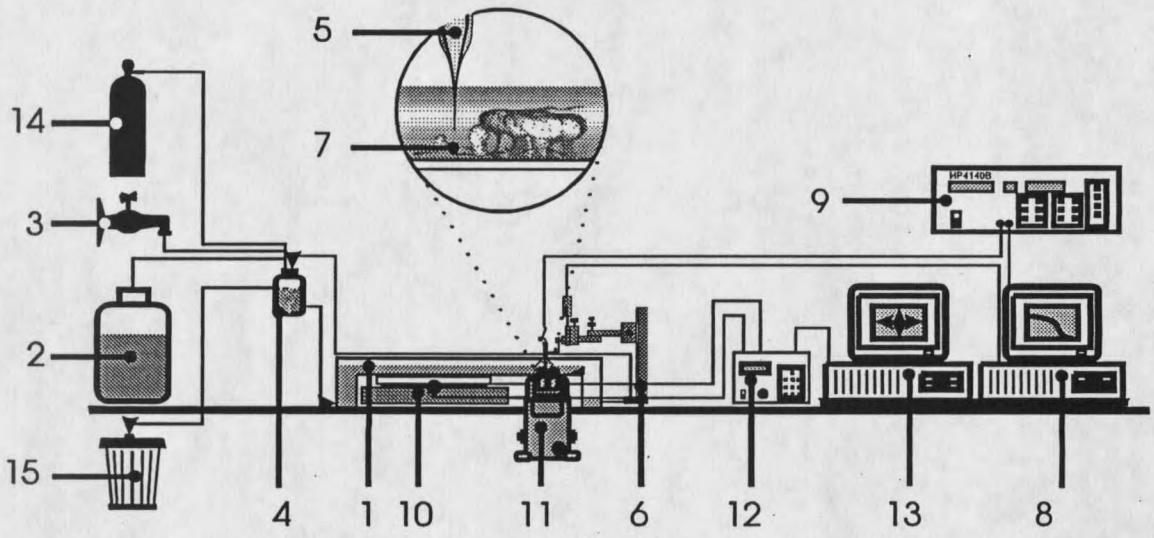

Figure 10. Experimental setup: 1. Open channel flow reactor; 2. Concentrated nutrient solution; 3. Tap water; 4. Mixing chamber; 5. Microelectrode; 6. Micromanipulator; 7. Biofilm; 8. Data acquisition system; 9.Pico-ammeter / DC-voltage source; 10. X-Y micropositioner stage; 11. Inverted microscope; 12. Controller; 13. Computer for stage movement; 14. Air tank; 15 Waste stream.

computer equipped with a custom made software was used to control the stage movement.

Biofilm growth

A concentrated nutrient solution and filtered tap water (PAC-filter, Model CBC-10, Cole-Parmer Instr. Co., Chicago, IL) was aerated in a mixing chamber before it was recycled through the reactor by a peristaltic pump (Cole-Parmer Instr. Co., Chicago, IL). The influent nutrient solution from the mixing chamber consisted of KH_2PO_4 (0.69 mM), K_2HPO_4 (1.5 mM), $(NH_4)_2SO_4$ (0.079 mM), $MgSO_4*7H_2O$ (0.013 mM), and yeast extract (0.031 g L^{-1}). The total reactor volume was 420 ml, and the hydraulic retention time was only 4 min and 30 sec to avoid suspended growth. 1-ml portions of stock cultures of: *Pseudomonas aeruginosa* ($7.7x10^9$ CFU/ml), *Pseudomonas fluorescens* ($4.8x10^{10}$ CFU/ml), and *Klebsiella pneumoniae* ($7.2x10^{10}$ CFU/ml) were used to inoculate the reactor. After inoculation the reactor was operated in a batch mode for 24 hours, followed by continuous flow mode for five days. During the period of continuous flow the reactor was tilted to obtain a shallow water depth, and hence, a high volumetric flow velocity set to 17 cm sec^{-1} (Reynolds number 1000). The high flow velocity during the growth phase was used to obtain strongly attached biofilms of high density (Van Loosdrecht et al., 1995, Christensen and Characklis, 1990). This was necessary to avoid detachment/change of structure during the experiments since different microelectrodes, flow velocities, and solutions were used.

Data acquisition system

The data acquisition system collected current data from the Picoammeter / DC Voltage Source. On the computer's monitor, the vertical profile of oxygen or local mass transfer coefficient was displayed in real time. At each step, 22 current readings were collected at a frequency of 1 KHz. The highest and lowest were rejected and a standard deviation was calculated for the remaining 20. If the deviation was higher than 5% the measurement was repeated, and if it was lower the electrode was moved to the next vertical position for a new measurement.

Measurement of local mass transfer coefficient profiles in sterile reactor

Instruments used in this experiment were the same as those described under "experimental setup". The ferricyanide solution was recycled through the reactor by a peristaltic pump. The local mass transfer coefficient microelectrode was attached to the micromanipulator and positioned 450 mm downstream from the reactor inlet. A standard calomel electrode (Model 13-620-51, Fisher Scientific, Pittsburgh, PA) was positioned close to the inlet, and a potential of -0.8 volts was applied between the two electrodes by the picoammeter / DC voltage source. Profiles of the local mass transfer coefficient were collected at the same location for three different flow velocities; 0.62, 1.53, and 2.60 cm sec^{-1}. The current signal was directed to the data acquisition system.

Local mass transfer coefficient- and oxygen profiles at same locations

Before the measurement a reference point was selected on the substratum using an inverted microscope (11) (Model CK-2, Olympus, Japan), and the DO-probe was positioned right above this point with a precision of 10 μm. The movement of the reactor relative to the reference point in X and Y directions was then recorded. At each location DO-profiles were collected at different volumetric flow velocities. The inverted microscope was also used to locate the tip of the microelectrode and to observe when the electrode reached the substratum. Before the local mass transfer coefficient measurements were performed, the reactor was drained, and the electrolyte solution was added. It was recycled through the reactor for 30 min to obtain a constant ferricyanide concentration throughout the biofilm (Yang and Lewandowski, 1995). The reference point was again found under the microscope, and the local mass transfer coefficient-electrode was positioned right above it with a precision of 10 μm. The reactor was then moved by the X-Y stage to the same locations that the DO profiles were collected, and local mass transfer coefficient profiles were measured for the same flow velocities.

Theoretical calculations

Calculation of the local mass transfer coefficient

Local mass transfer coefficient profiles were collected at different locations to study the nature of mass transport near and within the biofilm. Use of the local mass

transfer coefficient microelectrode in biofilms was described by Yang and Lewandowski (1995). A ferricyanide solution was used as electrolyte. Ferricyanide diffused to the tip of the microelectrode and was reduced to ferrocyanide according to the following reaction:

$$Fe(CN)_6^{3-} + e^- \rightarrow Fe(CN)_6^{4-} \quad (22)$$

The flux, J, of an ion to the tip of the electrode is related to the mass transfer coefficient, k:

$$J = k(C_\infty - C_s) \quad (23)$$

The surface reaction causes a current, I, which is also related to the flux:

$$I = JnAF \quad (24)$$

The limiting current technique is applied to create diffusion limiting conditions. Hence, the surface concentration is equal to zero. By combining equations 23 and 24 the following equation can be used to calculate the mass transfer coefficient:

$$k = I/(nAFC_b) \quad (25)$$

It is common to normalize the limiting current when comparing mass transfer rates (Macpherson et al., 1994, Gao et al., 1995). When compared to oxygen profiles, the limiting current is presented in a normalized form, obtained by dividing each data point by the highest current measured in each experiment.

Calculation of the effective diffusive boundary layer thickness

Oxygen profiles were measured at the same locations as the local mass transfer coefficient profiles. From the oxygen profiles the effective diffusive boundary layer

thickness (Revsbech and Jørgensen, 1986) was calculated to determine if convective mass transport occurred within the MBL. A method described by Lewandowski (1994) was applied to calculate the effective diffusive boundary layer thicknesses. It was found that the oxygen concentration above a biofilm can be described by the following empirical equation:

$$(C-C_S)/(C_\infty-C_S) = 1 - \exp(-Bx) \quad (26)$$

The first derivative of the local oxygen concentration, C, at the biofilm surface (x = 0) is:

$$(dC/dx)_{x=0} = B(C_\infty - C_S) \quad (27)$$

The flux, J of oxygen through the biofilm surface can be written as:

$$J = D(dC/dx)_{x=0} = k(C_\infty - C_S) = (D/L_D)(C_\infty - C_S) \quad (28)$$

From the last two equations it can be seen that B equals L^{-1}. Hence, B has to be determined to find the boundary layer thickness. The empirical equation can be written in a linearized form:

$$\ln[1-(C-C_S)/(C_\infty-C_S)] = -Bx \quad (29)$$

Then B can be found as the slope when plotting $\ln[1-(C-C_S)/(C_\infty-C_S)]$ versus x. The effective diffusive boundary layer is equal to the film described by the film theory. This is a fictitious liquid layer which contains the same amount of resistance to mass transfer as exists in the entire flowing fluid. Graphically the film thickness can be found as the distance from the biofilm liquid interface to the point where the tangent of the profile at the biofilm surface crosses the extended line through the bulk concentration.

RESULTS

Local mass transfer coefficient profiles in a sterile reactor

Figure 11 shows the local mass transfer coefficient profiles collected in a sterile reactor. The magnitude of the coefficient in the bulk liquid was approximately 3.4E-4 m sec^{-1}, 3.2E-4 m sec^{-1}, and 3.0E-4 m sec^{-1} at the flow velocities of 2.60 cm sec^{-1}, 1.53 cm sec^{-1}, and 0.62 cm sec^{-1}, respectively. It remained relatively constant until the electrode tip was located 15 μm from the substratum. At this point there was a sudden drop, and the local mass transfer coefficient was reduced by approximately 60% near the bottom compared to the values in the bulk liquid.

Dissolved oxygen- and local mass transfer coefficient profiles collected at the same locations

Thin cluster

The profiles in figures 12 and 13 were measured in a thin cluster with a thickness of approximately 70 microns. Flow velocities applied were 0.62 cm sec^{-1} and 1.53 cm sec^{-1} for the results shown in figures 12 and 13, respectively. The solid line perpendicular to the X-axis indicates the approximate location of the biofilm/liquid interface. The oxygen concentration in the bulk solution was close to 6 mg L^{-1}, and was depleted inside the biofilm at for the flow velocity of 0.62 cm sec^{-1}.

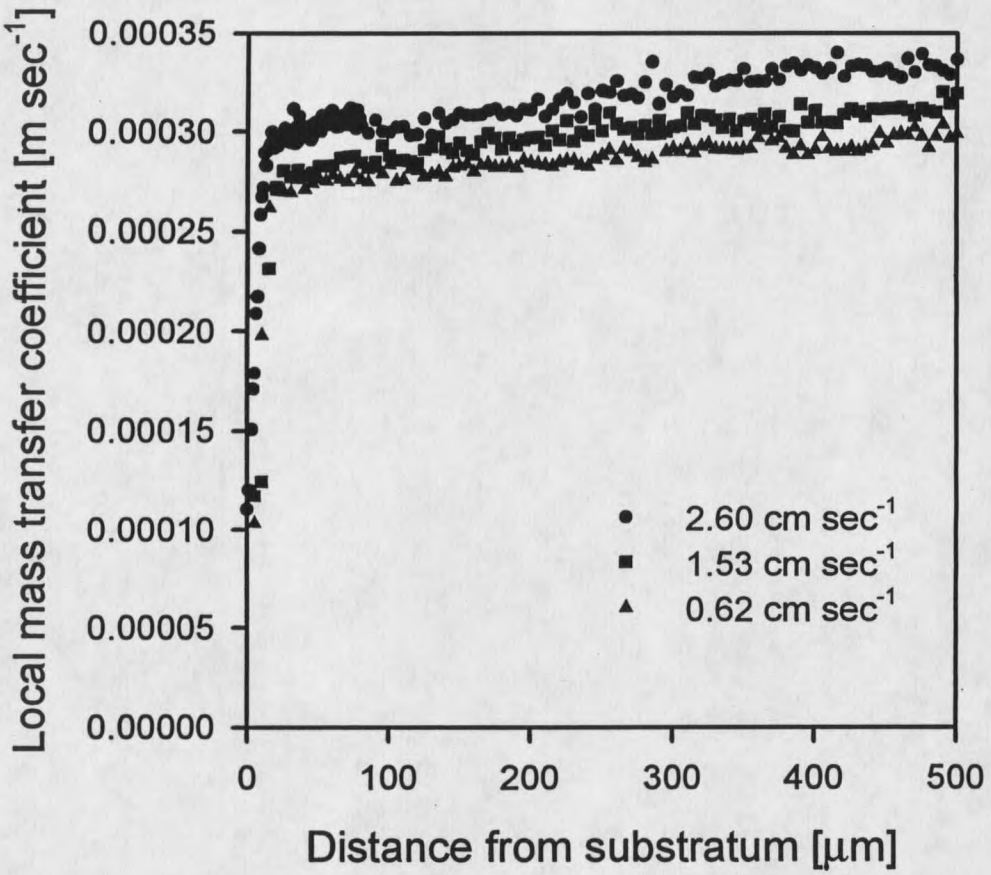

Figure 11. Local mass transfer coefficient profiles collected in a sterile reactor at three average flow velocities; 0.62, 1.53, and 2.60 cm sec^{-1}. The magnitude of the local mass transfer coefficient remained constant until 15 µm from the substratum. At this point the wall effect caused a sudden drop in the local mass transfer coefficient. A value close to 30 % of its bulk value was observed near the substratum.

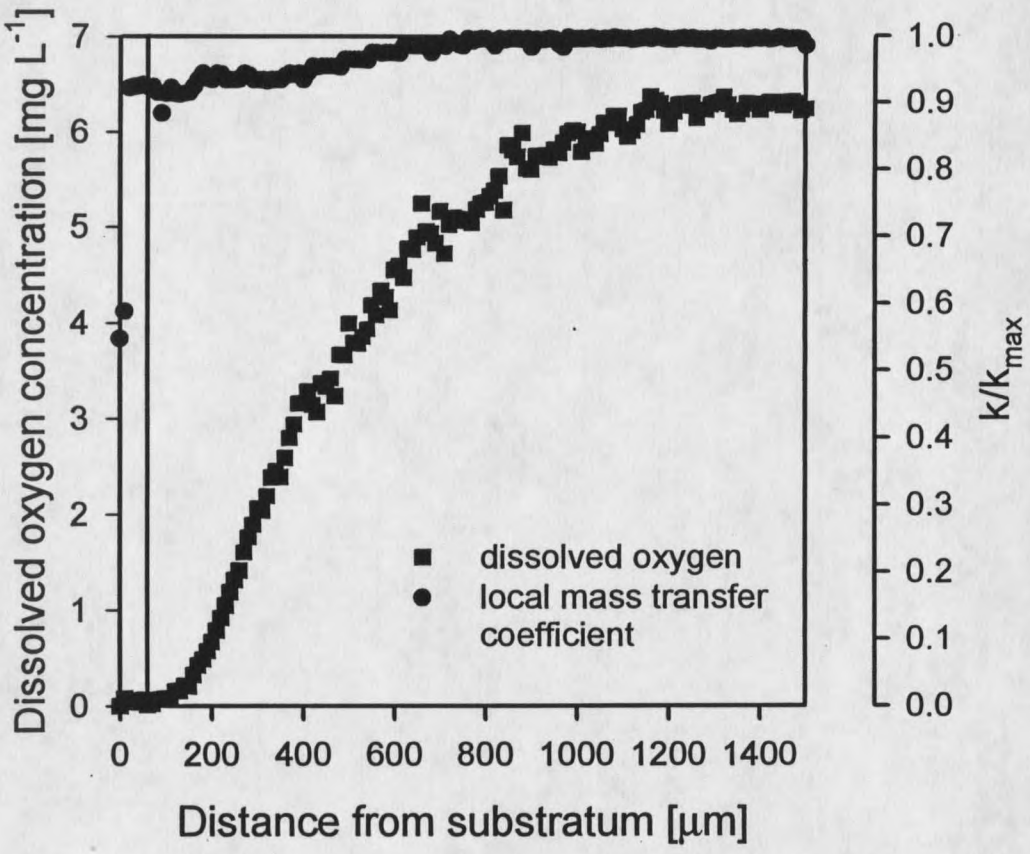

Figure 12. Dissolved oxygen and normalized local mass transfer coefficient profiles collected through a thin cluster at a flow velocity of 0.62 cm sec^{-1}. The biofilm thickness (ca. 70µm) is indicated by a solid line parallel to the Y-axis.

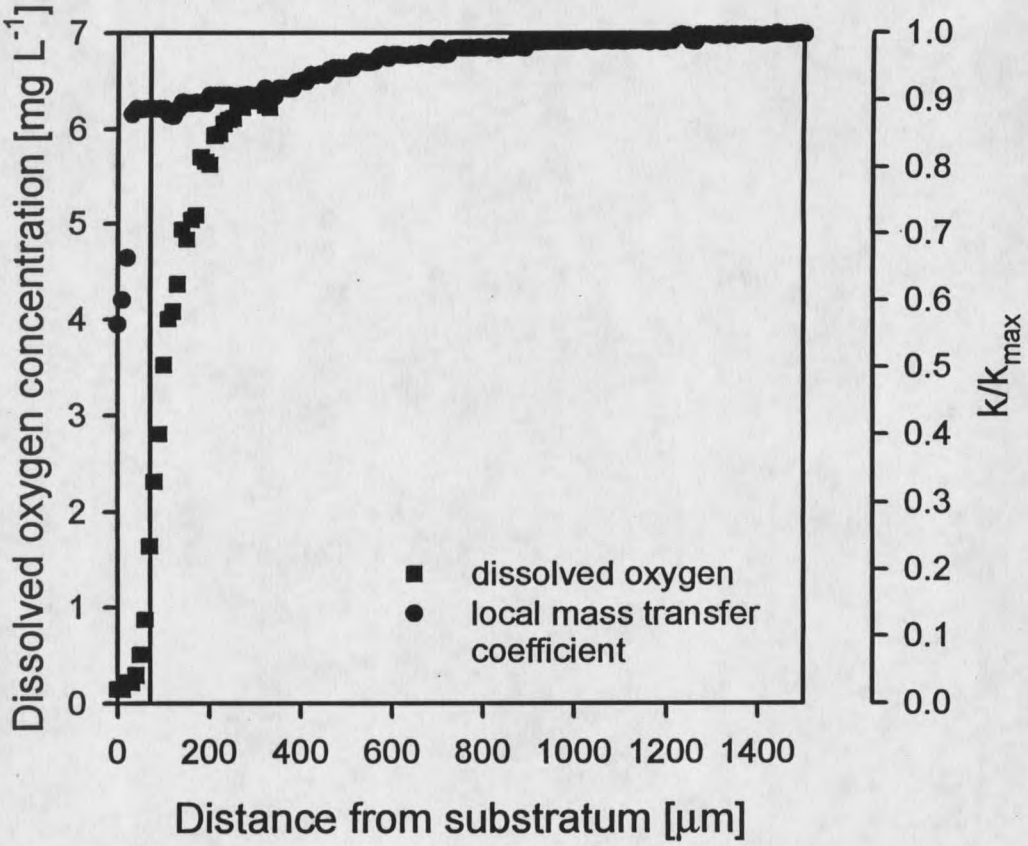

Figure 13. Dissolved oxygen and normalized local mass transfer coefficient profiles collected through a thin cluster at a flow velocity of 1.53 cm sec^{-1}. The biofilm thickness (ca. 70µm) is indicated by a solid line parallel to the Y-axis.

At this flow velocity the effective diffusive boundary layer thickness was 370 μm. At the flow velocity of 1.53 cm sec^{-1} the oxygen concentration was approximately 1.6 mg L^{-1} at the biofilm liquid interface, and 0.1 mg L^{-1} at the substratum. Corresponding effective diffusive boundary layer thickness was 60 μm. The local mass transfer coefficient near the biofilm surface decreased to approximately 90 % of its value in the bulk for both flow velocities. At a distance less than 30 μm from the substratum k/k_{max} dropped and reached 0.6 near the bottom.

Void filled with polymers

The profiles presented in figures 14, 15, and 16 were collected in a region between clusters. Through the inverted microscope this region appeared much brighter than the clusters. It was therefore assumed that the fraction of water and polymers was higher in this region of the biofilm. The thickness of this polymer layer was approximately 200 μm as indicated in the figures by a solid line parallel to the Y-axes. The oxygen concentration in the bulk liquid was approximately 6 mg L^{-1}. At a flow velocity of 0.62 cm sec^{-1} the entire biofilm was anaerobic as shown in figure 14. From figure 15 it can be seen that oxygen was depleted 100 μm from the substratum at the flow velocity of 1.53 cm sec^{-1}. At the biofilm liquid interface the oxygen concentration was 0.6 mg L^{-1}. By increasing the flow velocity to 2.60 cm sec^{-1} (figure 16) the biofilm became fully penetrated with an approximate oxygen concentration at the bottom of 1.3 mg L^{-1}. The oxygen concentration at the biofilm surface was 2.0 mg L^{-1}. At the flow velocity of 1.53 cm sec^{-1} significant noise was observed in the dissolved oxygen concentration data collected in the bulk liquid. For the flow

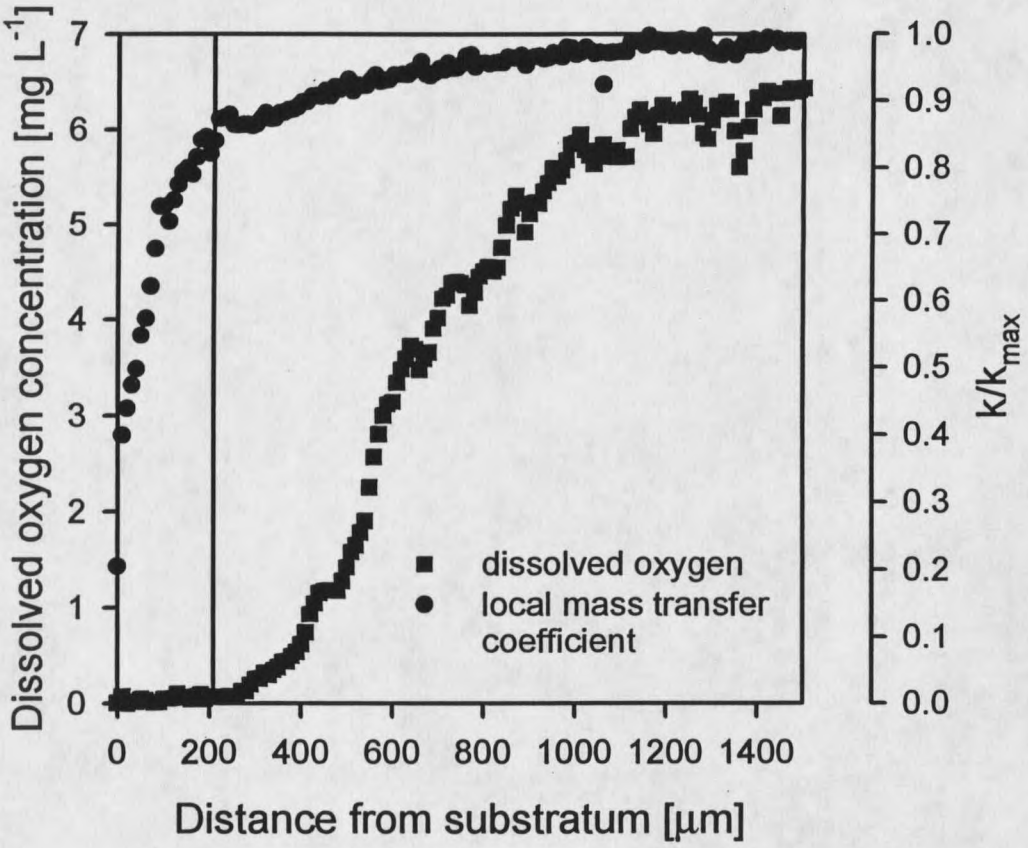

Figure 14. Dissolved oxygen and normalized local mass transfer coefficient profiles collected through a void filled with polymers at a flow velocity of 0.62 cm sec^{-1}. The biofilm thickness (ca. 200µm) is indicated by a solid line parallel to the Y-axis.

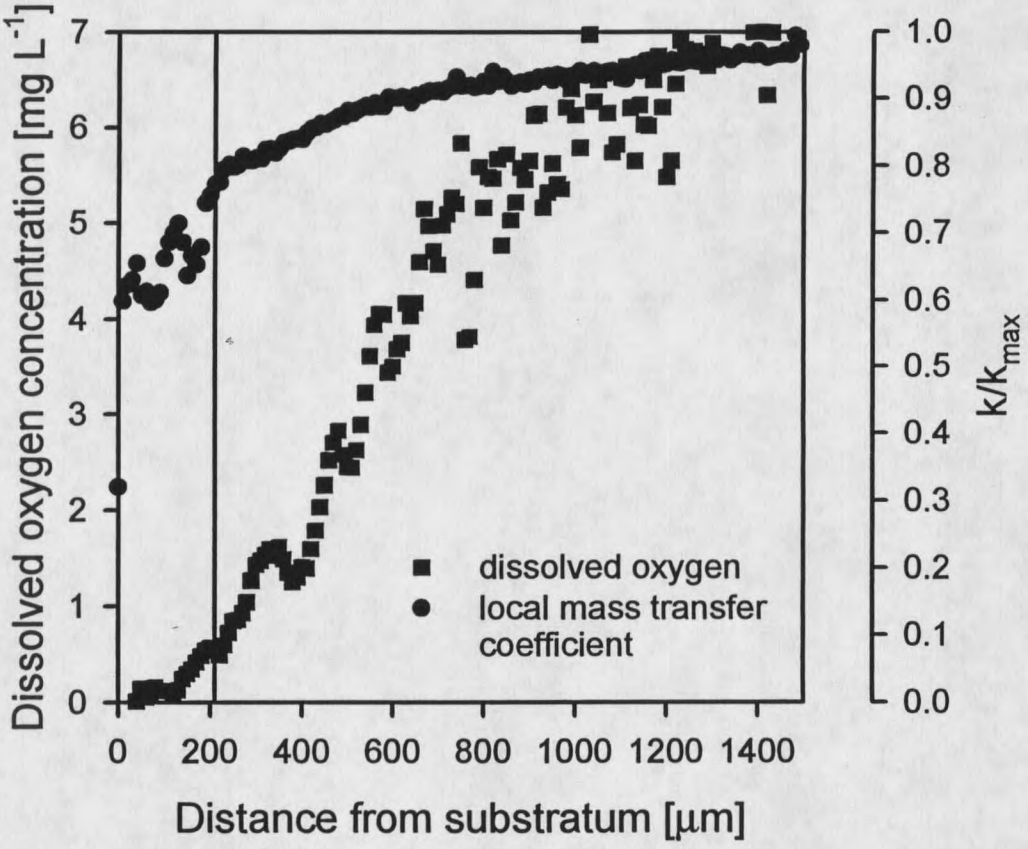

Figure 15. Dissolved oxygen and normalized local mass transfer coefficient profiles collected through a void filled with polymers at a flow velocity of 1.53 cm sec^{-1}. The biofilm thickness (ca. 200µm) is indicated by a solid line parallel to the Y-axis.

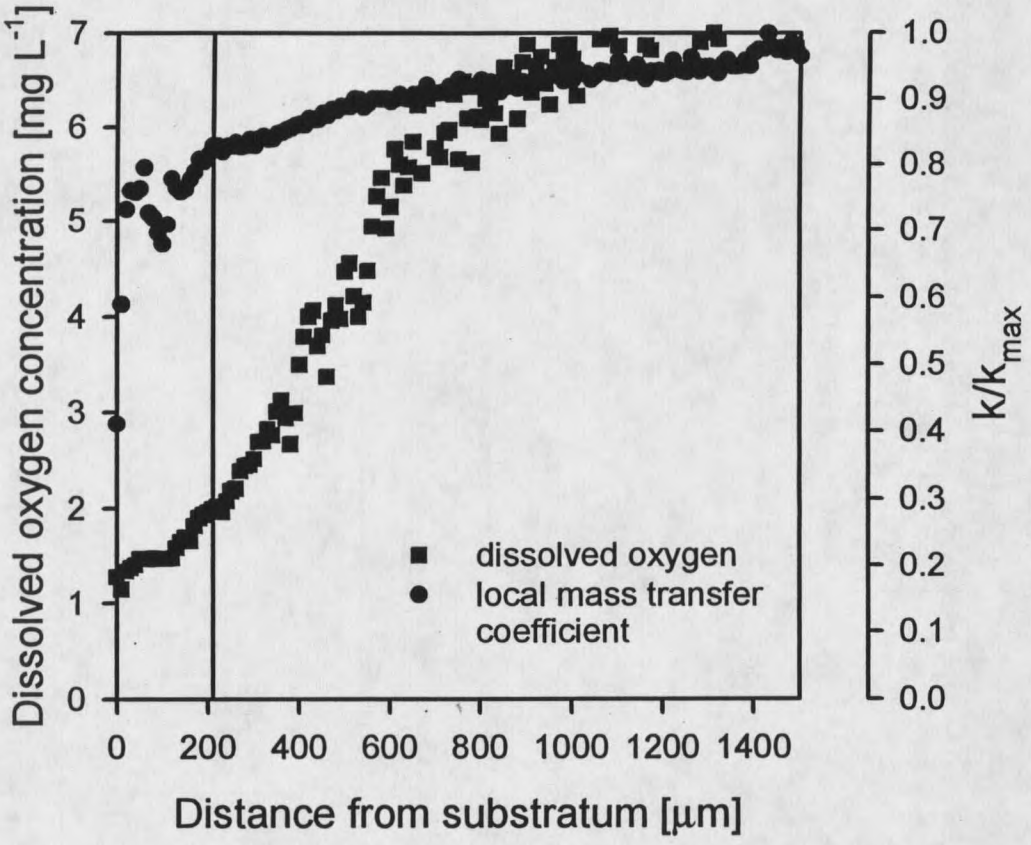

Figure 16. Dissolved oxygen and normalized local mass transfer coefficient profiles collected through a void filled with polymers at a flow velocity of 2.60 cm sec^{-1}. The biofilm thickness (ca. 200μm) is indicated by a solid line parallel to the Y-axis.

velocities 0.62 cm sec^{-1}, 1.53 cm sec^{-1}, and 2.60 cm sec^{-1} the effective diffusive boundary layer thickness was 440 μm, 420 μm, and 260 μm, respectively. The local mass transfer coefficient was reduced by approximately 15 % within the mass boundary layer at the flow velocity of 0.62 cm sec^{-1}. It decreased gradually below the biofilm surface, and k/k_{max} reached a value of 0.2 near the substratum. For the flow velocity of 1.53 cm sec^{-1} the local mass transfer coefficient was reduced by approximately 20 % through the mass boundary layer. k/k_{max} decreased only slightly inside the biofilm until the electrode tip was 10 μm from the substratum. Within the last 10 μm from the bottom the normalized local mass transfer coefficient decreased from 0.6 to 0.3. At the highest flow velocity the local mass transfer coefficient was reduced by approximately 20 % within the mass boundary layer. At a distance of 20 μm from the bottom k/k_{max} was 0.7, and decreased to 0.4 near the substratum.

Thick cluster

In figures 17, 18, and 19 oxygen- and local mass transfer coefficient profiles measured across a 350 μm thick cluster are shown. The cluster thickness is indicated by a solid line perpendicular to the X-axes. The oxygen concentration in the bulk liquid was approximately 6 mg L^{-1}. For the flow velocity of 0.62 cm sec^{-1} oxygen was depleted at a distance of 270 μm from the substratum as shown in figure 17. The oxygen concentration at the biofilm liquid interface was approximately 0.6 mg L^{-1}. Oxygen depletion was observed at a distance of 210 μm from the substratum at the flow velocity of 1.53 cm sec^{-1} which is shown in figure 18. At the biofilm surface the oxygen concentration was 1.5 mg L^{-1}. From figure 19 it can be seen that oxygen

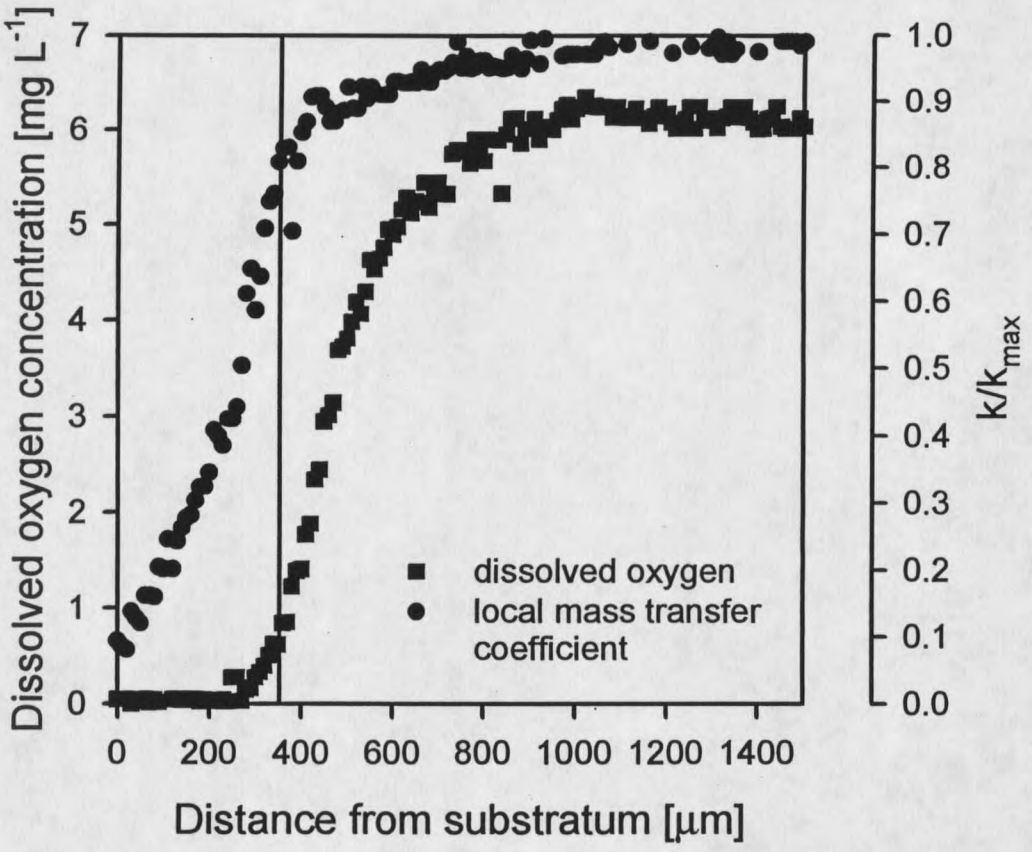

Figure 17. Dissolved oxygen and normalized local mass transfer coefficient profiles collected through a thick cluster at a flow velocity of 0.62 cm sec^{-1}. The biofilm thickness (ca. 350µm) is indicated by a solid line parallel to the Y-axis.

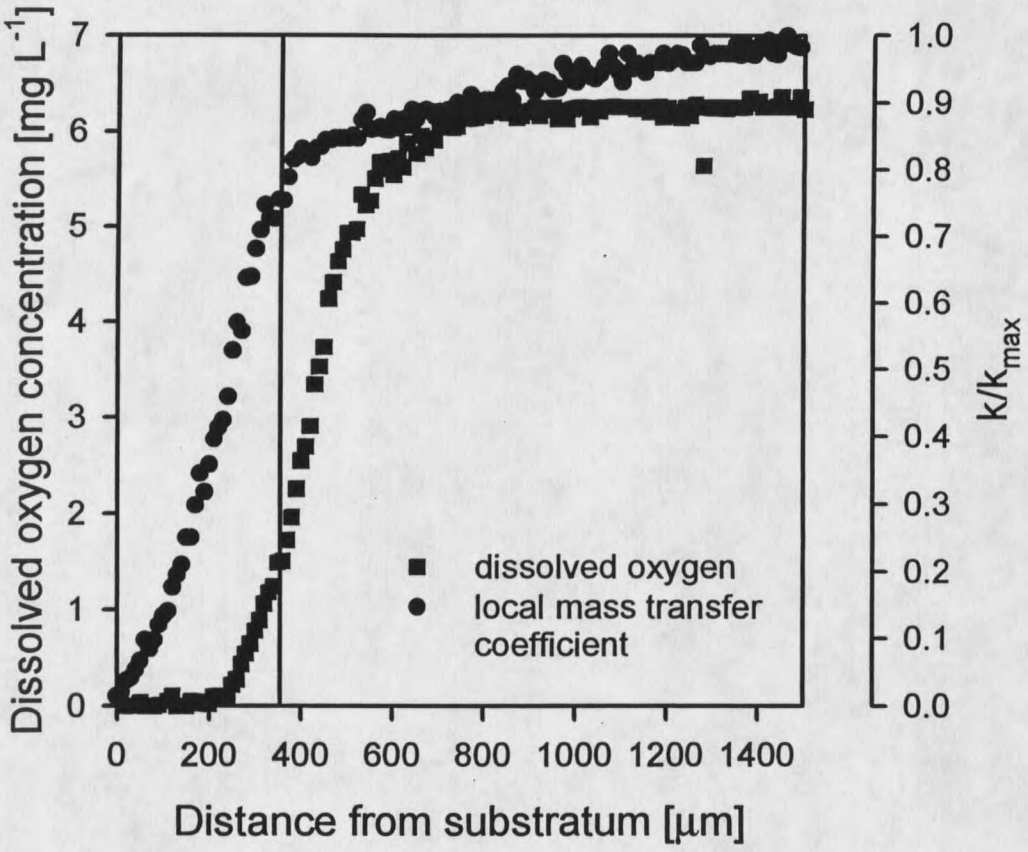

Figure 18. Dissolved oxygen and normalized local mass transfer coefficient profiles collected through a thick cluster at a flow velocity of 1.53 cm sec^{-1}. The biofilm thickness (ca. 350µm) is indicated by a solid line parallel to the Y-axis.

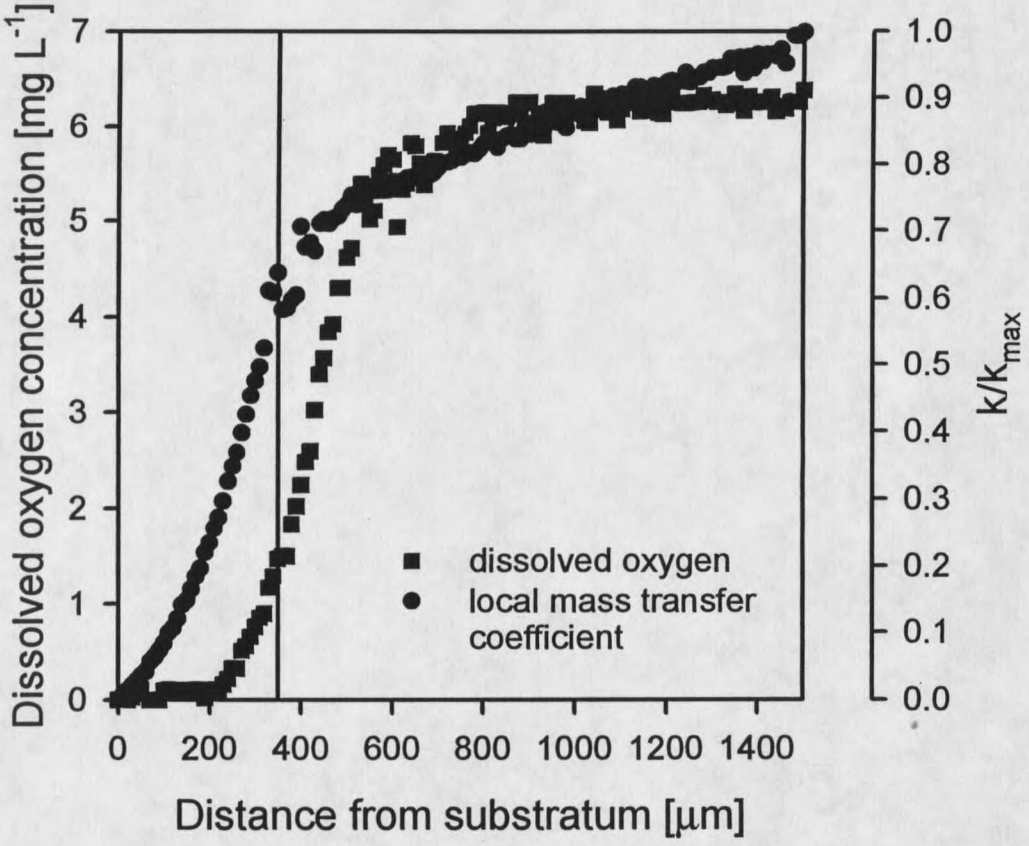

Figure 19. Dissolved oxygen and normalized local mass transfer coefficient profiles collected through a thick cluster at a flow velocity of 2.60 cm sec^{-1}. The biofilm thickness (ca. 350µm) is indicated by a solid line parallel to the Y-axis.

depletion occurred 200 μm from the substratum at a flow velocity of 2.60 cm sec^{-1}. The oxygen concentration was approximately 1.5 mg L^{-1} at the biofilm surface. For the flow velocities 0.62 cm sec^{-1}, 1.53 cm sec^{-1}, and 2.60 cm sec^{-1} the effective diffusive boundary layer thicknesses were 200 μm, 140 μm, and 140 μm, respectively. The local mass transfer coefficient was reduced by approximately 20 % within the mass boundary layer for the lowest flow velocity. It decreased gradually through the cluster, and k/k_{max} reached a value of 0.09 near the substratum. At the flow velocity of 1.53 cm sec^{-1} k/k_{max} was approximately 0.7 at the biofilm liquid interface. The local mass transfer coefficient decreased gradually through the biofilm and approached zero at the bottom. For the highest flow velocity the local mass transfer coefficient was reduced by almost 40 % through the mass boundary layer. k/k_{max} decreased gradually through the cluster and reached zero near the substratum.

DISCUSSION

Local mass transfer coefficient profiles in a sterile reactor

The shape of the local mass transfer coefficient profile depends on local hydrodynamics. Near a wall the hydrodynamics changes both with a biofilm present and absent. To be able to determine what are the effects of the biofilm, local mass transfer coefficient profiles were measured in a sterile reactor for comparison. Figure 11 shows that the flow velocity did not have any significant influence on the magnitude of the local mass transfer coefficient in the bulk liquid. The sudden drop observed close to the substratum is due to the presence of the wall. In the bulk liquid transport of ferricyanide occurs from behind, the sides, and the front of the reactive surface. When the electrode is close to the substratum the transport from the front ceases. This results in a drop in the limiting current. As the electrode moves further towards the bottom, the area of transport to the reactive surface decreases as well as the current. Ideally, if the tip of the electrode was perfectly flat, and the micromanipulator moved the electrode in such way that the tip was flush with the substratum, there would be no connection between the reacting surface and the electrolyte. In this case the current would be zero.

Dissolved oxygen- and local mass transfer coefficient profiles collected at the same locations

Thin cluster

From figures 12 and 13 it is clear that the local mass transfer coefficient remained high through the mass boundary layer and the biofilm cluster. For both flow velocities (0.62 cm sec^{-1} and 1.53 cm sec^{-1}) k/k_{max} was only reduced by 10 % through the mass boundary layer. The local mass transfer coefficient remained constant within the upper 50-60 μm layer of the cluster. These results indicate that convection was active both inside and outside the biofilm. The drop in local mass transfer coefficient close to the substratum is due to the wall effects also observed in a sterile reactor (figure 11). Although the change in velocity did not have any significant effect on the shape of the normalized local mass transfer coefficient profile, an increase in flow velocity from 0.62 cm sec^{-1} to 1.53 cm sec^{-1} resulted in a profound alteration of the oxygen profile. At the lowest flow velocity the cluster was anaerobic, while it was fully penetrated for the flow velocity of 1.53 cm sec^{-1}. The increase in flow velocity also caused an 80 % reduction of the effective diffusive boundary layer thickness.

Void filled with polymers

The flow velocity had a significant influence on the shape of both the oxygen- and local mass transfer coefficient profiles collected in the region consisting of extracellular polymers shown in figures 14, 15, and 16. At the lowest flow velocity oxygen was depleted throughout the biofilm. By increasing the velocity to 1.53 cm

sec^{-1} only the bottom half of the biofilm was anaerobic, and for the velocity of 2.60 cm sec^{-1} the biofilm was fully penetrated. The noise in the oxygen profile collected at the velocity of 1.53 cm sec^{-1} could be due to aggregated cells sticking to the tip of the electrode. Despite the large difference in the effective diffusive boundary layer thickness above the thin cluster (figures 12 and 13), the effective diffusive boundary layer thickness was only reduced by 5 % above the polymer layer when the flow velocity increased from 0.62 cm sec^{-1} to 1.53 cm sec^{-1}. There was a 40 % reduction in the thickness of the effective diffusive boundary layer when the flow velocity increased from 1.53 cm sec^{-1} to 2.60 cm sec^{-1}. The shape of the local mass transfer coefficient profiles appeared almost identical in the liquid phase for different flow velocities. Within the mass boundary layer k/k_{max} was reduced by 15 %, 20 %, and 20 % for the flow velocities of 0.62 cm sec^{-1}, 1.53 cm sec^{-1}, and 2.60 cm sec^{-1}, respectively. However, within the polymer layer the flow velocity had a profound influence on the profile. At the lowest flow velocity the normalized local mass transfer coefficient near the substratum decreased to 20 % of its bulk value. At the higher flow velocities the local mass transfer coefficient remained high within the biofilm. k/k_{max} was above 0.6 and 0.7 for the flow velocities of 1.53 cm sec^{-1}, and 2.60 cm sec^{-1}, respectively, at a distance further than 20 μm from the substratum. This indicates active convection within the polymer layer for these velocities. As in figures 11 through 13 the sudden drop in the local mass transfer coefficient is observed in figures 14, 15, and 16.

Thick cluster

The shape of the oxygen- and mass transfer coefficient profiles inside a cluster, shown in figure 17, 18, and 19, was not significantly affected by the flow velocity. This indicates a dense biofilm. A 270 μm thick anaerobic layer was observed at the bottom of the cluster at the lowest flow velocity. The anaerobic zone was approximately 200 μm thick for the velocities of 1.53 cm sec^{-1} and 2.60 cm sec^{-1}. At the biofilm liquid interface the oxygen concentration was approximately 0.6 mg L^{-1}, 1.5 mg L^{-1}, and 1.5 mg L^{-1} for the flow velocities of 0.62 cm sec^{-1}, 1.53 cm sec^{-1}, and 2.60 cm sec^{-1}, respectively. The effective diffusive boundary layer thickness was reduced by 30 % when the flow velocity increased from 0.62 cm sec^{-1} to 1.53 cm sec^{-1}. There was no change in this thickness when the velocity increased to 2.60 cm sec^{-1}. Effective diffusive boundary layer thicknesses for different locations and flow velocities are tabulated in table 1.

Table 1. Effective diffusive boundary layer thicknesses at different locations and flow velocities.

	Effective diffusive boundary layer thickness [μm]		
Flow velocity [cm sec^{-1}]	Thin cluster	Void w/polymer	Thick cluster
0.62	370	440	200
1.53	60	420	140
2.60	N.D.	260	140

The variation of the thickness at different locations, and the fractional change with flow velocity indicate that the mass boundary layer is not uniform. For all three flow

velocities the local mass transfer coefficient decreased gradually through the biofilm, and approached zero near the substratum. It has been mentioned before that the local mass transfer coefficient is a function of the effective diffusivity of ferricyanide and the thickness of the boundary layer surrounding the tip of the microelectrode. A change in either of these two parameters will cause a change in the local mass transfer coefficient. The shape of the profiles within the biofilm in figures 17, 18, and 19, can therefore, be due to a decreasing effective diffusivity or an increasing boundary layer thickness as the electrode tip approaches the bottom of the biofilm.

De Beer and Stoodley (1995) examined the hydrodynamics in biofilms by combining scanning confocal laser microscopy and microinjection of fluorescent dyes. They report that fluorescein was stagnant inside cell clusters, and conclude that mass transport inside these microbial aggregates, therefore, must be due to molecular diffusion only. Assuming a uniform distribution of cells and extracellular polymers in the cluster, the effective diffusivity and the thickness of the boundary layer, surrounding the microelectrode tip, should be constant within the biofilm. However, figures 17, 18, and 19 show that the local mass transfer coefficient decreased gradually within the cluster, and approached zero near the substratum.

If the flow around the tip of the local mass transfer coefficient microelectrode in the bulk liquid was turbulent, and transitional/laminar or absent in the biofilm, this could have explained the unexpected shape of the local mass transfer coefficient profile inside the biofilm. However, the Reynolds number was estimated based on the tip diameter of the microelectrode, and found to be 0.27 for the highest flow velocity

in the bulk liquid. For porous media, laminar flow occurs generally for Reynolds numbers less than 1 (Dullien, 1992). This means that the flow around the tip was laminar in the bulk liquid.

A co-worker suggested that the ferricyanide was utilized as an electron acceptor by the cells in the biofilm. However, figure 8 shows that oxygen was not depleted or used inside the biofilm when submerged in the electrolyte. In addition, Yang (1995) measured ferricyanide concentration profiles through biofilms. These showed that the electrolyte concentration was constant throughout the biofilm 30 minutes after the nutrient solution had been substituted with the ferricyanide solution.

Due to the high k/k_{max} observed in the upper region of the biofilm cluster convection occurs in this area. It is, therefore, likely that the thickness and shape of the boundary layer thickness around the tip of the microelectrode changes inside the biofilm. Longmire et al. (1990) determined the diffusivity of ferrocene solutes in polymer solvents by a microdisk electrode and cyclic voltammetry. They pointed out that one of the problems encountered was that the variability of the diffusion rates caused uncertainty about the diffusion geometry. Fang and Leddy (1995) presented results from a computer simulation for the effect of shield thickness on the cyclic voltammetric response of a microdisk. They explained three different scenarios of diffusion that depended on the scan rate, radius of the reactive surface (a), and radius of the reactive surface plus shield (b). The scan rate was converted to a scan parameter, δ_u;

$$\delta_u = [RTD/nFu]^{1/2} \qquad (30)$$

Their results showed that linear diffusion occurs if $\delta/a \ll 1$ and $\delta/b \ll 1$, radial, hemispherical diffusion occurs if $\delta/a > 1$ and $\delta/b < 1$, and radial, spherical diffusion occurs if $\delta/a \gg 1$ and $\delta/b > 1$.They report that the equations for infinitely thick insulators underestimate the current at a thinly shielded microdisk by up to 49%. Linear diffusion to the local mass transfer coefficient electrode would occur at a high flow velocity. A reduced velocity inside the biofilm could result in a change in the diffusion geometry to spherical diffusion. However, a transition from linear to spherical diffusion would increase the measured current inside the biofilm. It is, therefore, likely to believe that diffusion is either linear or spherical throughout the measurements. Although the diffusion geometry is the same, the boundary layer thickness may change if convection occurs within the cluster.

The gradual decrease in the local mass transfer coefficient through the biofilm can also be due to a gradual increase in the biofilm density. As the density increases, mass transport becomes more limited and the effective diffusivity decreases. It has been reported in literature that the density of some biofilms increases towards the substratum. Zhang and Bishop (1994 b) determined that the densities in the bottom layers of a heterotrophic biofilm were 5-10 times higher than those in the top layers. Fu et al. (1994) determined the effective diffusivity of oxygen in different layers of a biofilm. It varied from $0.25D_w$ at the substratum to $0.90D_w$ at the biofilm liquid interface. Yang (1995) measured a local mass transfer coefficient profile through a 650 μm thick 3% calcium alginate layer. The volumetric flow velocity was 1.15 cm sec^{-1}. It was found that in alginate the local mass transfer coefficient dropped rapidly

in the upper layer, and then leveled off towards the substratum. This is exactly what was expected to occur in a biofilm cluster, and supports the hypothesis that the effective diffusivity decreases down through a thick biofilm cluster. Experiments currently in progress also substantiate this hypothesis. A local mass transfer coefficient profile has been measured through a biofilm under stagnant conditions. The local mass transfer coefficient decreased gradually within clusters, approaching zero near the bottom, similar to profiles collected in a flow field (figures 17 through 19). Under stagnant conditions the thickness of the boundary layer surrounding the microelectrode tip is constant, and the only parameter that can cause the reduced local mass transfer coefficient is the effective diffusivity.

Tortuosity and porosity also influence the effective diffusivity. Zhang and Bishop (1994 a) developed two models for determining tortuosities, tortuosity factors, and effective diffusivities with porosity data as input. They report that for a biofilm with porosities of 0.84-0.93 in the top layers and 0.58-0.67 in the bottom layer, the tortuosity factor increased from 1.2 in the top layer to 1.6 in the bottom layer. In the same biofilm the ratio between the effective diffusivity to the diffusivity in bulk solution decreased from 68-81% in the top layer to 38-45% in the bottom layer. Zhang and Bishop (1994 a) defined pores as space between clusters. In their model the clusters obstructed the transport of substrate and, thereby, caused tortuosity. The concept of porosity and tortuosity can also be transferred to a smaller scale of the biofilm. Inside a cluster cells obstruct the transport of substrate. Substrate transport to cells in the bottom layer of a biofilm is more likely to occur around than through the

cells in the upper layers. Hence, the cells cause tortuosity. Regions with higher amounts of cells will have a higher tortuosity and lower porosity than regions containing less cells. Following is one of the equations used in the models of Zhang and Bishop (1994 a):

$$D_e = (\epsilon/\kappa)D_w \tag{31}$$

From this equation it is evident that if the porosity decreases and/or the tortuosity increases towards the bottom of the biofilm, the effective diffusivity as well as the local mass transfer coefficient will decrease.

Yang and Lewandowski (1995) observed very irregular profiles of the local mass transfer coefficient inside biofilm clusters. High peaks were believed to be due to channels inside the clusters facilitating convective flow. They also observed an increased local mass transfer coefficient just above the biofilm matrix which was suggested to be a result of active movement of the biofilm surface. These two effects were not observed in this work. However, the biofilm referred to in this thesis was grown at a much higher flow velocity, $v = 17$ cm sec^{-1} , whereas that of Yang and Lewandowski was grow at a flow velocity of $v = 1.3$ cm sec^{-1}. It is well known that biofilms growing at a high flow velocity are relatively rigid and dense (Van Loosdrecht et al., 1995, Christensen and Characklis, 1990). Therefore it is also possible that the secondary heterogeneity monitored by Yang and Lewandowski was in this case either less visible or absent.

Models of biofilms (Atkinson and Davies, 1974, Rittmann and McCarty, 1978, Wanner and Gujer, 1984) assume that there exists a thin diffusive boundary

layer in which the mass transport is dominated by molecular diffusion. If this was true a sudden drop should have been observed in the local mass transfer coefficient when entering this layer. Results presented in this thesis indicate that convective mass transport is active in the entire system down to the biofilm surface. A sudden decrease of the local mass transfer coefficient in the upper layer of the biofilm was also expected. However, clusters, 70 μm and less, and interstitial voids between clusters did not significantly influence the local mass transfer coefficient. The only significant reduction in local mass transfer coefficient was encountered in thick cell clusters. The question is now how this new knowledge about mass transport near and within biofilms can be applied in future biofilm modeling. As already mentioned it was obvious from results presented in this thesis that convective transport occurred near the biofilm surface. It was also shown that convection was present within thin clusters and polymer-layers. Assuming that molecular diffusion is dominating in this region underestimates the mass transfer to and within the biofilm. Modelers should, therefore, experiment with diffusivities higher than in stagnant water. In thick clusters it was found that the effective diffusivity decreased gradually towards the substratum. Mass transfer was convective in the top layer, and dominated by molecular diffusion in the bottom layers. If the biofilm model is built up by several compartments of the biofilm, different diffusivities can be applied in each compartment. Alternatively, one can develop an equation for the effective diffusivity as a function of known parameters e.g. porosity, density, or tortuosity. Wanner and Reichert (1996) extended an existing biofilm model. One of the improvements was to include a more flexible

description of transport of dissolved components in the biofilm. They did three calculations with different diffusivities of oxygen to predict the dissolved oxygen profile within the biofilm. In the first calculation the diffusivity was assumed to be equal to the molecular diffusivity of oxygen in water. The diffusivity was reduced due to tortuosity in the second calculation. In the third calculation the diffusivity was described by an exponential function which modeled convective oxygen transport into the biofilm. Results showed that when convective transport was accounted for in the model, the oxygen profile appeared significantly different than in the other two cases. This shows the importance of determining the degree of convective mass transport near and within biofilms.

CONCLUSIONS

Local mass transfer coefficient data presented in this thesis were measured with a microelectrode. The reliability of the technique was tested before any experiments were performed. It was found that the position of the reactive surface relative to the flow direction had a significant influence on the magnitude of the local mass transfer coefficient. This effect was avoided by keeping the microelectrode in a vertical position in each experiment. An oxygen profile measured through a biofilm submerged in electrolyte showed that respiration did not occur. Finally, oxygen was present in the system but did not have any influence on the local mass transfer coefficient measurement. The experiments presented were conducted at flow velocities between 0.6 and 2.6 cm/sec. For these flow velocities and for the specific experimental conditions employed in this work it was concluded that

1. Convection was active within the mass boundary layer and in the upper region of the biofilm independent of biofilm's thickness and flow velocity.

2. Thin biofilms, 70 μm or less, did not present any significant changes in local mass transfer resistance.

3. The polymers occupying the void space between clusters did not cause any significant changes in mass transfer resistance for flow velocities of 1.53 cm sec^{-1} and higher.

4. The local mass transfer coefficients in biofilm clusters, 350 μm thick and more, decreased gradually within the cluster approaching zero near the substratum. The decreased local mass transfer coefficient was found to be a result of a decreased effective diffusivity within the biofilm.

LITERATURE CITED

Atkinson, B., Davies, I. J. 1974. The overall rate of substrate uptake (reaction) by microbial films. Part I-A biological rate equation. Trans. Instn. Chem. Engrs. **52:** 248-259.

Bird, R. B., Stewart, W. E., Lightfoot, E. N. 1960. Transport phenomena. Wiley, New York.

Bishop, P. L., Rittmann, B. E. 1995. Modelling heterogeneity in biofilms: report of the discussion session. Wat. Sci. Tech. **32:** 263-265.

Blasius, H. 1908. Grenzshichten in Flüssigkeiten mit kleiner Reibung. Z. Math. U. Phys. Sci. **56:** 1-37; Engl. transl. in NACA TM 1256.

Chang, H. T., Rittmann, B. E. 1987 (a). Mathematical modeling of biofilm on activated carbon. Environ. Sci. Technol. **21:** 273-280.

Chang, H. T., Rittmann, B. E. 1987 (b). Verification of the model of biofilm on activated carbon. Environ. Sci. Technol. **21:** 280-288.

Chilton, T. H., Colburn, A. P. 1934. Ind. Eng. Chem. **26:** 1183.

Christensen, B. E., Characklis, W. G. 1990. Physical and chemical properties of biofilms, pp 93-130. In: W. G. Characklis and K. C. Marshall (eds.), Biofilms. Wiley, New York.

Christiansen, P., Hollesen, L., Harremoes, P. 1995. Liquid film diffusion on reaction rate in submerged biofilters. Wat. Res. **29:** 947-952.

Dalsgaard, T., De Zwart, J., Robertson, L. A., Kuenen, J. G., Revsbech, N. P. 1995. Nitrification, denitrification and growth in artificial thiosphaera biofilms as measured with combined microsensor for oxygen and nitrous oxide. FEMS Microbiol. Ecol. **17:** 137-148.

Dawson, D. A., Trass, O. 1972. Mass transfer at rough surfaces. J. Heat. Mass. Transfer. **15:** 1317-1336.

De Beer, D.; Stoodley, P. Relation between the structure of an aerobic biofilm and transport phenomena. *Wat. Sci. Tech.* **1995**, 32, 11-18.

De Beer, D., Stoodley, P., Roe, F., Lewandowski, Z. 1994 a. Effects of biofilm structures on oxygen distribution and mass transport. Biotechnol. Bioeng. **43:** 1131-1138.

De Beer, D., Stoodley, P., Lewandowski, Z. 1994 b. Liquid flow in heterogeneous biofilms. Biotechnol. Bioeng. **44:** 636-641.

Dullien, F. A. L. 1992. Porous media Fluid transport and pore structure. 2nd edition. Academic Press, California.

Fang, Y., Leddy, J. 1995. Cyclic voltammetric responses for inlaid microdisks with shields of thickness comparable to the electrode radius: a simulation of reversible electrode kinetics. Anal. Chem. **67:** 1259-1270.

Fetter, C. W. 1993. Contaminant hydrogeology. Macmillan publishing co. New York.

Fu, Y. -C., Zhang, T. C., Bishop, P. L. 1994. Determination of effective oxygen diffusivity in biofilms grown in a completely mixed biodrum reactor. Wat. Sci. Tech. **29:** 455-462.

Gantzer, C. J., Kollig, H. P., Rittmann, B. E., Lewis, D. L. 1988 (a). Predicting the rate of trace-organic compound removal by natural biofilms. Wat. Res. **22:** 191-200.

Gantzer, C. J., Rittmann, B. E., Herricks, E. E. 1988 (b). Mass transport to streambed biofilms. Wat. Res. **22:** 709-722.

Gao, X., Lee, J., White, H. S. 1995. Natural convection at microelectrodes. Anal. Chem. **67:** 1541-1545.

Hanratty, T. J. 1991. Use of the polarographic method to measure wall shear stress. J. Appl. Electrochem. **21:** 1038-1046.

Hermanowicz, S. W., Schindler, U., Wilderer. 1995. Fractal structure of biofilms: New tools for investigation of morphology. Wat. Sci. Tech. **32:** 99-105.

Horn, H., Hempel, D. C. 1995. Mass transfer coefficients for an autotrophic and a heterotrophic biofilm system. Wat. Sci. Tech. **32:** 199-204.

Juhasz, N. M., Deen, W. M. 1993. Electrochemical measurements of mass transfer at surfaces with discrete reactive areas. AIChE J. **39:** 1708-1715.

Keevil, C. W., Walker, J. T. 1992. Nomarski DIC microscopy and image analysis of biofilms. Binary. **4:** 93-95.

Korber, D. R., James, G. A., Costerton, J. W. 1994. Evaluation of fleroxacin activity against established Pseudomonas fluorescens biofilms. Appl. Environ. Microbiol. **60:** 1663-1669.

Kuenen, J. G., Jørgensen, B. B., Revsbech, N. P. 1986. Oxygen microprofiles of trickling filter biofilms. Wat. Res. **20:** 1589-1598.

Kühl, M., Jørgensen, B. B. 1992. Microsensor measurements of sulfate reduction and sulfide oxidation in compact microbial communities of aerobic biofilms. Appl. Environ. Micrbiol. **58:** 1164-1174.

Larsen, T. A., Harremoës, P. 1994. Combined reactor and microelectrode measurements in laboratory grown biofilms. Wat. Res. **28:** 1435-41.

Lawrence, J. R., Korber, D. R., Hoyle, B. D., Costerton, J. W., Caldwell, D. E. 1991. Optical sectioning of microbial biofilms. J. Bacteriol. **173:** 6558-6567.

Lewandowski, Z., Altobelli, S. A., Fukushima, E. 1993. NMR and microelectrode studies of hydrodynamics and kinetics in biofilms. Biotechnol. Prog. **9:** 40-45.

Lewandowski, Z. 1994. Dissolved oxygen gradients near microbially colonized surfaces, pp 175-188. In: G. G. Geesey, Z. Lewandowski, and H. C. Flemming (eds.), Biofouling and Biocorrosion in industrial water systems. Lewis Publishers, Florida.

Lewandowski, Z., Stoodley, P., Altobelli, S. 1995. Experimental and conceptual studies on mass transport in biofilms. Wat. Sci. Tech. **31:** 153-162.

Lide, D. R. (Ed.) 1994. Handbook of chemistry and physics. 74th edition. CRC Press.

Logan, B. E., Dettmer, J. W. 1990. Increased mass transfer to microorganisms with fluid motion. Biotechnol. Bioeng. **35:** 1135-1144.

Longmire, M. L.; Watanabe, M.; Zhang, H.; Wooster, T. T.; Murray, R. W. Voltammetric measurement of ultraslow diffusion rates in polymeric media with microdisk electrodes. *Anal. Chem.* **1990**, 62, 747-752.Longmire, M. L.; Watanabe, M.; Zhang, H.; Wooster, T. T.; Murray, R. W. Voltammetric measurement of ultraslow diffusion rates in polymeric media with microdisk electrodes. *Anal. Chem.* **1990**, 62, 747-752.

Macpherson, J. V., Marcar, S., Unwin, P. R. 1994. Microjet electrode: a hydrodynamic ultramicroelectrode with high mass transfer rates. Anal. Chem. **66:** 2175-2179.

Murga, R., Stewart, P. S., Daly, D. 1995. Quantitative analysis of biofilm thickness variability. Biotechnol. Bioeng. **45:** 503-510.

Revsbech, N. P. 1989 a. Microsensors: Spatial gradients in biofilms. In: W. G. Characklis and P. A. Wilderer (eds.), Structure and function of biofilms. Wiley, New York.

Revsbech, N. P. 1989 b. An oxygen microsensor with a guard cathode. Limnol. Oceanogr. **34:** 474-478.

Revsbech, N. P., Jørgensen, B. B. 1986. Microelectrodes: Their use in microbial ecology, pp. 293-352. In: Marshall, K. C. (Ed.) Advances in microbial ecology. Plenum, New York.

Reynolds, O. 1874. Proc. Manchester Lit. Phil. Soc. **8.**

Rittmann, B. E., McCarty, P. L. 1978. Variable-order model of bacterial-film kinetics. Journal of the Env. Eng. Div. **104:** 889-900

Siegrist, H., Gujer, W. 1985. Mass transfer mechanisms in a heterotrophic biofilm. Wat. Res. **19:** 1369-1378.

Stewart, P. S., Murga, R., Srinivasan, R., De Beer, D. 1995. Biofilm structural heterogeneity visualized by three microscopic methods. Wat. Res. **29:** 2006-2009.

Stoodley, P., DeBeer, D., Lewandowski, Z. 1994. Liquid flow in biofilm systems. Appl. Environ. Microbiol. **60:** 2711-2716.

Van Loosdrecht, M. C. M., Eikelboom, D., Gjaltema, A., Mulder, A., Tijhuis, L., Heijnen, J. J. 1995. Biofilm structures. Wat. Sci. Tech. **32:** 35-43.

Wanner, O., Gujer, W. 1986. A multispecies biofilm model. Biotechnol. Bioeng. **28:** 314-328.

Wanner, O., Reichert, P. 1996. Mathematical modeling of mixed-culture biofilms. **49:** 172-184.

Welty, J. R., Wicks, C. E., Wilson, R. E. 1976. Fundamentals of Momentum, Heat, and Mass Transfer. 2nd edition. Wiley, New York.

Wolfaardt, G. M., Lawrence, J. R., Robarts, R. D., Caldwell, S. J., Caldwell, D. E. 1994. Multicellular organization in a degradative biofilm community. Appl. Environ. Microbiol. **60:** 434-446.

Yang, S. 1995. Microelectrode measurement of local mass transfer coefficient in biofilms. Master's thesis, MSU Bozeman, MT.

Yang, S., Lewandowski, Z. 1995. Measurement of local mass transfer coefficient in biofilms. Biotechnol. Bioeng. **48:** 737-744.

Zhang, T. C., Bishop, P. L. 1994 c. Experimental determination of the dissolved oxygen boundary layer and mass transfer resistance near the fluid-biofilm interface. Wat.Sci.Tech. **30:** 47-58.

Zhang, T. C., Bishop, P. L. 1994 a. Evaluation of tortuosity factors and effective diffusivities in biofilms. Wat.Res. **28:** 2279-2287.

Zhang, T. C., Bishop, P. L. 1994 b. Density, porosity, and pore structure of biofilms. Wat.Res. **28:** 2267-2277.

NOMENCLATURE

[Units: M - mass, L - length, T - time]

a	radius of reactive surface	(L)
A	reactive surface area	(L^2)
b	radius of reactive surface plus shield	(L)
B	experimental coefficient	(L^{-1})
C	concentration	(ML^{-3})
c_p	heat capacity	(Joule $Kelvin^{-1}$ M^{-1})
C_s	surface concentration	(ML^{-3})
C_∞	bulk liquid concentration	(ML^{-3})
ΔC	concentration gradient	(ML^{-3})
d	inside diameter of reactor	(L)
D	molecular diffusivity	(L^2T^{-1})
D_e	effective diffusivity	(L^2T^{-1})
d_p	streambed particle size	(L)
D_p	particle diameter	(L)
D_w	diffusion coefficient in water	(L^2T^{-1})
e	void fraction	(-)

F	Faraday's constant	(96485 Coulomb $Mole^{-1}$)
I	electrical current	(Ampere)
J	flux of reactant	($MT^{-1}L^{-2}$)
j_D	j factor for mass transfer	(-)
j_H	j factor for heat transfer	(-)
k	mass transfer coefficient	(LT^{-1})
k_c	convective mass transfer coefficient	(LT^{-1})
L	characteristic length	(L)
L_D	film thickness	(L)
m	empirical constant	(-)
n	number of electrons transferred	(-)
n_1	empirical constant	(-)
n_3	empirical constant	(L)
Q	leucine uptake rate	(MT^{-1})
R	gas constant	(L^3 Pascal $Mole^{-1}$ $Kelvin^{-1}$)
T	absolute temperature	(Kelvin)
u	scan rate	(Volts T^{-1})
U_0	empty bed flow velocity	(LT^{-1})
v	velocity	(LT^{-1})
v_s	superficial flow velocity through column	(LT^{-1})

v_x	x-component of velocity	(LT^{-1})
v_∞	bulk liquid flow velocity	(LT^{-1})
x	rectangular coordinate	(-)
y	rectangular coordinate	(-)
α	cell radius	(L)
δ	hydrodynamic boundary layer thickness	(L)
δ_c	concentration boundary layer thickness	(L)
δ_u	scan rate parameter	(L)
ϵ	porosity	(-)
κ	tortuosity factor	(-)
ξ	constant	(-)
μ	viscosity	$(ML^{-1}T^{-1})$
ρ	density	(ML^{-3})
Nu	mass transfer Nusselt number	
Pe	Peclet number	
Pr	Prandtl number	
Re	Reynolds number	
Sh	Sherwood number	
St	Stanton number	

APPENDIX

Experimental raw data

Raw data of Fig. 6

Electrode position	Limiting current [x10^7A]	k [m/sec]	Electrode position	Limiting current [x10^7A]	k [m/sec]	Electrode position	Limiting current [x10^7A]	k [m/sec]
Facing	0.0794	4.2E-05	Facing	0.0802	4.3E-05	Vertical	0.111	5.9E-05
away	0.0759	4E-05	away	0.0801	4.3E-05	position	0.1118	6E-05
from	0.0798	4.2E-05	from	0.0803	4.3E-05	"	0.1155	6.1E-05
flow	0.0795	4.2E-05	flow	0.0794	4.2E-05	"	0.1141	6.1E-05
"	0.0779	4.1E-05	"	0.0812	4.3E-05	"	0.1104	5.9E-05
"	0.0796	4.2E-05	"	0.0815	4.3E-05	"	0.113	6E-05
"	0.0808	4.3E-05	"	0.0804	4.3E-05	"	0.1151	6.1E-05
"	0.0815	4.3E-05	"	0.0802	4.3E-05	"	0.112	6E-05
"	0.08	4.3E-05	"	0.0811	4.3E-05	"	0.1114	5.9E-05
"	0.0805	4.3E-05	"	0.0808	4.3E-05	"	0.1112	5.9E-05
"	0.0814	4.3E-05	"	0.0798	4.2E-05	"	0.1143	6.1E-05
"	0.0788	4.2E-05	"	0.0796	4.2E-05	"	0.1104	5.9E-05
"	0.0808	4.3E-05	"	0.0818	4.4E-05	"	0.1117	5.9E-05
"	0.0796	4.2E-05	"	0.0818	4.4E-05	"	0.1136	6E-05
"	0.08	4.3E-05	"	0.0829	4.4E-05	"	0.1118	6E-05
"	0.0794	4.2E-05	"	0.0823	4.4E-05	"	0.1118	6E-05
"	0.0791	4.2E-05	"	0.0838	4.5E-05	"	0.1125	6E-05
"	0.0781	4.2E-05	"	0.0823	4.4E-05	"	0.1114	5.9E-05
"	0.0803	4.3E-05	"	0.0827	4.4E-05	"	0.1132	6E-05
"	0.0782	4.2E-05	"	0.0809	4.3E-05	"	0.1107	5.9E-05
"	0.082	4.4E-05	"	0.0843	4.5E-05	"	0.1104	5.9E-05
"	0.0788	4.2E-05	"	0.0843	4.5E-05	"	0.1091	5.8E-05
"	0.0801	4.3E-05	"	0.0841	4.5E-05	"	0.111	5.9E-05
"	0.0803	4.3E-05	"	0.0836	4.4E-05	"	0.111	5.9E-05
"	0.0802	4.3E-05	"	0.0821	4.4E-05	"	0.1073	5.7E-05
"	0.0812	4.3E-05	"	0.084	4.5E-05	"	0.1133	6E-05
"	0.0807	4.3E-05	"	0.0826	4.4E-05	"	0.1167	6.2E-05
"	0.0798	4.2E-05	"	0.0832	4.4E-05	"	0.12	6.4E-05
"	0.0817	4.3E-05	"	0.0814	4.3E-05	"	0.1248	6.6E-05
"	0.0801	4.3E-05	Vertical	0.0886	4.7E-05	Facing	0.1305	6.9E-05
"	0.0818	4.4E-05	position	0.1048	5.6E-05	towards	0.1329	7.1E-05
"	0.0787	4.2E-05	"	0.1031	5.5E-05	flow	0.1308	7E-05
"	0.0791	4.2E-05	"	0.1073	5.7E-05	"	0.1285	6.8E-05

Diameter of the microelectrode: 10 microns

Ferricyanide concentration: 25 mM

Raw data of Fig. 6 CONT'D

Electrode position	Limiting current [x10^7A]	k [m/sec]
Facing	0.1347	7.2E-05
towards	0.1328	7.1E-05
flow	0.1327	7.1E-05
"	0.1354	7.2E-05
"	0.1364	7.3E-05
"	0.1322	7E-05
"	0.1269	6.8E-05
"	0.1367	7.3E-05
"	0.1398	7.4E-05
"	0.1355	7.2E-05
"	0.1383	7.4E-05
"	0.1362	7.2E-05
"	0.1388	7.4E-05
"	0.1382	7.4E-05
"	0.1361	7.2E-05
"	0.1353	7.2E-05
"	0.135	7.2E-05
"	0.1379	7.3E-05
"	0.1352	7.2E-05
"	0.1336	7.1E-05
"	0.136	7.2E-05
"	0.1346	7.2E-05
"	0.1347	7.2E-05
"	0.1343	7.1E-05
"	0.1306	7E-05
"	0.1309	7E-05
"	0.1325	7.1E-05

Raw data of Fig. 8

Vertical position [microns]	Oxygen concentration [mg/L]	Vertical position [microns]	Oxygen concentration [mg/L]
500	4.6991	240	4.2286
490	4.6991	230	4.1741
480	4.6514	220	4.2082
470	4.6036	210	4.2082
460	4.6241	200	4.1673
450	4.6105	190	4.1809
440	4.5968	180	4.1809
430	4.4741	170	4.0923
420	4.4945	160	4.0855
410	4.4673	150	4.0241
400	4.4673	140	4.065
390	4.4127	130	4.0241
380	4.44	120	4.0514
370	4.3377	110	4.0991
360	4.3582	100	4.1264
350	4.3377	90	4.1536
340	4.3105	80	4.1264
330	4.2423	70	4.1605
320	4.3105	60	4.1605
310	4.2627	50	4.1468
300	4.3445	40	4.1877
290	4.1809	30	4.0582
280	4.2559	20	4.0786
270	4.1536	10	4.0718
260	4.1673	0	4.2014
250	4.1468		

Raw data of Fig. 9

	Limiting current [x10^7A]		Limiting current [x10^7A]		Limiting current [x10^7A]		Limiting current [x10^7A]
Stagnant	0.3932	Stagn.	0.3903	Stagn.	0.39	AIR	0.7693
solution	0.3926	sol.	0.389	sol.	0.3925	ON	0.7416
"	0.3926	"	0.3897	"	0.3929	"	0.7763
"	0.392	"	0.3889	"	0.3945	"	0.7543
"	0.3941	"	0.3886	"	0.3944	"	0.8103
"	0.3945	"	0.3889	"	0.3949	"	0.6834
"	0.3942	"	0.3894	"	0.3944	"	0.7171
"	0.3943	"	0.3889	"	0.3951	AIR	0.7369
"	0.3945	"	0.3891	"	0.3948	OFF	0.7132
"	0.3942	"	0.3885	"	0.3943	"	0.5104
"	0.3944	"	0.3886	"	0.395	"	0.5514
"	0.3941	"	0.3872	"	0.3955	"	0.6377
"	0.394	"	0.3882	"	0.396	"	0.5671
"	0.3942	"	0.3872	"	0.3962	"	0.517
"	0.3938	"	0.3883	"	0.3966	"	0.4516
"	0.3922	"	0.3881	"	0.3966	"	0.462
"	0.3931	"	0.3867	"	0.3962	"	0.4692
"	0.3938	"	0.3865	"	0.3969	"	0.5114
"	0.393	"	0.3867	"	0.3978	"	0.5231
"	0.392	"	0.3869	"	0.3982	"	0.5324
"	0.3923	"	0.3846	"	0.3995	"	0.4331
"	0.3918	"	0.3852	"	0.3998	"	0.4405
"	0.3911	"	0.3849	"	0.398	"	0.4604
"	0.3914	"	0.3849	"	0.396	"	0.4668
"	0.3906	"	0.384	AIR	0.3943	"	0.4524
"	0.3909	"	0.385	ON	0.5426	"	0.4299
"	0.3917	"	0.3832	"	0.8193	"	0.4142
"	0.3914	"	0.3849	"	0.8139	"	0.4165
"	0.3903	"	0.3854	"	0.8908	"	0.4202
"	0.3909	"	0.3865	"	0.838	"	0.4189
"	0.3909	"	0.3863	"	0.8624	"	0.414
"	0.3906	"	0.387	"	0.8375	"	0.4089
"	0.3901	"	0.3888	"	0.8121	"	0.4047
"	0.3883	"	0.3901	"	0.8608	"	0.4004
"	0.3905	"	0.3898	"	0.7886	"	0.3982

Raw data of Fig. 9 CONT'D

	Limiting current [x10^7A]		Limiting current [x10^7A]		Limiting current [x10^7A]		Limiting current [x10^7A]		Limiting current [x10^7A]
AIR	0.3976	AIR	0.4121	AIR	0.3867	N2	0.7627	N2	0.4096
OFF	0.3981	OFF	0.4126	OFF	0.3867	ON	0.7947	OFF	0.4095
"	0.3979	"	0.4135	N2	0.3879	"	0.7904	"	0.4074
"	0.3962	"	0.4122	ON	0.8267	N2	0.7792	"	0.4038
"	0.3966	"	0.4121	"	0.6813	OFF	0.7783	"	0.4028
"	0.3959	"	0.412	"	0.7191	"	0.668	"	0.4005
"	0.3961	"	0.4104	"	0.6797	"	0.5776	"	0.3984
"	0.3972	"	0.4098	"	0.7104	"	0.5148	"	0.3973
"	0.396	"	0.4095	"	0.7384	"	0.4633	"	0.3962
"	0.3981	"	0.4082	"	0.7359	"	0.4208	"	0.3952
"	0.3984	"	0.4073	"	0.6902	"	0.4475	"	0.3946
"	0.3979	"	0.4077	"	0.6685	"	0.5663	"	0.3946
"	0.3969	"	0.4073	"	0.6826	"	0.4657	"	0.3946
"	0.3989	"	0.4078	"	0.6716	"	0.4287	"	0.3945
"	0.3986	"	0.4095	"	0.6236	"	0.4494	"	0.3916
"	0.3983	"	0.4106	"	0.7086	"	0.4678	"	0.3887
"	0.3975	"	0.4121	"	0.7452	"	0.4657	"	0.3864
"	0.397	"	0.4117	"	0.7249	"	0.433	"	0.3885
"	0.3973	"	0.4121	"	0.6886	"	0.4262	"	0.3888
"	0.3981	"	0.4103	"	0.7047	"	0.4305	"	0.3883
"	0.3974	"	0.4062	"	0.696	"	0.4259	"	0.3887
"	0.3973	"	0.4036	"	0.7966	"	0.4213	"	0.3881
"	0.3983	"	0.4022	"	0.7235	"	0.4198	"	0.3889
"	0.3981	"	0.4003	"	0.8158	"	0.4211	"	0.3873
"	0.3976	"	0.3984	"	0.7086	"	0.4216	"	0.3874
"	0.3966	"	0.3985	"	0.8457	"	0.4199	"	0.3867
"	0.396	"	0.3962	"	0.7225	"	0.4175	"	0.3861
"	0.3958	"	0.3969	"	0.8149	"	0.4157	"	0.3864
"	0.3987	"	0.3948	"	0.7162	"	0.4121	"	0.3866
"	0.4033	"	0.393	"	0.8307	"	0.4102	"	0.3869
"	0.4062	"	0.3908	"	0.831	"	0.4078	"	0.3883
"	0.4079	"	0.3899	"	0.8232	"	0.4085	"	0.3903
"	0.4082	"	0.3884	"	0.7277	"	0.4092	"	0.3929
"	0.4105	"	0.3873	"	0.7647	"	0.4104	"	0.3947
"	0.412	"	0.3868	"	0.7285	"	0.4105	"	0.3977

Raw data of Fig. 9 CONT'D

	Limiting current [x10^7A]		Limiting current [x10^7A]		Limiting current [x10^7A]
N2	0.4009	N2	0.3871	N2	0.3932
OFF	0.4042	OFF	0.387	OFF	0.3922
"	0.406	"	0.3864	"	0.392
"	0.4065	"	0.3863	"	0.3904
"	0.4062	"	0.3847	"	0.3903
"	0.4039	"	0.3839	"	0.3903
"	0.4021	"	0.3826	"	0.3889
"	0.4006	"	0.3829	"	0.3884
"	0.3969	"	0.3826	"	0.3905
"	0.3949	"	0.3825	"	0.3884
"	0.3948	"	0.383	"	0.3892
"	0.3926	"	0.3831	"	0.3901
"	0.3917	"	0.3842	"	0.3901
"	0.3917	"	0.3838	"	0.3899
"	0.3893	"	0.3862	"	0.3899
"	0.3863	"	0.3863	"	0.3906
"	0.387	"	0.3869		
"	0.3889	"	0.3882		
"	0.3925	"	0.3888		
"	0.394	"	0.3896		
"	0.3942	"	0.3903		
"	0.3942	"	0.3906		
"	0.3944	"	0.3904		
"	0.3931	"	0.3907		
"	0.3924	"	0.3922		
"	0.3907	"	0.3926		
"	0.3903	"	0.3944		
"	0.39	"	0.3945		
"	0.3883	"	0.3952		
"	0.3891	"	0.3938		
"	0.3884	"	0.3945		
"	0.3887	"	0.3958		
"	0.3883	"	0.3942		
"	0.3885	"	0.3944		
"	0.3884	"	0.3947		

Raw data of Fig. 11, v = 2.60 cm/sec

Vertical position [microns]	Limiting current [A]	k [m/sec]
500	1.5939E-08	0.0003367
495	1.5578E-08	0.000329
490	1.5675E-08	0.0003311
485	1.5776E-08	0.0003332
480	1.5803E-08	0.0003338
475	1.6068E-08	0.0003394
470	1.5624E-08	0.00033
465	1.5957E-08	0.000337
460	1.5503E-08	0.0003274
455	1.5566E-08	0.0003288
450	1.5725E-08	0.0003321
445	1.5647E-08	0.0003305
440	1.5646E-08	0.0003305
435	1.5787E-08	0.0003334
430	1.5805E-08	0.0003338
425	1.5768E-08	0.000333
420	1.5525E-08	0.0003279
415	1.6099E-08	0.00034
410	1.5716E-08	0.0003319
405	1.5594E-08	0.0003294
400	1.5733E-08	0.0003323
395	1.5795E-08	0.0003336
390	1.5683E-08	0.0003312
385	1.5843E-08	0.0003346
380	1.5769E-08	0.0003331
375	1.5455E-08	0.0003264
370	1.5696E-08	0.0003315
365	1.541E-08	0.0003255
360	1.5409E-08	0.0003255
355	1.5398E-08	0.0003252
350	1.5704E-08	0.0003317
345	1.5425E-08	0.0003258
340	1.5435E-08	0.000326

Vertical position [microns]	Limiting current [A]	k [m/sec]
335	1.5374E-08	0.0003247
330	1.5292E-08	0.000323
325	1.558E-08	0.0003291
320	1.5494E-08	0.0003273
315	1.5508E-08	0.0003276
310	1.507E-08	0.0003183
305	1.5155E-08	0.0003201
300	1.5035E-08	0.0003176
295	1.5317E-08	0.0003235
290	1.4861E-08	0.0003139
285	1.5881E-08	0.0003354
280	1.5386E-08	0.000325
279	1.5007E-08	0.000317
274	1.5103E-08	0.000319
269	1.5063E-08	0.0003182
264	1.5414E-08	0.0003256
259	1.5141E-08	0.0003198
254	1.5183E-08	0.0003207
249	1.4736E-08	0.0003112
244	1.5115E-08	0.0003193
239	1.4547E-08	0.0003073
234	1.4901E-08	0.0003147
229	1.511E-08	0.0003191
224	1.497E-08	0.0003162
219	1.4739E-08	0.0003113
214	1.4575E-08	0.0003078
209	1.4972E-08	0.0003162
204	1.473E-08	0.0003111
199	1.4741E-08	0.0003114
194	1.4595E-08	0.0003083
189	1.4657E-08	0.0003096
184	1.461E-08	0.0003086
179	1.4749E-08	0.0003115

Diameter of the microelectrode: 5 microns

Ferricyanide concentration: 25 mM

Raw data of Fig. 11CONT'D, v = 2.60 cm/sec

Vertical position [microns]	Limiting current [A]	k [m/sec]
174	1.471E-08	0.0003106
169	1.461E-08	0.0003086
164	1.46E-08	0.0003085
159	1.46E-08	0.0003084
154	1.465E-08	0.0003093
149	1.449E-08	0.0003061
144	1.441E-08	0.0003044
139	1.464E-08	0.0003093
134	1.412E-08	0.0002981
129	1.452E-08	0.0003066
124	1.414E-08	0.0002986
119	1.412E-08	0.0002983
114	1.433E-08	0.0003026
109	1.431E-08	0.0003023
104	1.419E-08	0.0002998
99	1.422E-08	0.0003002
94	1.448E-08	0.0003058
89	1.418E-08	0.0002994
84	1.435E-08	0.000303
79	1.453E-08	0.0003068
78	1.438E-08	0.0003037
77	1.472E-08	0.0003109
76	1.429E-08	0.0003018
75	1.473E-08	0.0003111
74	1.466E-08	0.0003096
73	1.443E-08	0.0003048
72	1.477E-08	0.0003119
71	1.47E-08	0.0003104
70	1.454E-08	0.0003071
69	1.437E-08	0.0003036
68	1.457E-08	0.0003077
67	1.46E-08	0.0003083
66	1.458E-08	0.000308
65	1.451E-08	0.0003065
64	1.433E-08	0.0003027

Vertical position [microns]	Limiting current [A]	k [m/sec]
63	1.457E-08	0.0003078
62	1.432E-08	0.0003025
61	1.459E-08	0.0003082
60	1.448E-08	0.0003059
59	1.471E-08	0.0003107
58	1.468E-08	0.00031
57	1.462E-08	0.0003087
56	1.452E-08	0.0003067
55	1.436E-08	0.0003034
54	1.447E-08	0.0003056
53	1.451E-08	0.0003064
52	1.458E-08	0.0003079
51	1.42E-08	0.0003
50	1.445E-08	0.0003052
49	1.435E-08	0.0003031
48	1.431E-08	0.0003023
47	1.441E-08	0.0003044
46	1.414E-08	0.0002987
45	1.407E-08	0.0002972
44	1.402E-08	0.0002961
43	1.434E-08	0.0003028
42	1.408E-08	0.0002973
41	1.414E-08	0.0002987
40	1.421E-08	0.0003001
39	1.423E-08	0.0003006
38	1.428E-08	0.0003015
37	1.412E-08	0.0002983
36	1.457E-08	0.0003077
35	1.398E-08	0.0002952
34	1.432E-08	0.0003024
33	1.391E-08	0.0002939
32	1.474E-08	0.0003114
31	1.4E-08	0.0002956
30	1.41E-08	0.0002978
29	1.395E-08	0.0002947

Raw data of Fig. 11CONT'D, v = 2.60 cm/sec

Vertical position [microns]	Limiting current [A]	k [m/sec]
28	1.4E-08	0.0002957
27	1.404E-08	0.0002965
26	1.428E-08	0.0003016
25	1.398E-08	0.0002953
24	1.411E-08	0.0002981
23	1.414E-08	0.0002986
22	1.393E-08	0.0002942
21	1.386E-08	0.0002927
20	1.411E-08	0.000298
19	1.383E-08	0.000292
18	1.38E-08	0.0002915
17	1.418E-08	0.0002995
16	1.39E-08	0.0002937
15	1.382E-08	0.0002919
14	1.375E-08	0.0002904
13	1.339E-08	0.0002829
12	1.369E-08	0.0002891
11	1.286E-08	0.0002717
10	1.265E-08	0.0002671
9	1.222E-08	0.0002582
8	1.144E-08	0.0002415
7	1.029E-08	0.0002174
6	9.891E-09	0.0002089
5	8.452E-09	0.0001785
4	8.086E-09	0.0001708
3	7.131E-09	0.0001506
2	5.685E-09	0.0001201
1	5.681E-09	0.00012
0	5.222E-09	0.0001103

Raw data of Fig. 11 CONT'D, v = 1.53 cm/sec

Vertical position [microns]	Limiting current [A]	k [m/sec]	Vertical position [microns]	Limiting current [A]	k [m/sec]	Vertical position [microns]	Limiting current [A]	k [m/sec]
495	1.5E-08	0.00032	330	1.4E-08	0.0003	165	1.4E-08	0.0003
490	1.5E-08	0.00031	325	1.4E-08	0.00031	160	1.4E-08	0.00029
485	1.5E-08	0.00032	320	1.5E-08	0.00031	155	1.4E-08	0.00029
480	1.5E-08	0.00031	315	1.5E-08	0.00031	150	1.4E-08	0.00029
475	1.5E-08	0.00031	310	1.4E-08	0.0003	145	1.4E-08	0.00029
470	1.5E-08	0.00031	305	1.5E-08	0.00031	140	1.4E-08	0.00029
465	1.5E-08	0.00031	300	1.4E-08	0.0003	135	1.4E-08	0.00029
460	1.5E-08	0.00031	295	1.4E-08	0.0003	130	1.4E-08	0.0003
455	1.5E-08	0.00031	290	1.4E-08	0.0003	125	1.4E-08	0.00029
450	1.5E-08	0.00031	285	1.4E-08	0.00031	120	1.4E-08	0.00029
445	1.5E-08	0.00031	280	1.4E-08	0.0003	115	1.3E-08	0.00028
440	1.5E-08	0.00031	275	1.4E-08	0.0003	110	1.4E-08	0.00029
435	1.5E-08	0.00031	270	1.4E-08	0.0003	105	1.4E-08	0.00029
430	1.5E-08	0.00031	265	1.4E-08	0.0003	100	1.4E-08	0.00029
425	1.5E-08	0.00031	260	1.4E-08	0.0003	95	1.4E-08	0.00029
420	1.5E-08	0.00031	255	1.4E-08	0.0003	90	1.4E-08	0.00029
415	1.5E-08	0.00031	250	1.5E-08	0.00031	85	1.3E-08	0.00028
410	1.4E-08	0.0003	245	1.4E-08	0.0003	80	1.3E-08	0.00028
405	1.4E-08	0.0003	240	1.5E-08	0.00031	75	1.3E-08	0.00028
400	1.4E-08	0.0003	235	1.4E-08	0.0003	70	1.4E-08	0.00029
395	1.5E-08	0.00031	230	1.4E-08	0.0003	65	1.4E-08	0.00029
390	1.4E-08	0.0003	225	1.4E-08	0.0003	60	1.4E-08	0.00029
385	1.5E-08	0.00031	220	1.4E-08	0.00031	55	1.3E-08	0.00028
380	1.4E-08	0.0003	215	1.4E-08	0.0003	50	1.3E-08	0.00028
375	1.4E-08	0.0003	210	1.4E-08	0.0003	45	1.3E-08	0.00028
370	1.5E-08	0.00031	205	1.4E-08	0.00029	40	1.3E-08	0.00028
365	1.4E-08	0.0003	200	1.4E-08	0.0003	35	1.3E-08	0.00028
360	1.5E-08	0.00031	195	1.4E-08	0.0003	30	1.3E-08	0.00028
355	1.4E-08	0.0003	190	1.4E-08	0.0003	25	1.3E-08	0.00028
350	1.4E-08	0.00031	185	1.4E-08	0.00029	20	1.3E-08	0.00028
345	1.4E-08	0.00031	180	1.4E-08	0.0003	15	1.3E-08	0.00027
340	1.4E-08	0.0003	175	1.4E-08	0.00029	10	1.1E-08	0.00023
335	1.4E-08	0.00031	170	1.4E-08	0.0003	5	5.9E-09	0.00012
						0	5.5E-09	0.00012

Diameter of the microelectrode: 5 microns

Ferricyanide concentration: 25 mM

Raw data of Fig. 11 CONT'D, v = 0.62 cm/sec

Vertical position [microns]	Limiting current [A]	k [m/sec]	Vertical position [microns]	Limiting current [A]	k [m/sec]	Vertical position [microns]	Limiting current [A]	k [m/sec]
495	1.4E-08	0.0003	330	1.4E-08	0.00029	165	1.3E-08	0.00028
490	1.4E-08	0.0003	325	1.4E-08	0.00029	160	1.3E-08	0.00028
485	1.4E-08	0.0003	320	1.4E-08	0.00029	155	1.3E-08	0.00028
480	1.4E-08	0.0003	315	1.4E-08	0.00029	150	1.3E-08	0.00028
475	1.4E-08	0.00029	310	1.4E-08	0.00029	145	1.3E-08	0.00028
470	1.4E-08	0.0003	305	1.4E-08	0.00029	140	1.3E-08	0.00028
465	1.4E-08	0.0003	300	1.4E-08	0.00029	135	1.3E-08	0.00028
460	1.4E-08	0.0003	295	1.4E-08	0.00029	130	1.3E-08	0.00028
455	1.4E-08	0.0003	290	1.4E-08	0.00029	125	1.3E-08	0.00028
450	1.4E-08	0.0003	285	1.4E-08	0.0003	120	1.3E-08	0.00028
445	1.4E-08	0.00029	280	1.4E-08	0.00029	115	1.3E-08	0.00028
440	1.4E-08	0.0003	275	1.3E-08	0.00028	110	1.3E-08	0.00028
435	1.4E-08	0.00029	270	1.4E-08	0.00029	105	1.3E-08	0.00028
430	1.4E-08	0.00029	265	1.4E-08	0.00029	100	1.3E-08	0.00028
425	1.4E-08	0.00029	260	1.4E-08	0.00029	95	1.3E-08	0.00028
420	1.4E-08	0.00029	255	1.4E-08	0.00029	90	1.3E-08	0.00028
415	1.4E-08	0.00029	250	1.4E-08	0.00029	85	1.3E-08	0.00028
410	1.4E-08	0.00029	245	1.4E-08	0.00029	80	1.3E-08	0.00027
405	1.4E-08	0.00029	240	1.4E-08	0.00029	75	1.3E-08	0.00028
400	1.4E-08	0.0003	235	1.3E-08	0.00028	70	1.3E-08	0.00028
395	1.4E-08	0.00029	230	1.3E-08	0.00028	65	1.3E-08	0.00027
390	1.4E-08	0.00029	225	1.4E-08	0.00029	60	1.3E-08	0.00028
385	1.4E-08	0.00029	220	1.4E-08	0.00029	55	1.3E-08	0.00028
380	1.4E-08	0.00029	215	1.3E-08	0.00028	50	1.3E-08	0.00028
375	1.4E-08	0.00029	210	1.3E-08	0.00028	45	1.3E-08	0.00028
370	1.4E-08	0.0003	205	1.3E-08	0.00028	40	1.3E-08	0.00027
365	1.4E-08	0.0003	200	1.3E-08	0.00028	35	1.3E-08	0.00027
360	1.4E-08	0.0003	195	1.3E-08	0.00028	30	1.3E-08	0.00028
355	1.4E-08	0.0003	190	1.4E-08	0.00029	25	1.3E-08	0.00027
350	1.4E-08	0.00029	185	1.3E-08	0.00028	20	1.3E-08	0.00027
345	1.4E-08	0.00029	180	1.3E-08	0.00028	15	1.3E-08	0.00027
340	1.4E-08	0.00029	175	1.3E-08	0.00028	10	1.2E-08	0.00026
335	1.4E-08	0.00029	170	1.3E-08	0.00028	5	9.4E-09	0.0002
						0	4.9E-09	0.0001

Diameter of the microelectrode: 5 microns

Ferricyanide concentration: 25 mM

Raw data of Fig. 12

Vertical position [microns]	Limiting current [A]	k [m/sec]	k/kmax	Oxygen conc. [mg/L]
1500	1.875E-08	0.0002021	0.98563	6.23214
1490	1.894E-08	0.0002041	0.99541	6.21071
1480	1.896E-08	0.0002043	0.99646	6.28929
1470	1.895E-08	0.0002042	0.99593	6.31071
1460	1.893E-08	0.000204	0.99488	6.28929
1450	1.897E-08	0.0002045	0.99741	6.26429
1440	1.898E-08	0.0002046	0.99793	6.3
1430	1.895E-08	0.0002042	0.99593	6.29286
1420	1.894E-08	0.0002041	0.99541	6.30357
1410	1.896E-08	0.0002044	0.99688	6.27857
1400	1.895E-08	0.0002042	0.99593	6.22143
1390	1.896E-08	0.0002044	0.99688	6.28214
1380	1.895E-08	0.0002042	0.99593	6.28214
1370	1.893E-08	0.000204	0.99488	6.28929
1360	1.896E-08	0.0002044	0.99688	6.21786
1350	1.895E-08	0.0002042	0.99593	6.17143
1340	1.895E-08	0.0002042	0.99593	6.21786
1330	1.894E-08	0.0002041	0.99541	6.27857
1320	1.894E-08	0.0002041	0.99541	6.35714
1310	1.895E-08	0.0002042	0.99593	6.30357
1300	1.895E-08	0.0002042	0.99593	6.28929
1290	1.888E-08	0.0002034	0.99225	6.275
1280	1.894E-08	0.0002041	0.99541	6.22143
1270	1.894E-08	0.0002041	0.99541	6.22143
1260	1.894E-08	0.0002041	0.99541	6.13214
1250	1.896E-08	0.0002044	0.99688	6.28929
1240	1.895E-08	0.0002042	0.99593	6.25714
1230	1.896E-08	0.0002044	0.99688	6.28214
1220	1.896E-08	0.0002043	0.99646	6.275
1210	1.894E-08	0.0002041	0.99541	6.19643
1200	1.894E-08	0.0002041	0.99541	6.075
1190	1.895E-08	0.0002042	0.99593	6.21429
1180	1.897E-08	0.0002045	0.99741	6.28929

Diameter of the microelectrode: 7 microns

Ferricyanide concentration: 25 mM

Raw data of Fig. 12 CONT'D

Vertical position [microns]	Limiting current [A]	k [m/sec]	k/kmax	Oxygen conc. [mg/L]
1170	1.9E-08	0.0002048	0.99898	6.325
1160	1.895E-08	0.0002042	0.99593	6.36071
1150	1.898E-08	0.0002046	0.99793	6.21786
1140	1.896E-08	0.0002044	0.99688	6.19643
1130	1.895E-08	0.0002042	0.99593	6.06786
1120	1.894E-08	0.0002041	0.99541	6
1110	1.896E-08	0.0002043	0.99646	5.94286
1100	1.896E-08	0.0002043	0.99646	6.01786
1090	1.896E-08	0.0002044	0.99688	6.15357
1080	1.899E-08	0.0002047	0.99846	6.15714
1070	1.895E-08	0.0002042	0.99593	6.07857
1060	1.895E-08	0.0002042	0.99593	6.08214
1050	1.893E-08	0.000204	0.99488	5.96786
1040	1.895E-08	0.0002042	0.99593	5.86786
1030	1.896E-08	0.0002044	0.99688	5.92857
1020	1.895E-08	0.0002042	0.99593	5.86071
1010	1.895E-08	0.0002042	0.99593	5.78571
1000	1.895E-08	0.0002042	0.99593	5.99286
990	1.893E-08	0.000204	0.99488	6.00714
980	1.899E-08	0.0002047	0.99846	5.975
970	1.872E-08	0.0002017	0.98405	5.87857
960	1.881E-08	0.0002027	0.98868	5.76786
950	1.894E-08	0.0002041	0.99541	5.80357
940	1.895E-08	0.0002042	0.99593	5.72143
930	1.894E-08	0.0002041	0.99541	5.74286
920	1.892E-08	0.0002038	0.99436	5.72857
910	1.894E-08	0.0002041	0.99541	5.73929
900	1.872E-08	0.0002017	0.98405	5.6
890	1.895E-08	0.0002042	0.99593	5.60714
880	1.893E-08	0.000204	0.99488	5.98214
870	1.895E-08	0.0002042	0.99593	5.73214
860	1.895E-08	0.0002042	0.99593	5.80357
850	1.895E-08	0.0002042	0.99593	5.85357
840	1.892E-08	0.0002038	0.99436	5.16786
830	1.895E-08	0.0002042	0.99593	5.525

Raw data of Fig. 12 CONT'D

Vertical position [microns]	Limiting current [A]	k [m/sec]	k/kmax	Oxygen conc. [mg/L]
820	1.875E-08	0.0002021	0.98563	5.375
810	1.89E-08	0.0002036	0.99331	5.31429
800	1.895E-08	0.0002042	0.99593	5.25
790	1.895E-08	0.0002042	0.99593	5.23929
780	1.893E-08	0.000204	0.99488	5.175
770	1.888E-08	0.0002034	0.99225	5.03571
760	1.895E-08	0.0002042	0.99593	5.075
750	1.875E-08	0.0002021	0.98563	5.05357
740	1.878E-08	0.0002024	0.98721	5.07857
730	1.884E-08	0.000203	0.99026	5.08929
720	1.894E-08	0.0002041	0.99541	5.01786
710	1.873E-08	0.0002018	0.98458	4.71786
700	1.876E-08	0.0002022	0.98616	5.15714
690	1.876E-08	0.0002022	0.98616	4.825
680	1.855E-08	0.0001999	0.97533	4.925
670	1.871E-08	0.0002016	0.98353	4.94286
660	1.875E-08	0.0002021	0.98563	5.23929
650	1.875E-08	0.0002021	0.98563	4.88214
640	1.875E-08	0.0002021	0.98563	4.75714
630	1.875E-08	0.0002021	0.98563	4.76429
620	1.875E-08	0.0002021	0.98563	4.46786
610	1.853E-08	0.0001996	0.97386	4.58929
600	1.855E-08	0.0001999	0.97533	4.54643
590	1.855E-08	0.0001999	0.97533	4.125
580	1.855E-08	0.0001999	0.97533	4.26071
570	1.854E-08	0.0001997	0.97438	4.33214
560	1.855E-08	0.0001999	0.97533	4.075
550	1.855E-08	0.0001999	0.97533	4.17857
540	1.833E-08	0.0001975	0.96355	3.92857
530	1.835E-08	0.0001977	0.9646	3.85
520	1.836E-08	0.0001979	0.96513	3.775
510	1.836E-08	0.0001979	0.96513	3.78929
500	1.835E-08	0.0001977	0.9646	3.98929
490	1.836E-08	0.0001979	0.96513	3.65714
480	1.814E-08	0.0001955	0.95378	3.66429

Raw data of Fig. 12 CONT'D

Vertical position [microns]	Limiting current [A]	k [m/sec]	k/kmax	Oxygen conc. [mg/L]
470	1.8164E-08	0.0001957	0.95483	3.22857
460	1.8164E-08	0.0001957	0.95483	3.41071
450	1.8164E-08	0.0001957	0.95483	3.32857
440	1.8164E-08	0.0001957	0.95483	3.36071
430	1.8144E-08	0.0001955	0.95378	3.06429
420	1.8154E-08	0.0001956	0.9543	3.13929
410	1.7978E-08	0.0001937	0.94505	3.27857
400	1.7774E-08	0.0001915	0.93433	3.15714
390	1.7968E-08	0.0001936	0.94452	3.15357
380	1.793E-08	0.0001932	0.94253	2.93571
370	1.7958E-08	0.0001935	0.944	2.79643
360	1.789E-08	0.0001928	0.94042	2.58929
350	1.7774E-08	0.0001915	0.93433	2.38929
340	1.7774E-08	0.0001915	0.93433	2.45357
330	1.7774E-08	0.0001915	0.93433	2.38214
320	1.7734E-08	0.0001911	0.93222	2.18571
310	1.7774E-08	0.0001915	0.93433	2.03571
300	1.7774E-08	0.0001915	0.93433	2.06071
290	1.7774E-08	0.0001915	0.93433	1.88929
280	1.791E-08	0.000193	0.94147	1.75714
270	1.7958E-08	0.0001935	0.944	1.6
260	1.7792E-08	0.0001917	0.93527	1.41071
250	1.7774E-08	0.0001915	0.93433	1.31071
240	1.7774E-08	0.0001915	0.93433	1.18571
230	1.7774E-08	0.0001915	0.93433	1.04643
220	1.795E-08	0.0001934	0.94358	0.91786
210	1.7968E-08	0.0001936	0.94452	0.78929
200	1.7784E-08	0.0001916	0.93485	0.66786
190	1.7822E-08	0.0001921	0.93685	0.57143
180	1.7958E-08	0.0001935	0.944	0.48571
170	1.7774E-08	0.0001915	0.93433	0.425
160	1.7578E-08	0.0001894	0.92402	0.325
150	1.7422E-08	0.0001877	0.91582	0.20357
140	1.7392E-08	0.0001874	0.91425	0.21071
130	1.7364E-08	0.0001871	0.91277	0.15714

Raw data of Fig. 12 CONT'D

Vertical position [microns]	Limiting current [A]	k [m/sec]	k/kmax	Oxygen conc. [mg/L]
120	1.7374E-08	0.0001872	0.9133	0.15357
110	1.7548E-08	0.0001891	0.92245	0.08214
100	1.7382E-08	0.0001873	0.91372	0.08214
90	1.6826E-08	0.0001813	0.88449	0.07143
80	1.7412E-08	0.0001876	0.9153	0.06786
70	1.7578E-08	0.0001894	0.92402	0.02143
60	1.7578E-08	0.0001894	0.92402	0.01429
50	1.7646E-08	0.0001902	0.9276	0.06786
40	1.7598E-08	0.0001896	0.92507	0.06429
30	1.7578E-08	0.0001894	0.92402	0.03571
20	1.7548E-08	0.0001891	0.92245	0.05714
10	1.1202E-08	0.0001207	0.58886	0.08214
0	1.042E-08	0.0001123	0.54775	0

Raw data of Fig. 13

Vertical position [microns]	Limiting current [A]	k [m/sec]	k/kmax
1500	1.9356E-08	0.0002086	0.99801
1490	1.9376E-08	0.0002088	0.99904
1480	1.9366E-08	0.0002087	0.99853
1470	1.9336E-08	0.0002084	0.99698
1460	1.9336E-08	0.0002084	0.99698
1450	1.9346E-08	0.0002085	0.9975
1440	1.9384E-08	0.0002089	0.99946
1430	1.9346E-08	0.0002085	0.9975
1420	1.9336E-08	0.0002084	0.99698
1410	1.9306E-08	0.000208	0.99544
1400	1.9326E-08	0.0002083	0.99647
1390	1.9336E-08	0.0002084	0.99698
1380	1.9336E-08	0.0002084	0.99698
1370	1.9336E-08	0.0002084	0.99698
1360	1.9296E-08	0.0002079	0.99492
1350	1.9336E-08	0.0002084	0.99698
1340	1.9336E-08	0.0002084	0.99698
1330	1.9296E-08	0.0002079	0.99492
1320	1.9336E-08	0.0002084	0.99698
1310	1.9336E-08	0.0002084	0.99698
1300	1.9296E-08	0.0002079	0.99492
1290	1.9336E-08	0.0002084	0.99698
1280	1.9336E-08	0.0002084	0.99698
1270	1.9336E-08	0.0002084	0.99698
1260	1.914E-08	0.0002063	0.98688
1250	1.915E-08	0.0002064	0.98739
1240	1.9326E-08	0.0002083	0.99647
1230	1.9336E-08	0.0002084	0.99698
1220	1.9278E-08	0.0002077	0.99399
1210	1.916E-08	0.0002065	0.98791
1200	1.915E-08	0.0002064	0.98739
1190	1.9112E-08	0.000206	0.98543
1180	1.915E-08	0.0002064	0.98739

Diameter of the microelectrode: 7 microns

Ferricyanide concentration: 25 mM

Raw data of Fig. 13 CONT'D

Vertical position [microns]	Limiting current [A]	k [m/sec]	k/kmax
1170	1.918E-08	0.0002067	0.98894
1160	1.9112E-08	0.000206	0.98543
1150	1.915E-08	0.0002064	0.98739
1140	1.918E-08	0.0002067	0.98894
1130	1.915E-08	0.0002064	0.98739
1120	1.919E-08	0.0002068	0.98945
1110	1.914E-08	0.0002063	0.98688
1100	1.914E-08	0.0002063	0.98688
1090	1.916E-08	0.0002065	0.98791
1080	1.914E-08	0.0002063	0.98688
1070	1.915E-08	0.0002064	0.98739
1060	1.916E-08	0.0002065	0.98791
1050	1.914E-08	0.0002063	0.98688
1040	1.9112E-08	0.000206	0.98543
1030	1.917E-08	0.0002066	0.98842
1020	1.917E-08	0.0002066	0.98842
1010	1.915E-08	0.0002064	0.98739
1000	1.914E-08	0.0002063	0.98688
990	1.914E-08	0.0002063	0.98688
980	1.914E-08	0.0002063	0.98688
970	1.914E-08	0.0002063	0.98688
960	1.914E-08	0.0002063	0.98688
950	1.914E-08	0.0002063	0.98688
940	1.914E-08	0.0002063	0.98688
930	1.914E-08	0.0002063	0.98688
920	1.9112E-08	0.000206	0.98543
910	1.9122E-08	0.0002061	0.98595
900	1.914E-08	0.0002063	0.98688
890	1.8956E-08	0.0002043	0.97739
880	1.8964E-08	0.0002044	0.9778
870	1.914E-08	0.0002063	0.98688
860	1.8956E-08	0.0002043	0.97739
850	1.8956E-08	0.0002043	0.97739
840	1.8964E-08	0.0002044	0.9778
830	1.8916E-08	0.0002038	0.97533

Raw data of Fig. 13 CONT'D

Vertical position [microns]	Limiting current [A]	k [m/sec]	k/kmax
820	1.8984E-08	0.0002046	0.97883
810	1.8946E-08	0.0002042	0.97687
800	1.8946E-08	0.0002042	0.97687
790	1.8964E-08	0.0002044	0.9778
780	1.8946E-08	0.0002042	0.97687
770	1.8946E-08	0.0002042	0.97687
760	1.8946E-08	0.0002042	0.97687
750	1.8956E-08	0.0002043	0.97739
740	1.8946E-08	0.0002042	0.97687
730	1.8936E-08	0.0002041	0.97636
720	1.877E-08	0.0002023	0.9678
710	1.875E-08	0.0002021	0.96677
700	1.8936E-08	0.0002041	0.97636
690	1.876E-08	0.0002022	0.96728
680	1.875E-08	0.0002021	0.96677
670	1.876E-08	0.0002022	0.96728
660	1.878E-08	0.0002024	0.96831
650	1.875E-08	0.0002021	0.96677
640	1.875E-08	0.0002021	0.96677
630	1.872E-08	0.0002017	0.96522
620	1.874E-08	0.0002019	0.96625
610	1.875E-08	0.0002021	0.96677
600	1.875E-08	0.0002021	0.96677
590	1.8662E-08	0.0002011	0.96223
580	1.875E-08	0.0002021	0.96677
570	1.8692E-08	0.0002014	0.96378
560	1.8574E-08	0.0002002	0.95769
550	1.8536E-08	0.0001997	0.95573
540	1.8536E-08	0.0001997	0.95573
530	1.8544E-08	0.0001998	0.95615
520	1.8544E-08	0.0001998	0.95615
510	1.8378E-08	0.000198	0.94759
500	1.836E-08	0.0001979	0.94666
490	1.836E-08	0.0001979	0.94666
480	1.836E-08	0.0001979	0.94666

Raw data of Fig. 13 CONT'D

Vertical position [microns]	Limiting current [A]	k [m/sec]	k/kmax	Oxygen conc. [mg/L]
470	1.836E-08	0.0001979	0.94666	
460	1.831E-08	0.0001973	0.94408	
450	1.815E-08	0.0001956	0.93604	
440	1.817E-08	0.0001958	0.93707	
430	1.813E-08	0.0001954	0.93501	
420	1.816E-08	0.0001957	0.93655	
410	1.798E-08	0.0001937	0.92696	
400	1.8E-08	0.000194	0.92799	
390	1.796E-08	0.0001935	0.92593	
380	1.777E-08	0.0001915	0.91644	
370	1.777E-08	0.0001915	0.91644	
360	1.777E-08	0.0001915	0.91644	
350	1.777E-08	0.0001915	0.91644	
340	1.755E-08	0.0001891	0.90479	
330	1.758E-08	0.0001894	0.90634	6.21833
320	1.777E-08	0.0001915	0.91644	6.24722
310	1.761E-08	0.0001897	0.90788	6.28694
300	1.758E-08	0.0001894	0.90634	6.28694
290	1.758E-08	0.0001894	0.90634	6.28694
280	1.759E-08	0.0001895	0.90685	6.3375
270	1.757E-08	0.0001893	0.90582	6.21833
260	1.752E-08	0.0001888	0.90335	6.21833
250	1.756E-08	0.0001892	0.90531	6.11
240	1.758E-08	0.0001894	0.90634	6.09194
230	1.758E-08	0.0001894	0.90634	6.04861
220	1.758E-08	0.0001894	0.90634	5.9475
210	1.757E-08	0.0001893	0.90582	5.92944
200	1.758E-08	0.0001894	0.90634	5.6225
190	1.735E-08	0.000187	0.89479	5.655
180	1.737E-08	0.0001872	0.89582	5.70194
170	1.737E-08	0.0001872	0.89582	5.08444
160	1.736E-08	0.0001871	0.8953	5.0375
150	1.735E-08	0.000187	0.89479	4.82806
140	1.738E-08	0.0001873	0.89623	4.93639
130	1.719E-08	0.0001852	0.88623	4.36222

Raw data of Fig. 13 CONT'D

Vertical position [microns]	Limiting current [A]	k [m/sec]	k/kmax	Oxygen conc. [mg/L]
120	1.698E-08	0.000183	0.87561	4.07694
110	1.702E-08	0.00018343	0.87767	4.00111
100	1.719E-08	0.00018522	0.88623	3.52083
90	1.719E-08	0.00018522	0.88623	2.80222
80	1.719E-08	0.00018522	0.88623	2.31472
70	1.722E-08	0.00018552	0.88767	1.64306
60	1.719E-08	0.00018522	0.88623	0.87028
50	1.717E-08	0.00018501	0.8852	0.50556
40	1.719E-08	0.00018522	0.88623	0.2925
30	1.705E-08	0.00018373	0.87911	0.21667
20	1.285E-08	0.0001385	0.66266	0.22389
10	1.163E-08	0.00012533	0.59965	0.14444
0	1.094E-08	0.00011787	0.56397	0.14806

Raw data of Fig. 14

Vertical position [microns]	Limiting current [A]	k [m/sec]	k/kmax	Oxygen conc. [mg/L]
1500	ND	ND	ND	6.42543
1490	ND	ND	ND	6.40368
1480	2.362E-08	0.0004989	0.9879	6.39125
1470	2.367E-08	0.0004999	0.98999	6.41922
1460	2.366E-08	0.0004997	0.98957	6.37572
1450	2.359E-08	0.0004983	0.98664	6.14269
1440	2.373E-08	0.0005012	0.9925	6.37572
1430	2.392E-08	0.0005052	1.00044	6.3695
1420	2.378E-08	0.0005023	0.99459	6.39747
1410	2.355E-08	0.0004974	0.98497	6.326
1400	2.349E-08	0.0004961	0.98246	6.326
1390	2.37E-08	0.0005006	0.99124	6.20483
1380	2.349E-08	0.0004961	0.98246	6.02462
1370	2.361E-08	0.0004987	0.98748	5.77294
1360	2.34E-08	0.0004942	0.9787	5.60516
1350	2.316E-08	0.0004892	0.96866	5.98423
1340	2.326E-08	0.0004913	0.97284	6.21415
1330	2.344E-08	0.0004951	0.98037	6.2794
1320	2.316E-08	0.0004892	0.96866	6.20793
1310	2.32E-08	0.00049	0.97033	6.24211
1300	2.322E-08	0.0004904	0.97117	6.09608
1290	2.337E-08	0.0004936	0.97744	5.90033
1280	2.383E-08	0.0005033	0.99668	5.95937
1270	2.346E-08	0.0004955	0.9812	6.15201
1260	2.359E-08	0.0004983	0.98664	6.26697
1250	2.363E-08	0.0004991	0.98831	6.31358
1240	2.35E-08	0.0004964	0.98288	6.20483
1230	2.37E-08	0.0005006	0.99124	6.13958
1220	2.362E-08	0.0004989	0.9879	6.14269
1210	2.348E-08	0.0004959	0.98204	6.16754
1200	2.363E-08	0.0004991	0.98831	6.20172
1190	2.362E-08	0.0004989	0.9879	6.24833
1180	2.369E-08	0.0005004	0.99082	6.1489

Diameter of the microelectrode: 5 microns
Ferricyanide concentration: 25 mM

Raw data of Fig. 14 CONT'D

Vertical position [microns]	Limiting current [A]	k [m/sec]	k/kmax	Oxygen conc. [mg/L]
1170	2.362E-08	0.0004989	0.9879	5.95626
1160	2.383E-08	0.0005033	0.99668	6.05258
1150	2.349E-08	0.0004961	0.98246	6.12715
1140	2.363E-08	0.0004991	0.98831	6.20172
1130	2.363E-08	0.0004991	0.98831	6.13337
1120	2.362E-08	0.0004989	0.9879	6.00908
1110	2.326E-08	0.0004913	0.97284	5.71702
1100	2.327E-08	0.0004915	0.97326	5.7077
1090	2.326E-08	0.0004913	0.97284	5.77916
1080	2.324E-08	0.0004909	0.972	5.76362
1070	2.322E-08	0.0004904	0.97117	5.7077
1060	2.209E-08	0.0004666	0.92391	5.83819
1050	2.324E-08	0.0004909	0.972	5.77916
1040	2.321E-08	0.0004902	0.97075	5.63934
1030	2.331E-08	0.0004923	0.97493	5.72945
1020	2.343E-08	0.0004949	0.97995	5.78227
1010	2.325E-08	0.0004911	0.97242	5.94383
1000	2.318E-08	0.0004896	0.96949	5.85684
990	2.34E-08	0.0004942	0.9787	5.8413
980	2.344E-08	0.0004951	0.98037	5.67663
970	2.31E-08	0.0004879	0.96615	5.57098
960	2.313E-08	0.0004885	0.9674	5.50884
950	2.322E-08	0.0004904	0.97117	5.59273
940	2.306E-08	0.0004871	0.96447	5.43738
930	2.303E-08	0.0004864	0.96322	5.35349
920	2.312E-08	0.0004883	0.96698	5.22299
910	2.309E-08	0.0004877	0.96573	5.23853
900	2.304E-08	0.0004866	0.96364	5.11114
890	2.28E-08	0.0004816	0.9536	4.9185
880	2.313E-08	0.0004885	0.9674	5.22299
870	2.305E-08	0.0004868	0.96406	5.30378
860	2.304E-08	0.0004866	0.96364	5.16707
850	2.306E-08	0.0004871	0.96447	4.98996
840	2.29E-08	0.0004837	0.95778	4.75072
830	2.289E-08	0.0004835	0.95736	4.53944

Raw data of Fig. 14 CONT'D

Vertical position [microns]	Limiting current [A]	k [m/sec]	k/kmax	Oxygen conc. [mg/L]
820	2.288E-08	0.0004833	0.95695	4.49594
810	2.284E-08	0.0004824	0.95527	4.54876
800	2.288E-08	0.0004833	0.95695	4.50215
790	2.288E-08	0.0004833	0.95695	4.44312
780	2.272E-08	0.0004799	0.95025	4.27223
770	2.317E-08	0.0004894	0.96908	4.14173
760	2.311E-08	0.0004881	0.96657	4.35301
750	2.283E-08	0.0004822	0.95486	4.37476
740	2.27E-08	0.0004795	0.94942	4.38719
730	2.268E-08	0.000479	0.94858	4.37476
720	2.286E-08	0.0004828	0.95611	4.24737
710	2.262E-08	0.0004778	0.94607	4.21319
700	2.267E-08	0.0004788	0.94816	4.01123
690	2.253E-08	0.0004759	0.94231	3.90249
680	2.241E-08	0.0004733	0.93729	3.65392
670	2.249E-08	0.000475	0.94063	3.58867
660	2.292E-08	0.0004841	0.95862	3.47371
650	2.265E-08	0.0004784	0.94733	3.68499
640	2.258E-08	0.0004769	0.9444	3.71917
630	2.247E-08	0.0004746	0.9398	3.58556
620	2.247E-08	0.0004746	0.9398	3.47682
610	2.245E-08	0.0004742	0.93896	3.34011
600	2.245E-08	0.0004742	0.93896	3.14125
590	2.227E-08	0.0004704	0.93143	3.1164
580	2.226E-08	0.0004702	0.93102	2.99833
570	2.221E-08	0.0004691	0.92892	2.80569
560	2.245E-08	0.0004742	0.93896	2.56644
550	2.226E-08	0.0004702	0.93102	2.24952
540	2.208E-08	0.0004664	0.92349	1.89842
530	2.205E-08	0.0004657	0.92223	1.78035
520	2.207E-08	0.0004661	0.92307	1.64986
510	2.187E-08	0.0004619	0.9147	1.57839
500	2.227E-08	0.0004704	0.93143	1.41993
490	2.206E-08	0.0004659	0.92265	1.27701
480	2.191E-08	0.0004628	0.91638	1.17758

Raw data of Fig. 14 CONT'D

Vertical position [microns]	Limiting current [A]	k [m/sec]	k/kmax	Oxygen conc. [mg/L]
470	2.2E-08	0.0004647	0.92014	1.17447
460	2.169E-08	0.0004581	0.90718	1.18069
450	2.187E-08	0.0004619	0.9147	1.17447
440	2.166E-08	0.0004575	0.90592	1.15272
430	2.169E-08	0.0004581	0.90718	1.04398
420	2.166E-08	0.0004575	0.90592	0.93212
410	2.148E-08	0.0004537	0.89839	0.74259
400	2.146E-08	0.0004533	0.89756	0.6152
390	2.131E-08	0.0004501	0.89128	0.53752
380	2.122E-08	0.0004482	0.88752	0.49402
370	2.12E-08	0.0004478	0.88668	0.4381
360	2.111E-08	0.0004459	0.88292	0.43499
350	2.108E-08	0.0004452	0.88166	0.37906
340	2.09E-08	0.0004414	0.87413	0.34799
330	2.088E-08	0.000441	0.8733	0.29828
320	2.109E-08	0.0004455	0.88208	0.32003
310	2.087E-08	0.0004408	0.87288	0.25789
300	2.069E-08	0.000437	0.86535	0.25478
290	2.062E-08	0.0004355	0.86242	0.19575
280	2.067E-08	0.0004366	0.86451	0.12739
270	2.068E-08	0.0004368	0.86493	0.12739
260	2.066E-08	0.0004364	0.8641	0.07146
250	2.067E-08	0.0004366	0.86451	0.07457
240	2.102E-08	0.000444	0.87915	0.07768
230	2.092E-08	0.0004419	0.87497	0.06836
220	2.087E-08	0.0004408	0.87288	0.06836
210	2.009E-08	0.0004243	0.84026	0.06525
200	1.963E-08	0.0004146	0.82102	0.07457
190	2.023E-08	0.0004273	0.84611	0.04661
180	2.012E-08	0.000425	0.84151	0.09632
170	1.95E-08	0.0004119	0.81558	0.07146
160	1.889E-08	0.000399	0.79007	0.04661
150	1.911E-08	0.0004036	0.79927	0.06525
140	1.895E-08	0.0004003	0.79258	0.06836
130	1.852E-08	0.0003912	0.77459	0.09943

Raw data of Fig. 14 CONT'D

Vertical position [microns]	Limiting current [A]	k [m/sec]	k/kmax	Oxygen conc. [mg/L]
120	1.797E-08	0.0003796	0.75159	0.05593
110	1.719E-08	0.0003631	0.71896	0.04971
100	1.775E-08	0.0003749	0.74239	0.04971
90	1.773E-08	0.0003745	0.74155	0.01554
80	1.619E-08	0.000342	0.67714	0.00932
70	1.484E-08	0.0003134	0.62068	-0.0435
60	1.369E-08	0.0002892	0.57258	0.03418
50	1.309E-08	0.0002765	0.54748	0.04971
40	1.191E-08	0.0002516	0.49813	0.02175
30	1.134E-08	0.0002395	0.47429	0.01864
20	1.051E-08	0.000222	0.43958	0
10	9.56E-09	0.0002019	0.39984	0.07146
0	4.9E-09	0.0001035	0.20494	0.00621

Raw data of Fig. 15

Vertical position [microns]	Limiting current [A]	k [m/sec]	k/kmax	Oxygen conc. [mg/L]
1500	2.511E-08	0.0005304	1.00068	7.20789
1490	2.458E-08	0.0005192	0.97956	7.21418
1480	2.496E-08	0.0005272	0.9947	7.25194
1470	2.423E-08	0.0005118	0.96561	7.22362
1460	2.438E-08	0.0005149	0.97159	7.24564
1450	2.422E-08	0.0005116	0.96521	7.22677
1440	2.422E-08	0.0005116	0.96521	7.17328
1430	2.418E-08	0.0005107	0.96361	6.98766
1420	2.411E-08	0.0005092	0.96083	6.33011
1410	2.421E-08	0.0005113	0.96481	6.9971
1400	2.438E-08	0.0005149	0.97159	7.08833
1390	2.42E-08	0.0005111	0.96441	6.99395
1380	2.422E-08	0.0005116	0.96521	7.12294
1370	2.422E-08	0.0005116	0.96521	7.12294
1360	2.431E-08	0.0005135	0.9688	7.2425
1350	2.413E-08	0.0005097	0.96162	7.23621
1340	2.403E-08	0.0005075	0.95764	7.1198
1330	2.417E-08	0.0005105	0.96322	7.2425
1320	2.421E-08	0.0005113	0.96481	7.24564
1310	2.402E-08	0.0005073	0.95724	7.17014
1300	2.402E-08	0.0005073	0.95724	6.88069
1290	2.4E-08	0.0005069	0.95644	6.63843
1280	2.405E-08	0.000508	0.95843	6.67933
1270	2.396E-08	0.0005061	0.95485	6.76742
1260	2.396E-08	0.0005061	0.95485	6.79259
1250	2.418E-08	0.0005107	0.96361	7.03485
1240	2.396E-08	0.0005061	0.95485	6.81462
1230	2.389E-08	0.0005046	0.95206	6.90271
1220	2.392E-08	0.0005052	0.95325	6.44966
1210	2.403E-08	0.0005075	0.95764	5.64739
1200	2.387E-08	0.0005042	0.95126	5.47749
1190	2.384E-08	0.0005035	0.95007	6.20426
1180	2.385E-08	0.0005037	0.95046	6.74226

Diameter of the microelectrode: 5 microns

Ferricyanide concentration: 25 mM

Raw data of Fig. 15 CONT'D

Vertical position [microns]	Limiting current [A]	k [m/sec]	k/kmax	Oxygen conc. [mg/L]
1170	2.38E-08	0.00050269	0.94847	6.49371
1160	2.399E-08	0.0005067	0.95604	6.01234
1150	2.397E-08	0.00050628	0.95525	6.02807
1140	2.361E-08	0.00049868	0.9409	6.22943
1130	2.383E-08	0.00050332	0.94967	5.64739
1120	2.364E-08	0.00049931	0.94209	6.20111
1110	2.332E-08	0.00049255	0.92934	6.63529
1100	2.334E-08	0.00049297	0.93014	6.51573
1090	2.358E-08	0.00049804	0.9397	5.81728
1080	2.363E-08	0.0004991	0.9417	5.73548
1070	2.36E-08	0.00049847	0.9405	6.14448
1060	2.354E-08	0.0004972	0.93811	6.55978
1050	2.351E-08	0.00049656	0.93691	6.49056
1040	2.362E-08	0.00049889	0.9413	6.26404
1030	2.356E-08	0.00049762	0.93891	6.96878
1020	2.344E-08	0.00049509	0.93412	7.12294
1010	2.363E-08	0.0004991	0.9417	5.78582
1000	2.343E-08	0.00049487	0.93373	6.12561
990	2.344E-08	0.00049509	0.93412	6.39932
980	2.326E-08	0.00049128	0.92695	6.20426
970	2.344E-08	0.00049509	0.93412	5.35165
960	2.349E-08	0.00049614	0.93612	5.40513
950	2.327E-08	0.0004915	0.92735	5.61907
940	2.344E-08	0.00049509	0.93412	5.31389
930	2.337E-08	0.00049361	0.93133	5.15973
920	2.338E-08	0.00049382	0.93173	6.13819
910	2.322E-08	0.00049044	0.92536	6.12246
900	2.326E-08	0.00049128	0.92695	5.64424
890	2.313E-08	0.00048854	0.92177	5.45232
880	2.319E-08	0.00048981	0.92416	5.57502
870	2.314E-08	0.00048875	0.92217	5.21321
860	2.304E-08	0.00048664	0.91818	5.02759
850	2.321E-08	0.00049023	0.92496	5.71346
840	2.341E-08	0.00049445	0.93293	4.76331
830	2.322E-08	0.00049044	0.92536	5.66626

Raw data of Fig. 15 CONT'D

Vertical position [microns]	Limiting current [A]	k [m/sec]	k/kmax	Oxygen conc. [mg/L]
820	2.36E-08	0.00049847	0.9405	5.46491
810	2.306E-08	0.00048706	0.91898	5.48379
800	2.323E-08	0.00049065	0.92576	5.15973
790	2.305E-08	0.00048685	0.91858	5.58446
780	2.301E-08	0.000486	0.91699	4.40465
770	2.307E-08	0.00048727	0.91938	3.80687
760	2.307E-08	0.00048727	0.91938	3.77856
750	2.304E-08	0.00048664	0.91818	5.83301
740	2.339E-08	0.00049403	0.93213	5.20063
730	2.305E-08	0.00048685	0.91858	5.2667
720	2.297E-08	0.00048516	0.91539	5.09051
710	2.283E-08	0.0004822	0.90981	4.9741
700	2.288E-08	0.00048326	0.91181	4.5651
690	2.285E-08	0.00048262	0.91061	4.70353
680	2.285E-08	0.00048262	0.91061	4.96781
670	2.279E-08	0.00048136	0.90822	5.144
660	2.268E-08	0.00047903	0.90384	4.59027
650	2.269E-08	0.00047924	0.90424	4.16239
640	2.243E-08	0.00047375	0.89387	4.03025
630	2.26E-08	0.00047734	0.90065	4.16239
620	2.264E-08	0.00047819	0.90224	3.7471
610	2.26E-08	0.00047734	0.90065	3.68103
600	2.26E-08	0.00047734	0.90065	3.49855
590	2.263E-08	0.00047798	0.90184	3.43562
580	2.229E-08	0.0004708	0.88829	4.04284
570	2.228E-08	0.00047059	0.8879	4.04913
560	2.241E-08	0.00047333	0.89308	3.93587
550	2.226E-08	0.00047016	0.8871	3.60866
540	2.231E-08	0.00047122	0.88909	3.22168
530	2.223E-08	0.00046953	0.8859	2.88504
520	2.214E-08	0.00046763	0.88232	2.61762
510	2.204E-08	0.00046552	0.87833	2.43829
500	2.212E-08	0.00046721	0.88152	2.44458
490	2.19E-08	0.00046256	0.87275	2.57043
480	2.191E-08	0.00046277	0.87315	2.82212

Raw data of Fig. 15 CONT'D

Vertical position [microns]	Limiting current [A]	k [m/sec]	k/kmax	Oxygen conc. [mg/L]
470	2.18E-08	0.0004604	0.86877	2.69627
460	2.171E-08	0.0004585	0.86518	2.51379
450	2.163E-08	0.0004569	0.86199	2.25581
440	2.166E-08	0.0004575	0.86319	2.02928
430	2.15E-08	0.0004541	0.85681	1.78388
420	2.146E-08	0.0004533	0.85522	1.59197
410	2.129E-08	0.0004497	0.84844	1.39061
400	2.105E-08	0.0004446	0.83888	1.40634
390	2.109E-08	0.0004455	0.84047	1.29622
380	2.105E-08	0.0004446	0.83888	1.25218
370	2.099E-08	0.0004433	0.83649	1.34656
360	2.094E-08	0.0004423	0.8345	1.48814
350	2.072E-08	0.0004376	0.82573	1.6077
340	2.053E-08	0.0004336	0.81816	1.52275
330	2.07E-08	0.0004372	0.82493	1.59197
320	2.069E-08	0.000437	0.82453	1.52904
310	2.033E-08	0.0004294	0.81019	1.46926
300	2.037E-08	0.0004302	0.81178	1.42522
290	2.026E-08	0.0004279	0.8074	1.26476
280	2.024E-08	0.0004275	0.8066	1.03824
270	2.043E-08	0.0004315	0.81417	0.92812
260	2.009E-08	0.0004243	0.80062	0.85891
250	2.002E-08	0.0004229	0.79783	0.84318
240	2.011E-08	0.0004248	0.80142	0.72362
230	1.994E-08	0.0004212	0.79464	0.59148
220	1.945E-08	0.0004108	0.77512	0.48451
210	1.937E-08	0.0004091	0.77193	0.54429
200	1.896E-08	0.0004005	0.75559	0.56317
190	1.866E-08	0.0003941	0.74363	0.53485
180	1.699E-08	0.0003589	0.67708	0.48136
170	1.637E-08	0.0003458	0.65237	0.4153
160	1.67E-08	0.0003527	0.66552	0.33979
150	1.596E-08	0.0003371	0.63603	0.29574
140	1.718E-08	0.0003629	0.68465	0.24226
130	1.791E-08	0.0003783	0.71374	0.12585

Raw data of Fig. 15 CONT'D

Vertical position [microns]	Limiting current [A]	k [m/sec]	k/kmax	Oxygen conc. [mg/L]
120	1.754E-08	0.0003705	0.699	0.10068
110	1.719E-08	0.0003631	0.68505	0.11641
100	1.659E-08	0.0003504	0.66114	-0.00629
90	1.531E-08	0.0003234	0.61013	0.11955
80	1.505E-08	0.0003179	0.59977	0.15416
70	1.497E-08	0.0003162	0.59658	0.10068
60	1.537E-08	0.0003246	0.61252	0.05348
50	1.523E-08	0.0003217	0.60694	0.13843
40	1.641E-08	0.0003466	0.65397	0.00944
30	1.58E-08	0.0003337	0.62966	-0.04719
20	1.56E-08	0.0003295	0.62169	-0.00315
10	1.501E-08	0.000317	0.59817	-0.06292
0	8.03E-09	0.0001696	0.32001	-0.11326

Raw data of Fig. 16

Vertical position [microns]	Limiting current [A]	k [m/sec]	k/kmax	Oxygen conc. [mg/L]
1500	1.884E-08	0.0003979	0.9635	7.11036
1490	1.905E-08	0.0004024	0.97424	6.83349
1480	1.926E-08	0.0004068	0.98498	7.10092
1470	1.897E-08	0.0004007	0.97015	7.18587
1460	1.911E-08	0.0004036	0.97731	7.18587
1450	1.903E-08	0.0004019	0.97322	7.30857
1440	1.912E-08	0.0004038	0.97782	7.27396
1430	1.953E-08	0.0004125	0.99879	7.30542
1420	1.906E-08	0.0004026	0.97476	7.32115
1410	1.906E-08	0.0004026	0.97476	7.31171
1400	1.895E-08	0.0004003	0.96913	7.22677
1390	1.856E-08	0.000392	0.94919	7.23621
1380	1.872E-08	0.0003954	0.95737	7.28969
1370	1.857E-08	0.0003922	0.9497	7.21418
1360	1.854E-08	0.0003916	0.94816	7.34947
1350	1.855E-08	0.0003918	0.94867	7.17328
1340	1.873E-08	0.0003956	0.95788	7.06002
1330	1.861E-08	0.0003931	0.95174	7.18272
1320	1.835E-08	0.0003876	0.93845	6.92788
1310	1.846E-08	0.0003899	0.94407	6.9971
1300	1.854E-08	0.0003916	0.94816	7.29913
1290	1.854E-08	0.0003916	0.94816	7.26452
1280	1.84E-08	0.0003886	0.941	6.89327
1270	1.858E-08	0.0003924	0.95021	7.24564
1260	1.882E-08	0.0003975	0.96248	7.1607
1250	1.838E-08	0.0003882	0.93998	7.2834
1240	1.842E-08	0.0003891	0.94203	7.29913
1230	1.846E-08	0.0003899	0.94407	7.22677
1220	1.872E-08	0.0003954	0.95737	7.29913
1210	1.84E-08	0.0003886	0.941	7.24879
1200	1.833E-08	0.0003872	0.93742	7.35891
1190	1.842E-08	0.0003891	0.94203	7.09777
1180	1.836E-08	0.0003878	0.93896	7.32115

Diameter of the microelectrode: 5 microns
Ferricyanide concentration: 25 mM

Raw data of Fig. 16 CONT'D

Vertical position [microns]	Limiting current [A]	k [m/sec]	k/kmax	Oxygen conc. [mg/L]
1170	1.841E-08	0.0003888	0.94151	6.81147
1160	1.817E-08	0.0003838	0.92924	6.8681
1150	1.836E-08	0.0003878	0.93896	7.1544
1140	1.859E-08	0.0003926	0.95072	7.36205
1130	1.834E-08	0.0003874	0.93793	7.23935
1120	1.844E-08	0.0003895	0.94305	7.2834
1110	1.839E-08	0.0003884	0.94049	7.10721
1100	1.87E-08	0.000395	0.95634	6.85866
1090	1.833E-08	0.0003872	0.93742	7.16699
1080	1.835E-08	0.0003876	0.93845	6.96563
1070	1.838E-08	0.0003882	0.93998	7.06317
1060	1.84E-08	0.0003886	0.941	6.92788
1050	1.827E-08	0.0003859	0.93435	7.25508
1040	1.816E-08	0.0003836	0.92873	7.33688
1030	1.832E-08	0.0003869	0.93691	7.18272
1020	1.835E-08	0.0003876	0.93845	7.23621
1010	1.846E-08	0.0003899	0.94407	6.32696
1000	1.814E-08	0.0003831	0.92771	6.71709
990	1.816E-08	0.0003836	0.92873	6.88069
980	1.813E-08	0.0003829	0.92719	6.70765
970	1.852E-08	0.0003912	0.94714	6.87439
960	1.83E-08	0.0003865	0.93589	6.63214
950	1.825E-08	0.0003855	0.93333	6.23572
940	1.813E-08	0.0003829	0.92719	6.45595
930	1.812E-08	0.0003827	0.92668	6.73911
920	1.817E-08	0.0003838	0.92924	6.64472
910	1.795E-08	0.0003791	0.91799	6.36157
900	1.803E-08	0.0003808	0.92208	6.87125
890	1.81E-08	0.0003823	0.92566	6.68877
880	1.79E-08	0.0003781	0.91543	6.0847
870	1.795E-08	0.0003791	0.91799	6.52517
860	1.796E-08	0.0003793	0.9185	6.45281
850	1.805E-08	0.0003812	0.9231	6.6227
840	1.779E-08	0.0003757	0.90981	5.93054
830	1.797E-08	0.0003796	0.91901	6.14134

Raw data of Fig. 16 CONT'D

Vertical position [microns]	Limiting current [A]	k [m/sec]	k/kmax	Oxygen conc. [mg/L]
820	1.808E-08	0.0003819	0.92464	6.24516
810	1.796E-08	0.0003793	0.9185	6.29864
800	1.815E-08	0.0003834	0.92822	6.07527
790	1.795E-08	0.0003791	0.91799	6.10987
780	1.795E-08	0.0003791	0.91799	5.61592
770	1.797E-08	0.0003796	0.91901	6.08785
760	1.793E-08	0.0003787	0.91697	6.48112
750	1.816E-08	0.0003836	0.92873	5.65682
740	1.796E-08	0.0003793	0.9185	6.34584
730	1.796E-08	0.0003793	0.9185	5.96515
720	1.777E-08	0.0003753	0.90878	5.93683
710	1.777E-08	0.0003753	0.90878	5.67885
700	1.777E-08	0.0003753	0.90878	5.77638
690	1.775E-08	0.0003749	0.90776	6.34898
680	1.799E-08	0.00038	0.92003	6.29864
670	1.777E-08	0.0003753	0.90878	5.50895
660	1.761E-08	0.0003719	0.9006	6.22943
650	1.771E-08	0.0003741	0.90571	5.84245
640	1.758E-08	0.0003713	0.89907	5.56873
630	1.76E-08	0.0003717	0.90009	5.37996
620	1.771E-08	0.0003741	0.90571	5.60019
610	1.758E-08	0.0003713	0.89907	5.76694
600	1.751E-08	0.0003698	0.89549	5.14714
590	1.758E-08	0.0003713	0.89907	4.92062
580	1.758E-08	0.0003713	0.89907	5.45862
570	1.758E-08	0.0003713	0.89907	5.26041
560	1.758E-08	0.0003713	0.89907	4.9395
550	1.745E-08	0.0003686	0.89242	4.47386
540	1.734E-08	0.0003662	0.88679	4.14037
530	1.756E-08	0.0003709	0.89804	3.99879
520	1.758E-08	0.0003713	0.89907	4.20958
510	1.736E-08	0.0003667	0.88782	4.54937
500	1.736E-08	0.0003667	0.88782	4.46757
490	1.737E-08	0.0003669	0.88833	3.97677
480	1.725E-08	0.0003643	0.88219	4.11205

Raw data of Fig. 16 CONT'D

Vertical position [microns]	Limiting current [A]	k [m/sec]	k/kmax	Oxygen conc. [mg/L]
470	1.728E-08	0.00036498	0.88372	3.95789
460	1.71E-08	0.00036118	0.87452	3.36955
450	1.716E-08	0.00036244	0.87759	3.80373
440	1.698E-08	0.00035864	0.86838	3.69046
430	1.697E-08	0.00035843	0.86787	4.05857
420	1.701E-08	0.00035928	0.86992	3.99879
410	1.682E-08	0.00035526	0.8602	3.788
400	1.684E-08	0.00035568	0.86122	3.4954
390	1.68E-08	0.00035484	0.85918	2.99201
380	1.673E-08	0.00035336	0.8556	2.66796
370	1.667E-08	0.00035209	0.85253	2.94167
360	1.66E-08	0.00035062	0.84895	3.12101
350	1.656E-08	0.00034977	0.8469	3.00774
340	1.642E-08	0.00034681	0.83974	2.76234
330	1.64E-08	0.00034639	0.83872	2.82212
320	1.649E-08	0.00034829	0.84332	2.69942
310	1.642E-08	0.00034681	0.83974	2.69313
300	1.62E-08	0.00034217	0.82849	2.51379
290	1.64E-08	0.00034639	0.83872	2.45087
280	1.621E-08	0.00034238	0.829	2.43829
270	1.616E-08	0.00034132	0.82645	2.3848
260	1.63E-08	0.00034428	0.83361	2.20232
250	1.618E-08	0.00034174	0.82747	2.17715
240	1.619E-08	0.00034196	0.82798	2.07333
230	1.603E-08	0.00033858	0.8198	1.96321
220	1.621E-08	0.00034238	0.829	2.0167
210	1.621E-08	0.00034238	0.829	1.99468
200	1.593E-08	0.00033646	0.81468	1.96007
190	1.573E-08	0.00033224	0.80445	1.93175
180	1.58E-08	0.00033372	0.80803	1.89714
170	1.543E-08	0.0003259	0.78911	1.81534
160	1.521E-08	0.00032126	0.77786	1.65489
150	1.492E-08	0.00031513	0.76303	1.69264
140	1.484E-08	0.00031344	0.75894	1.6486
130	1.494E-08	0.00031555	0.76405	1.57938

Raw data of Fig. 16 CONT'D

Vertical position [microns]	Limiting current [A]	k [m/sec]	k/kmax	Oxygen conc. [mg/L]
120	1.523E-08	0.0003217	0.77888	1.47556
110	1.386E-08	0.0002927	0.70882	1.46926
100	1.329E-08	0.0002807	0.67967	1.46926
90	1.363E-08	0.0002879	0.69706	1.46926
80	1.405E-08	0.0002968	0.71854	1.47556
70	1.42E-08	0.0002999	0.72621	1.46612
60	1.556E-08	0.0003286	0.79576	1.46297
50	1.493E-08	0.0003153	0.76354	1.46926
40	1.481E-08	0.0003128	0.7574	1.40319
30	1.487E-08	0.0003141	0.76047	1.37173
20	1.432E-08	0.0003025	0.73235	1.33712
10	1.153E-08	0.0002435	0.58966	1.14521
0	8.05E-09	0.00017	0.41169	1.2742

Raw data of Fig. 17

Vertical position [microns]	Limiting current [A]	k [m/sec]	k/kmax	Oxygen conc. [mg/L]
1500	9.57E-09	0.0002021	0.99084	6.03069
1490	9.51E-09	0.0002009	0.98463	6.11868
1480	9.57E-09	0.0002021	0.99084	6.00722
1470	9.57E-09	0.0002021	0.99084	6.00722
1460	9.57E-09	0.0002021	0.99084	6.00722
1450	9.57E-09	0.0002021	0.99084	6.03069
1440	9.66E-09	0.000204	1.00016	6.23601
1430	9.96E-09	0.0002104	1.03122	6.12455
1420	9.96E-09	0.0002104	1.03122	6.10695
1410	9.96E-09	0.0002104	1.03122	6.00722
1400	9.42E-09	0.000199	0.97531	6.00135
1390	9.77E-09	0.0002064	1.01155	6.07175
1380	9.96E-09	0.0002104	1.03122	6.11868
1370	9.87E-09	0.0002085	1.0219	6.23601
1360	9.95E-09	0.0002102	1.03019	6.21841
1350	9.46E-09	0.0001998	0.97945	6.12455
1340	9.38E-09	0.0001981	0.97117	6.23601
1330	9.57E-09	0.0002021	0.99084	6.13628
1320	9.38E-09	0.0001981	0.97117	6.11282
1310	9.63E-09	0.0002034	0.99706	6.01309
1300	9.52E-09	0.0002011	0.98567	6.11868
1290	9.47E-09	0.0002	0.98049	6.08935
1280	9.96E-09	0.0002104	1.03122	6.10695
1270	9.78E-09	0.0002066	1.01259	6.23601
1260	9.96E-09	0.0002104	1.03122	6.00722
1250	9.5E-09	0.0002007	0.9836	6.23601
1240	9.77E-09	0.0002064	1.01155	6.11282
1230	9.93E-09	0.0002097	1.02812	6.00722
1220	9.76E-09	0.0002061	1.01051	6.00722
1210	9.4E-09	0.0001985	0.97324	6.07175
1200	9.89E-09	0.0002089	1.02397	6.17148
1190	9.79E-09	0.0002068	1.01362	6.13628
1180	9.79E-09	0.0002068	1.01362	6.23601

Diameter of the microelectrode: 5 microns

Ferricyanide concentration: 25 mM

Raw data of Fig. 17 CONT'D

Vertical position [microns]	Limiting current [A]	k [m/sec]	k/kmax	Oxygen conc. [mg/L]
1170	9.78E-09	0.0002066	1.01259	6.14215
1160	9.57E-09	0.0002021	0.99084	6.06002
1150	9.79E-09	0.0002068	1.01362	6.12455
1140	9.83E-09	0.0002076	1.01776	6.11868
1130	9.77E-09	0.0002064	1.01155	6.22428
1120	9.74E-09	0.0002057	1.00844	6.12455
1110	9.53E-09	0.0002013	0.9867	6.11868
1100	9.79E-09	0.0002068	1.01362	6.14215
1090	9.8E-09	0.000207	1.01466	6.23601
1080	9.75E-09	0.0002059	1.00948	6.13042
1070	9.48E-09	0.0002002	0.98152	6.23601
1060	9.57E-09	0.0002021	0.99084	6.24188
1050	9.49E-09	0.0002004	0.98256	6.23014
1040	9.38E-09	0.0001981	0.97117	6.25361
1030	9.38E-09	0.0001981	0.97117	6.23601
1020	9.38E-09	0.0001981	0.97117	6.34161
1010	9.68E-09	0.0002045	1.00223	6.23601
1000	9.38E-09	0.0001981	0.97117	6.21255
990	9.38E-09	0.0001981	0.97117	6.10695
980	9.38E-09	0.0001981	0.97117	6.26534
970	9.36E-09	0.0001977	0.9691	6.21841
960	9.68E-09	0.0002045	1.00223	6.10108
950	9.77E-09	0.0002064	1.01155	5.99549
940	9.77E-09	0.0002064	1.01155	6.03069
930	9.61E-09	0.000203	0.99498	6.00135
920	9.25E-09	0.0001954	0.95771	5.88989
910	9.77E-09	0.0002064	1.01155	6.10695
900	9.58E-09	0.0002023	0.99188	6.00722
890	9.32E-09	0.0001969	0.96496	6.00135
880	9.17E-09	0.0001937	0.94943	5.84883
870	9.22E-09	0.0001947	0.95461	6.11868
860	9.37E-09	0.0001979	0.97014	6.10695
850	9.19E-09	0.0001941	0.9515	5.94269
840	9.17E-09	0.0001937	0.94943	5.32085
830	9.19E-09	0.0001941	0.9515	5.88403

Raw data of Fig. 17 CONT'D

Vertical position [microns]	Limiting current [A]	k [m/sec]	k/kmax	Oxygen conc. [mg/L]
820	9.21E-09	0.0001945	0.95357	5.88403
810	9.18E-09	0.0001939	0.95046	5.88989
800	9.29E-09	0.0001962	0.96185	5.6611
790	9.29E-09	0.0001962	0.96185	5.72563
780	9.2E-09	0.0001943	0.95253	5.88989
770	9.17E-09	0.0001937	0.94943	5.63764
760	9.36E-09	0.0001977	0.9691	5.75496
750	9.18E-09	0.0001939	0.95046	5.77843
740	9.56E-09	0.0002019	0.98981	5.77843
730	9.27E-09	0.0001958	0.95978	5.73736
720	9.18E-09	0.0001939	0.95046	5.31498
710	9.14E-09	0.0001931	0.94632	5.32085
700	9.16E-09	0.0001935	0.94839	5.43231
690	9.11E-09	0.0001924	0.94322	5.31498
680	8.97E-09	0.0001895	0.92872	5.17419
670	8.98E-09	0.0001897	0.92976	5.43231
660	9.16E-09	0.0001935	0.94839	5.22699
650	8.96E-09	0.0001892	0.92769	5.24458
640	8.98E-09	0.0001897	0.92976	5.11552
630	8.96E-09	0.0001892	0.92769	5.27392
620	8.96E-09	0.0001892	0.92769	5.15072
610	8.98E-09	0.0001897	0.92976	4.96886
600	8.98E-09	0.0001897	0.92976	4.88673
590	8.79E-09	0.0001857	0.91008	4.9454
580	8.79E-09	0.0001857	0.91008	4.75181
570	8.79E-09	0.0001857	0.91008	4.63448
560	8.8E-09	0.0001859	0.91112	4.52301
550	8.9E-09	0.000188	0.92147	4.62274
540	8.72E-09	0.0001842	0.90284	4.28836
530	8.91E-09	0.0001882	0.92251	4.05957
520	8.58E-09	0.0001812	0.88834	4.18276
510	8.59E-09	0.0001814	0.88938	3.97744
500	8.9E-09	0.000188	0.92147	3.80144
490	8.55E-09	0.0001806	0.88524	3.71931
480	8.53E-09	0.0001802	0.88317	3.68412

Raw data of Fig. 17 CONT'D

Vertical position [microns]	Limiting current [A]	k [m/sec]	k/kmax	Oxygen conc. [mg/L]
470	8.4E-09	0.0001774	0.86971	3.13854
460	8.4E-09	0.0001774	0.86971	3.00948
450	8.61E-09	0.0001819	0.89145	2.94495
440	8.77E-09	0.0001852	0.90801	2.44043
430	8.77E-09	0.0001852	0.90801	2.3407
420	8.75E-09	0.0001848	0.90594	1.87726
410	8.39E-09	0.0001772	0.86867	1.76579
400	8.23E-09	0.0001738	0.8521	1.40208
390	7.81E-09	0.000165	0.80862	1.38448
380	6.8E-09	0.0001436	0.70405	1.22608
370	8.01E-09	0.0001692	0.82933	0.85063
360	8E-09	0.000169	0.82829	0.8389
350	7.8E-09	0.0001647	0.80758	0.61597
340	7.34E-09	0.000155	0.75996	0.62184
330	7.23E-09	0.0001527	0.74857	0.50451
320	6.84E-09	0.0001445	0.70819	0.39305
310	6.14E-09	0.0001297	0.63571	0.32852
300	5.66E-09	0.0001195	0.58602	0.27572
290	6.25E-09	0.000132	0.6471	0.16426
280	5.89E-09	0.0001244	0.60983	0.14666
270	4.86E-09	0.0001027	0.50319	0.02933
260	4.27E-09	9.019E-05	0.4421	0.27572
250	4.1E-09	8.66E-05	0.4245	0.27572
240	4.1E-09	8.66E-05	0.4245	0.02347
230	3.72E-09	7.857E-05	0.38516	0.04106
220	3.86E-09	8.153E-05	0.39965	0.0352
210	3.94E-09	8.322E-05	0.40793	0.02347
200	3.33E-09	7.033E-05	0.34478	0.0352
190	3.13E-09	6.611E-05	0.32407	0.04106
180	3.12E-09	6.59E-05	0.32303	0.02347
170	2.93E-09	6.189E-05	0.30336	0.04693
160	2.72E-09	5.745E-05	0.28162	0.04106
150	2.67E-09	5.639E-05	0.27644	0.04693
140	2.53E-09	5.344E-05	0.26195	0.0352
130	2.34E-09	4.942E-05	0.24228	0.04693

Raw data of Fig. 17 CONT'D

Vertical position [microns]	Limiting current [A]	k [m/sec]	k/kmax	Oxygen conc. [mg/L]
120	1.94E-09	4.098E-05	0.20086	0.04693
110	2.37E-09	5.006E-05	0.24538	-0.01173
100	1.94E-09	4.098E-05	0.20086	-0.00587
90	1.97E-09	4.161E-05	0.20397	0.0176
80	1.54E-09	3.253E-05	0.15945	0.04106
70	1.56E-09	3.295E-05	0.16152	0.01173
60	1.56E-09	3.295E-05	0.16152	0.04693
50	1.16E-09	2.45E-05	0.1201	0.04106
40	1.24E-09	2.619E-05	0.12839	0.02933
30	1.33E-09	2.809E-05	0.1377	0
20	7.8E-10	1.647E-05	0.08076	0.04693
10	8.3E-10	1.753E-05	0.08594	0.04693
0	9.1E-10	1.922E-05	0.09422	0.04693

Raw data of Fig. 18

Vertical position [microns]	Limiting current [A]	k [m/sec]	k/kmax	Oxygen conc. [mg/L]
1500	1.381E-08	0.0002917	0.98211	6.22963
1490	1.383E-08	0.0002921	0.98353	6.35654
1480	1.387E-08	0.000293	0.98638	6.2517
1470	1.405E-08	0.0002968	0.99918	6.2517
1460	1.387E-08	0.000293	0.98638	6.2517
1450	1.366E-08	0.0002885	0.97144	6.35654
1440	1.368E-08	0.0002889	0.97287	6.26273
1430	1.395E-08	0.0002946	0.99207	6.2517
1420	1.378E-08	0.0002911	0.97998	6.2517
1410	1.384E-08	0.0002923	0.98424	6.2517
1400	1.365E-08	0.0002883	0.97073	6.30688
1390	1.367E-08	0.0002887	0.97215	6.29032
1380	1.386E-08	0.0002927	0.98567	6.33998
1370	1.364E-08	0.0002881	0.97002	6.2517
1360	1.386E-08	0.0002927	0.98567	6.24618
1350	1.367E-08	0.0002887	0.97215	6.2517
1340	1.367E-08	0.0002887	0.97215	6.2517
1330	1.368E-08	0.0002889	0.97287	6.23514
1320	1.367E-08	0.0002887	0.97215	6.24618
1310	1.367E-08	0.0002887	0.97215	6.2517
1300	1.362E-08	0.0002877	0.9686	6.24066
1290	1.367E-08	0.0002887	0.97215	6.2517
1280	1.384E-08	0.0002923	0.98424	5.6337
1270	1.348E-08	0.0002847	0.95864	6.24618
1260	1.349E-08	0.0002849	0.95935	6.27377
1250	1.348E-08	0.0002847	0.95864	6.15789
1240	1.365E-08	0.0002883	0.97073	6.2517
1230	1.367E-08	0.0002887	0.97215	6.14134
1220	1.354E-08	0.000286	0.96291	6.19652
1210	1.347E-08	0.0002845	0.95793	6.16341
1200	1.367E-08	0.0002887	0.97215	6.24066
1190	1.348E-08	0.0002847	0.95864	6.14686
1180	1.348E-08	0.0002847	0.95864	6.25722

Diameter of the microelectrode: 5 microns

Ferricyanide concentration: 25 mM

Raw data of Fig. 18 CONT'D

Vertical position [microns]	Limiting current [A]	k [m/sec]	k/kmax	Oxygen conc. [mg/L]
1170	1.348E-08	0.0002847	0.95864	6.21859
1160	1.328E-08	0.0002805	0.94442	6.20204
1150	1.337E-08	0.0002824	0.95082	6.2517
1140	1.348E-08	0.0002847	0.95864	6.23514
1130	1.336E-08	0.0002822	0.95011	6.23514
1120	1.367E-08	0.0002887	0.97215	6.2517
1110	1.309E-08	0.0002765	0.93091	6.2517
1100	1.33E-08	0.0002809	0.94584	6.2517
1090	1.34E-08	0.000283	0.95295	6.2517
1080	1.367E-08	0.0002887	0.97215	6.25722
1070	1.341E-08	0.0002832	0.95366	6.2517
1060	1.325E-08	0.0002799	0.94229	6.2517
1050	1.315E-08	0.0002777	0.93517	6.20756
1040	1.319E-08	0.0002786	0.93802	6.24618
1030	1.328E-08	0.0002805	0.94442	6.14686
1020	1.342E-08	0.0002834	0.95438	6.24618
1010	1.309E-08	0.0002765	0.93091	6.2517
1000	1.312E-08	0.0002771	0.93304	6.24618
990	1.33E-08	0.0002809	0.94584	6.22963
980	1.346E-08	0.0002843	0.95722	6.13031
970	1.296E-08	0.0002737	0.92166	6.21859
960	1.293E-08	0.0002731	0.91953	6.12479
950	1.308E-08	0.0002763	0.9302	6.2517
940	1.312E-08	0.0002771	0.93304	6.24066
930	1.305E-08	0.0002756	0.92806	6.21859
920	1.289E-08	0.0002723	0.91668	6.15789
910	1.306E-08	0.0002758	0.92877	6.2517
900	1.315E-08	0.0002777	0.93517	6.21859
890	1.31E-08	0.0002767	0.93162	6.20204
880	1.324E-08	0.0002796	0.94157	6.15789
870	1.27E-08	0.0002682	0.90317	6.14134
860	1.3E-08	0.0002746	0.92451	6.23514
850	1.289E-08	0.0002723	0.91668	6.18548
840	1.27E-08	0.0002682	0.90317	6.19652
830	1.27E-08	0.0002682	0.90317	6.23514

Raw data of Fig. 18 CONT'D

Vertical position [microns]	Limiting current [A]	k [m/sec]	k/kmax	Oxygen conc. [mg/L]
820	1.27E-08	0.0002682	0.90317	6.2517
810	1.27E-08	0.0002682	0.90317	6.191
800	1.262E-08	0.0002666	0.89748	6.15789
790	1.27E-08	0.0002682	0.90317	6.20756
780	1.281E-08	0.0002706	0.91099	6.14134
770	1.254E-08	0.0002649	0.89179	6.13582
760	1.251E-08	0.0002642	0.88966	6.12479
750	1.265E-08	0.0002672	0.89962	6.19652
740	1.249E-08	0.0002638	0.88824	6.04754
730	1.25E-08	0.000264	0.88895	6.0365
720	1.245E-08	0.000263	0.88539	6.0365
710	1.247E-08	0.0002634	0.88681	6.11375
700	1.236E-08	0.0002611	0.87899	6.0365
690	1.246E-08	0.0002632	0.8861	5.89856
680	1.25E-08	0.000264	0.88895	5.92615
670	1.246E-08	0.0002632	0.8861	5.82131
660	1.23E-08	0.0002598	0.87473	5.95374
650	1.25E-08	0.000264	0.88895	5.76061
640	1.229E-08	0.0002596	0.87401	6.05306
630	1.231E-08	0.00026	0.87544	5.87097
620	1.211E-08	0.0002558	0.86121	5.61715
610	1.23E-08	0.0002598	0.87473	5.71095
600	1.208E-08	0.0002551	0.85908	5.5399
590	1.209E-08	0.0002554	0.85979	5.68888
580	1.214E-08	0.0002564	0.86335	5.60059
570	1.211E-08	0.0002558	0.86121	5.67233
560	1.209E-08	0.0002554	0.85979	5.50127
550	1.244E-08	0.0002628	0.88468	5.26401
540	1.229E-08	0.0002596	0.87401	5.21986
530	1.191E-08	0.0002516	0.84699	5.33022
520	1.196E-08	0.0002526	0.85055	4.96604
510	1.191E-08	0.0002516	0.84699	4.92742
500	1.191E-08	0.0002516	0.84699	4.92742
490	1.19E-08	0.0002513	0.84628	4.75085
480	1.191E-08	0.0002516	0.84699	4.62946

Raw data of Fig. 18 CONT'D

Vertical position [microns]	Limiting current [A]	k [m/sec]	k/kmax	Oxygen conc. [mg/L]
470	1.186E-08	0.0002505	0.84343	4.40874
460	1.186E-08	0.0002505	0.84343	4.23769
450	1.172E-08	0.0002475	0.83348	3.73005
440	1.169E-08	0.0002469	0.83134	3.52589
430	1.149E-08	0.0002427	0.81712	3.33829
420	1.156E-08	0.0002442	0.8221	2.90238
410	1.168E-08	0.0002467	0.83063	2.68718
400	1.152E-08	0.0002433	0.81925	2.54372
390	1.146E-08	0.0002421	0.81499	2.25127
380	1.108E-08	0.000234	0.78796	1.95883
370	1.059E-08	0.0002237	0.75312	1.72156
360	1.061E-08	0.0002241	0.75454	1.50085
350	1.02E-08	0.0002154	0.72538	1.4843
340	1.022E-08	0.0002159	0.7268	1.24151
330	1.05E-08	0.0002218	0.74672	1.1753
320	9.96E-09	0.0002104	0.70831	1.05942
310	9.56E-09	0.0002019	0.67987	0.88837
300	8.98E-09	0.0001897	0.63862	0.77801
290	8.96E-09	0.0001892	0.6372	0.64007
280	7.83E-09	0.0001654	0.55684	0.54075
270	8.01E-09	0.0001692	0.56964	0.43039
260	7.42E-09	0.0001567	0.52768	0.27037
250	6.45E-09	0.0001362	0.4587	0.2152
240	5.96E-09	0.0001259	0.42385	0.0938
230	5.8E-09	0.0001225	0.41247	0.10484
220	5.57E-09	0.0001176	0.39612	0.10484
210	5.03E-09	0.0001062	0.35771	0.0938
200	4.46E-09	9.42E-05	0.31718	0.01655
190	4.85E-09	0.0001024	0.34491	0.04414
180	4.19E-09	8.85E-05	0.29798	0.02207
170	3.51E-09	7.414E-05	0.24962	0.03311
160	3.52E-09	7.435E-05	0.25033	0.04966
150	2.95E-09	6.231E-05	0.20979	0
140	2.73E-09	5.766E-05	0.19415	0
130	2.48E-09	5.238E-05	0.17637	0

Raw data of Fig. 18 CONT'D

Vertical position [microns]	Limiting current [A]	k [m/sec]	k/kmax	Oxygen conc. [mg/L]
120	1.98E-09	4.182E-05	0.14081	0.10484
110	1.88E-09	3.971E-05	0.1337	0.04966
100	1.69E-09	3.57E-05	0.12019	-0.00552
90	1.37E-09	2.894E-05	0.09743	0.01104
80	1.19E-09	2.513E-05	0.08463	0
70	1.37E-09	2.894E-05	0.09743	0
60	9.4E-10	1.985E-05	0.06685	0
50	7.5E-10	1.584E-05	0.05334	0.03311
40	5.9E-10	1.246E-05	0.04196	0.00552
30	5.3E-10	1.119E-05	0.03769	-0.00552
20	2.8E-10	5.914E-06	0.01991	0
10	2E-10	4.224E-06	0.01422	-0.01104
0	-5E-11	-1.056E-06	0	-0.02207

Raw data of Fig. 19

Vertical position [microns]	Limiting current [A]	k [m/sec]	k/kmax	Oxygen conc. [mg/L]
1500	2.749E-08	0.0005806	0.99936	6.37309
1490	2.733E-08	0.0005772	0.99354	6.2517
1480	2.733E-08	0.0005772	0.99354	6.2517
1470	2.457E-08	0.000519	0.89321	6.2517
1460	2.617E-08	0.0005527	0.95137	6.17997
1450	2.675E-08	0.000565	0.97246	6.21307
1440	2.647E-08	0.0005591	0.96228	6.15238
1430	2.654E-08	0.0005606	0.96482	6.30136
1420	2.655E-08	0.0005608	0.96519	6.2517
1410	2.626E-08	0.0005546	0.95464	6.2517
1400	2.654E-08	0.0005606	0.96482	6.25722
1390	2.597E-08	0.0005485	0.9441	6.24618
1380	2.643E-08	0.0005582	0.96082	6.30688
1370	2.578E-08	0.0005445	0.93719	6.15789
1360	2.642E-08	0.000558	0.96046	6.2517
1350	2.617E-08	0.0005527	0.95137	6.33447
1340	2.637E-08	0.000557	0.95864	6.24066
1330	2.606E-08	0.0005504	0.94737	6.21859
1320	2.6E-08	0.0005492	0.94519	6.2517
1310	2.598E-08	0.0005487	0.94447	6.2517
1300	2.598E-08	0.0005487	0.94447	6.27377
1290	2.578E-08	0.0005445	0.93719	6.27377
1280	2.578E-08	0.0005445	0.93719	6.32343
1270	2.559E-08	0.0005405	0.93029	6.2517
1260	2.559E-08	0.0005405	0.93029	6.2517
1250	2.539E-08	0.0005363	0.92302	6.24618
1240	2.578E-08	0.0005445	0.93719	6.24066
1230	2.541E-08	0.0005367	0.92374	6.24066
1220	2.536E-08	0.0005356	0.92193	6.24618
1210	2.546E-08	0.0005378	0.92556	6.3455
1200	2.539E-08	0.0005363	0.92302	6.25722
1190	2.524E-08	0.0005331	0.91756	6.13031
1180	2.5E-08	0.000528	0.90884	6.14134

Diameter of the microelectrode: 5 microns

Ferricyanide concentration: 25 mM

Raw data of Fig. 19 CONT'D

Vertical position [microns]	Limiting current [A]	k [m/sec]	k/kmax	Oxygen conc. [mg/L]
1170	2.523E-08	0.0005329	0.9172	6.2517
1160	2.506E-08	0.0005293	0.91102	6.15789
1150	2.499E-08	0.0005278	0.90848	6.21859
1140	2.52E-08	0.0005323	0.91611	6.15238
1130	2.519E-08	0.000532	0.91575	6.2517
1120	2.492E-08	0.0005263	0.90593	6.24066
1110	2.478E-08	0.0005234	0.90084	6.24618
1100	2.489E-08	0.0005257	0.90484	6.17445
1090	2.459E-08	0.0005194	0.89393	6.06409
1080	2.48E-08	0.0005238	0.90157	6.14134
1070	2.46E-08	0.0005196	0.8943	6.14134
1060	2.47E-08	0.0005217	0.89793	6.2517
1050	2.47E-08	0.0005217	0.89793	6.29032
1040	2.423E-08	0.0005118	0.88085	6.33447
1030	2.422E-08	0.0005116	0.88048	6.0365
1020	2.402E-08	0.0005073	0.87321	6.05306
1010	2.439E-08	0.0005152	0.88666	6.14686
1000	2.429E-08	0.000513	0.88303	6.15789
990	2.422E-08	0.0005116	0.88048	6.13031
980	2.351E-08	0.0004966	0.85467	6.24618
970	2.377E-08	0.0005021	0.86412	6.24066
960	2.373E-08	0.0005012	0.86267	6.21307
950	2.399E-08	0.0005067	0.87212	6.24066
940	2.373E-08	0.0005012	0.86267	6.15238
930	2.345E-08	0.0004953	0.85249	5.89856
920	2.344E-08	0.0004951	0.85213	6.13582
910	2.341E-08	0.0004945	0.85104	6.0365
900	2.324E-08	0.0004909	0.84486	6.2517
890	2.354E-08	0.0004972	0.85576	6.24066
880	2.305E-08	0.0004868	0.83795	6.11927
870	2.305E-08	0.0004868	0.83795	6.2517
860	2.324E-08	0.0004909	0.84486	6.13582
850	2.318E-08	0.0004896	0.84268	6.09168
840	2.305E-08	0.0004868	0.83795	6.11375
830	2.269E-08	0.0004792	0.82486	6.14134

Raw data of Fig. 19 CONT'D

Vertical position [microns]	Limiting current [A]	k [m/sec]	k/kmax	Oxygen conc. [mg/L]
820	2.304E-08	0.0004866	0.83759	6.08065
810	2.305E-08	0.0004868	0.83795	5.93166
800	2.285E-08	0.0004826	0.83068	6.14134
790	2.262E-08	0.0004778	0.82232	6.13031
780	2.244E-08	0.000474	0.81577	6.13031
770	2.249E-08	0.000475	0.81759	5.99788
760	2.24E-08	0.0004731	0.81432	5.92615
750	2.227E-08	0.0004704	0.80959	5.87097
740	2.227E-08	0.0004704	0.80959	5.76613
730	2.214E-08	0.0004676	0.80487	5.82131
720	2.207E-08	0.0004661	0.80232	5.92615
710	2.207E-08	0.0004661	0.80232	5.82131
700	2.185E-08	0.0004615	0.79433	5.60059
690	2.166E-08	0.0004575	0.78742	5.6337
680	2.153E-08	0.0004547	0.78269	5.49576
670	2.148E-08	0.0004537	0.78087	5.37436
660	2.15E-08	0.0004541	0.7816	5.60611
650	2.141E-08	0.0004522	0.77833	5.7882
640	2.144E-08	0.0004528	0.77942	5.82131
630	2.142E-08	0.0004524	0.77869	5.3854
620	2.129E-08	0.0004497	0.77397	5.3247
610	2.109E-08	0.0004455	0.7667	4.92742
600	2.128E-08	0.0004495	0.7736	5.64474
590	2.092E-08	0.0004419	0.76052	5.6944
580	2.09E-08	0.0004414	0.75979	5.58956
570	2.089E-08	0.0004412	0.75943	5.4792
560	2.086E-08	0.0004406	0.75834	5.09847
550	2.105E-08	0.0004446	0.76524	5.01019
540	2.07E-08	0.0004372	0.75252	5.17572
530	2.07E-08	0.0004372	0.75252	5.39092
520	2.029E-08	0.0004286	0.73761	5.19779
510	2.07E-08	0.0004372	0.75252	4.70671
500	2.03E-08	0.0004288	0.73798	4.6129
490	2.012E-08	0.000425	0.73143	4.29839
480	1.983E-08	0.0004188	0.72089	4.29839

Raw data of Fig. 19 CONT'D

Vertical position [microns]	Limiting current [A]	k [m/sec]	k/kmax	Oxygen conc. [mg/L]
470	1.972E-08	0.0004165	0.71689	3.91766
460	1.953E-08	0.0004125	0.70998	3.83489
450	1.968E-08	0.0004157	0.71544	3.559
440	1.953E-08	0.0004125	0.70998	3.39346
430	1.84E-08	0.0003886	0.66891	3.01825
420	1.875E-08	0.000396	0.68163	2.58786
410	1.855E-08	0.0003918	0.67436	2.4775
400	1.939E-08	0.0004095	0.7049	2.24024
390	1.66E-08	0.0003506	0.60347	2.01952
380	1.643E-08	0.000347	0.59729	1.83192
370	1.607E-08	0.0003394	0.5842	1.49533
360	1.6E-08	0.0003379	0.58166	1.50637
350	1.751E-08	0.0003698	0.63655	1.46774
340	1.67E-08	0.0003527	0.6071	1.28565
330	1.679E-08	0.0003546	0.61038	1.16978
320	1.443E-08	0.0003048	0.52458	0.89389
310	1.365E-08	0.0002883	0.49623	0.84975
300	1.307E-08	0.0002761	0.47514	0.75594
290	1.246E-08	0.0002632	0.45297	0.6511
280	1.169E-08	0.0002469	0.42497	0.55178
270	1.094E-08	0.0002311	0.39771	0.50764
260	1.013E-08	0.000214	0.36826	0.32555
250	9.57E-09	0.0002021	0.3479	0.32555
240	8.96E-09	0.0001892	0.32573	0.2152
230	8.16E-09	0.0001724	0.29665	0.16002
220	7.47E-09	0.0001578	0.27156	0.10484
210	7.04E-09	0.0001487	0.25593	0.11036
200	6.45E-09	0.0001362	0.23448	0.09932
190	6.04E-09	0.0001276	0.21958	0.01655
180	5.39E-09	0.0001138	0.19595	0.09932
170	5.06E-09	0.0001069	0.18395	0.11036
160	4.54E-09	9.589E-05	0.16505	0.0938
150	4.07E-09	8.596E-05	0.14796	-0.11036
140	3.9E-09	8.237E-05	0.14178	0.09932
130	3.32E-09	7.012E-05	0.12069	0.10484

Raw data of Fig. 19 CONT'D

Vertical position [microns]	Limiting current [A]	k [m/sec]	k/kmax	Oxygen conc. [mg/L]
120	2.93E-09	6.189E-05	0.10652	0.08277
110	2.73E-09	5.766E-05	0.09925	0.11036
100	2.29E-09	4.837E-05	0.08325	0.0938
90	2.01E-09	4.245E-05	0.07307	0
80	1.76E-09	3.717E-05	0.06398	-0.12139
70	1.56E-09	3.295E-05	0.05671	0
60	1.17E-09	2.471E-05	0.04253	-0.00552
50	9.8E-10	2.07E-05	0.03563	0.11036
40	7.8E-10	1.647E-05	0.02836	-0.02207
30	5.9E-10	1.246E-05	0.02145	0.02759
20	3.9E-10	8.237E-06	0.01418	0
10	1.6E-10	3.379E-06	0.00582	-0.00552
0	-1.5E-10	-3.168E-06	-0.00545	0